A Theoretical Analysis of Chemical and Physical Processes in an Ozone Flame

Edwin S. Campbell

Department of Chemistry
New York University
New York 53, N.Y.

1. Introduction.

A new solution of the one-dimensional time-independent hydrodynamic equations for an ozone flame which avoids some approximations made in earlier calculations yields some qualitatively different results.

The mathematical model is summarized in Section 2, the physical model and numerical parameters in Section 3, the numerical methods and the character of the eigenvalue problem in Section 4. The solution curves are analyzed in Section 5 in terms of the physical and chemical processes within the flame as a part of a study of how these processes depend upon fuel properties. The main conclusions are summarized in Section 6.

2. Mathematical Model.

This study uses the one-dimensional time-independent hydrodynamic equations in the forms suggested by Hirschfelder and Curtiss [1]

Continuity of species i: $dG_i / dZ = m_i R_i / M$ (1a)

Diffusion of species i: $dx_i / dZ = (M / n) \sum_{j \neq i} D_{ij}^{-1} \{(x_i G_j)/m_j - (x_j G_i)/m_i\}$ (1b)

Energy balance: $dT / dZ =$

$$(M / \lambda) \sum_j \{(H_j G_j)/m_j - \lim_{Z \to \infty} (H_j G_j)/m_j\} \quad (1c)$$

$$P = n R T \quad (1d)$$

where

G_i = the fractional mass-flow rate of species i $= m_i n_i v_i / M$ (1e)

m_j: the mass of species j in g./ gmol

n_j: the concentration of species j in molecules/ cc.

v_j: the average velocity of particles of type j with respect to a fixed axis system.

M: the total mass-flow rate with respect to a fixed axis system $= \sum_j n_j m_j v_j$.

D_{ij}: the binary diffusion coefficient for the pair i, j in $cm.^2\text{-}sec.^{-1}$

$x_j = n_j / n$, the mol-fraction of species j

n: the total concentration in molecules / cc. $= \sum_j n_j$

H_j: the enthalpy of species j in cal. / gmol

λ: the thermal conductivity of the gas mixture in $cal.\text{-}cm.^{-1}\text{-}sec.^{-1}\text{-}deg.^{-1}$

P: the pressure in atm.

R: the ideal gas constant in $cc.\text{-}atm.\text{-}deg.^{-1}\text{-}gmol^{-1}$

T: the absolute temperature.

The approximations required to derive these equations have been discussed elsewhere [2]. However, for the ozone flame, special justification is required for the omission of terms in kinetic-energy of gas flow in the equation of energy balance (cf. Section 4).

The Hirschfelder-Curtiss model assumes that the hot boundary is defined by an asymptotic approach to chemical, thermal, and diffusion equilibrium

$$\lim_{Z\to\infty} dT / dZ = \lim_{Z\to\infty} dx_i / dZ = \lim_{Z\to\infty} dG_i / dZ. \qquad (2)$$

The cold boundary is defined by a non-zero value of the temperature gradient,

$$(dT / dZ)_{Z\ \mathrm{cold}} > 0 \qquad (3)$$

Z cold: cold boundary,

and the continuity of the fractional mass-flow rates.

The mol-fractions may be subject to a discontinuity and are mathematically unspecified. For one class of idealized systems, it has been shown that: (a) the discontinuity exists; (b) its magnitude depends upon $(dT / dZ)_{Z\ \mathrm{cold}}$. The latter quantity can be varied over a range of values which will leave the discontinuity experimentally insignificant and which will not affect the flame solution as much as 0.01%. [3]

It has been shown that M can be viewed as an eigenvalue to be adjusted in fitting the cold-boundary conditions on the fractional mass-flow rates for one of the major constituents of the fuel. [4]

3. Physical Model and Numerical Parameters.

A critical review of experimental studies of oxygen and ozone-oxygen reaction kinetics [5] supported Hirschfelder and Curtiss' [6] choice of the three following reactions to describe the ozone flame:

$$(1)\ O_3 + M \rightleftarrows O_2 + O + M \qquad (4)$$

$$(2)\ O_3 + O \rightleftarrows 2O_2$$

$$(4)\ 2O + M \rightleftarrows O_2 + M.$$

Let: f_i^f (f_i^r): specific rate with respect to mol-fractions for the i-th forward (reverse) reaction at a total pressure of 1 atm. (5)

The specific rates have been assigned a functional form recommended for use in flame studies [7]

$$f_i^p(T) = a_i^p T^{b_i} \exp(-\epsilon_i^p / T), \quad p = f, r \qquad (6)$$

a_i^p, b_i^p, ϵ_i^p: constants.

If the reactions occur at a rate which allows approximate equilibration among the states of the reacting species, then the forward and reverse rates must approximately satisfy the thermodynamic equation

$$K_i^x = f_i^f / f_i^r \qquad (7)$$

K_i^x: the equilibrium constant with respect to mol-fractions for the i-th reaction.

The equations given in the review for the equilibrium constants were changed for mol-fractions. [5a] The parameters are recorded in Table 1.

Table 1

Parameters In Mol-Fraction Equilibrium Constants At $\mathcal{P}$ = 1 atm.

Reaction	a_i^x	b_i^x	ϵ_i^x
1	(+6) + 1.2799 33367	(-1) + 2.5	(+4) + 1.2920 85
2	(+2) + 6.0937 32368	(-1) - 7.5	(+4) - 4.6783 15
4	(-4) + 4.7609 76251	(+0) - 1.0	(+4) - 5.9704 00

Legend: The parameters are for the equation

$$K_i^x = a_i^x T^{b_i^x} \exp(-\epsilon_i^x / T).$$

The reaction numbers refer to Eq. (4).

(±Z) y.yy is (y.yy) x $10^{\pm Z}$.

The equations for reactions ($\overset{f}{1}$, M = O_2) and ($\overset{f}{2}$) were taken from the review [5b] and changed for mol-fractions. The thermodynamically consistent reverse rates were obtained from the data of Table 1. The results are shown in Table 2.

Table 2

Parameters In Eq. (6) For Mol-Fraction Specific Rates When $\mathcal{P}$ = 1 atm.

i	p	a_i^p	b_i^p	ϵ_i^p
1, M=O_3*	f	(+12) 1.98	- 2.0	(+4) + 1.243
	r	(+6) 1.546 9555	- 2.25	(+2) - 4.902 5
2+	f	(+8) 8.08	- 2.0	(+3) + 2.133
	r	(+6) 1.325 9520	- 1.25	(+4) + 4.691 615
4,** M=O_2	f	(+12) 4.6	- 4.0	0
	r	(+15) 9.661 8839	- 3.0	(+4) + 5.970 400

Legend: An entry (±Z) y.yy denotes the number (y.yy) x$10^{\pm Z}$. A line beneath digits of a_i^p or ϵ_i^p for i = 1,2 indicates that according to the review, the digits are uncertain. They are retained to maintain thermodynamic consistency to eight significant figures.

* Within the accuracy of existing data, $a_{1,M} \equiv f^p_{1,M} / f^p_{1,O_3}$ is constant. a_{1,O_2} = 0.33 [5c]. a_O was arbitrarily assigned the value a_{O_3} = 1.5.

+ The specific rates for reaction 2 are for the consumption of O_3 (i.e., one-half of the rates for the production of O_2).

** The specific rates for reaction 4 are for the production of O_2, i.e., one half of the values for the consumption of O. $a_{4,M} \equiv f^p_{4,M} / f^p_{4,O_2}$ was assumed to be constant. The following values were arbitrarily assumed: a_{4,O_3} = 2, $a_{4,O}$ = 1.33....

Several investigators have published data on reaction (4) since the preparation of the review. Unfortunately, there is only order of magnitude agreement for specific rates as shown in Table 3.

Table 3

$10^{-14}\ k^{f}_{4,M}$ $cc.^2\text{-}mol^{-2}\text{-}sec.^{-1}$ at 3500°

M	Reference [8]	[9]	[10]
A	—	0.52	0.45
Xe	1.3	—	—
O_2	4.6	1.6	4.8
O	14.	13.	9.9

Legend: The data are taken from reference [8]. They are for

$$d[O_2] / dt = k^{f}_{4,M} [M] [O]^2.$$

The most reliable determinations of recombination rates have been made by inserting dissociation rates measured in a shock tube into the thermodynamic equation between forward and reverse rates. The applicability of the equilibrium relation has been checked in shock tube studies of the coupling between dissociation and recombination [11]. Under the conditions of the experiment, the vibrational relaxation in dissociating O_2 - A mixtures was sufficiently rapid that the coupling was completely negligible up to 5000°.

Since it seemed difficult to select one significantly more reliable value, the equation suggested by reference [8] was arbitrarily adopted. It should be recognized that the temperature dependence for recombination was selected arbitrarily by the authors on the basis of other people's results. Their equation for recombination was changed for use with mol-fractions and the thermodynamically consistent dissociation rate was obtained using the parameters of Table 1. The results are recorded in Table 2.

While reactions (2) and (4) are important for determination of the asymptotic equilibrium values as $Z \to +\infty$, because of the large activation energies, they would not be expected to affect the first few digits in calculations at any other point in the flame. Comparisons with rates used in previous theoretical studies are made in Sections (5.1, 5.6).

The transport coefficients suggested in the review [5] have been adopted. They will be tabulated for reference.

Table 4

Parameters For Binary Diffusion Coefficients At P = 1 atm.

β	γ	$d_{\beta\gamma} \times 10^5$ $cm.^2\text{-}sec.^{-1}\text{-}deg.^{-3/2}$	$d^{\circ}_{\beta\gamma} \times 10^{-2}$ deg.
O_2	O_3	4.59	1.808
O_2	O	7.36	1.471
O	O_3	5.81	1.808

Legend: The parameters are taken from the review [5d] for use in the empirical equation

$$D_{\beta\gamma}(T) = d_{\beta\gamma} T^{3/2} / (1 + d^{\circ}_{\beta\gamma} T^{-1}).$$

A line beneath a digit indicates that in the review that digit was considered to be uncertain.

Table 5

Parameters For The Thermal Conductivity of The Pure Gases

	a(cal.-cm.$^{-1}$-sec.$^{-1}$-deg.$^{-1}$)deg.$^{-1/2}$	b°K	c°K
O_2	6.726×10^{-6}	265.9	10
O_3	$\underline{5.83} \times 10^{-6}$	467	10
O*	3×10^{-6}	400	0

Legend: The parameters are taken from the review [5e] for use in the empirical equation

$$\lambda = a\, T^{1/2} / \left\{ 1 + bT^{-1} \exp\left[-cT^{-1} / \ln 10 \right] \right\} .$$

A line underneath a digit indicates that in the review that digit was considered to be uncertain.

* As a result of an error, parameters for O atom were used which predict a lower thermal conductivity for O than for O_2. At 1097°, where x_O has its maximum, the thermal conductivity for O is about a factor of 3 smaller than recent theoretical estimates. However, the maximum in x_O is less than three per cent and the estimated error in λ_{mix} is only 2.6%.

The thermal conductivity of the gaseous mixture was estimated from the thermal conductivity of the pure components by the simple linear combination rule [5f]:

$$\lambda_{mix} = \sum_i \lambda_i x_i . \qquad (8)$$

The enthalpies were assumed to be linear functions of temperature given by the review [5g]. The values used for the heat capacities were averages taken over the range [300°K, 1300°K], rounded to the nearest one-quarter in C_α/R. The parameters are summarized for reference in Table 6.

Table 6

Parameters For The Enthalpy Equations

α	$H_\alpha(1300^\circ)$ cal./ gmol	C_α/R
O	(+4) 6.56$\underline{36}$	2.5
O_2	(+4) 1.004$\underline{5}$ $\underline{2}$	4.0
O_3	(+4) 4.93$\underline{59}$	6.25

Legend: The parameters are for $H_\alpha(T) = H_\alpha(1300^\circ) + C_\alpha(T-1300^\circ)$. (±Z) y.yy denotes the number (y.yy)x$10^{\pm Z}$. The review [5g] considered the underlined digits to be uncertain.

The total mass-flow rate, M, is an eigenvalue. The value required for solution of the flame equations can be compared with one calculated from the experimental burning velocity, $v(Z_c)$,

$$M = \rho(Z_c)\, v\,(Z_c) \qquad (9)$$

$\rho(Z_c)$: gas density at the burner in g./cm^3.

$v(Z_c)$: mass average velocity at the burner in cm./sec.

Z_c: the (arbitrary) distance coordinate for the burner.

Streng and Grosse measured the burning velocity of a set of ozone-oxygen mixtures [12]. The data in this paper are for their mixture with the parameters

$$
\begin{aligned}
P &= 1 \text{ atm.} \\
T(Z_c) &= 300^{\circ}K \\
x_{O_3}(Z_c) &= 0.28 \\
x_{O_2}(Z_c) &= 0.72 \\
v(Z_c) &= 52.2 \text{ cm./sec.}
\end{aligned}
\qquad (10)
$$

The Hirschfelder-Curtiss model for the flame holder has been shown for one idealized flame to require an experimentally negligible discontinuity in the mol-fractions at Z_c (vide Section 2). Thus, for the mathematical model the mol-fractions of Eq. (10) represent $\lim_{Z \to Z_c^-} x_\alpha(Z) \neq \lim_{Z \to Z_c^+} x_\alpha(Z)$. The remaining boundary values were calculated using the boundary conditions for the Hirschfelder-Curtiss model (cf. Section 2). The entire set of values is summarized for reference • :

$$M = 0.07736 \text{ g.-cm.}^{-2}\text{-sec.}^{-1}$$

	$Z = Z_c$	$\lim Z \to +\infty$
G_0	0.0	(-7) 1.904 4986
G_{O_2}	(-1) 6.315 7895	(-1) 9.999 9981
G_{O_3}	(-1) 3.684 2105	(-9) 1.101 6955
X_0	——	(-7) 3.808 9965
X_{O_2}	——	(-1) 9.999 9962
X_{O_3}	——	(-10) 7.344 6352
T^+	(+2) 3.00	(+3) 1.344 2328

(11)

4. Methods of Numerical Integration; Character of the Eigenvalue Problem.

Previously published techniques[13] were used to construct a Taylor Series of the thirtieth order about the hot boundary temperature, T_{max} (which is a singular point of the differential equation system), as a local solution over an interval

$$[T_1, T_{max}] \qquad (12)$$

$$T_{max} = \lim_{Z \to \infty} T(Z) \text{ . } **$$

• (± Z) y.yy denotes the number (y.yy) x $10^{\pm Z}$.

+ This value corresponds to $(dT/dZ)_{Z_c} = 0$. The actual value of $T(Z_c)$ must be such that $(dT/dZ)_{Z_c}$ has a positive value. The exact value is of no importance [3].

•• In order to scale the magnitudes of successive power series coefficients, it is essential to use a reduced temperature. $t = (T-T_{max})/T_{max}$ has been found to be a suitable choice [4].

The power series coefficients were checked by a test which has been used repeatedly to detect any errors of inconsistency [13a].

Mathematical instability of the equation system [4] prevents continuation of the solution from T_1 by a straightforward application of conventional methods of numerical integration. Alteration of the last of eight digits in single precision computer calculations was sufficient to cause the solution to diverge either positively or negatively along *a priori* ridiculous curves (*e.g.*, dG_{O_3}/dT goes to zero in the high temperature region). Furthermore, the first stage of a previously published method of successive approximation could be constructed over only a part of the remaining temperature range of interest [4]. Therefore, the results discussed in this paper were obtained by further development of previous work [14]. A computer program was developed in which the machine made the necessary logical choices to correct its integration and to follow the desired solution [15]. The validity of the procedure was tested with: (a) the check discussed at the end of this Section; (b) comparison of the solution with that obtained by the first stage of the successive approximation technique. Over a temperature range common to both, the difference between the function values for the two solutions was at most a few per cent *.

All previous calculations on ozone which took diffusion into account were based either on the kinetic steady-state [18,19] or on improved algebraic approximation related to the kinetic steady-state [20] which gave solutions approximately following the kinetic steady-state. It has been shown that [4]: (a) the kinetic steady-state insures a solution with a satisfactory approximation to the boundary condition $G_O = 0$; (b) with this approximation any three component system requires only a single eigenvalue, M.

Since the present calculation neither assumes nor predicts any reasonable approximation to the kinetic steady-state, it is surprising that the solution for this mixture could be constructed with M as the sole eigenvalue. The basis for the last statement consists of the following facts: (1) Starting values at T_1 off the hot boundary which give negative or positive divergence agreed with the sum of the series constructed at T_{max} to within one unit in the eighth digit; (2) Solutions which approximately satisfy the cold boundary conditions $G_O = 0$, $\varkappa_O \cong 0$ were obtained (in the sense that (a) $\varkappa_O$ and $|G_O|$ decreased to less than 0.01 of their maximum values; (b) Inspection of the bounding curves showed that the ratios would have been lowered if the bounds were brought closer); (3) M could be adjusted to fit $G_{O_3}(Z_c)$.

Conversely, for richer ozone flames (*i.e.*, higher T_{max}) calculations already performed show that: (1) the series solution including ε^2 terms in some cases predicts starting values which differ by a factor; (2) it seems impossible to fit the cold boundary value on $G_{O_3}(Z_c)$ and G_O using only a single eigenvalue and the equations present a two eigenvalue problem.

---

* In previous studies, similar numerical techniques were applied to a hypothetical flame (with the difference that all decisions were made manually). A similar comparison supported the validity of the solution for the idealized system [14b, 17].

Contrary to previous belief [18, 19, 20, 21], it seems that a single eigenvalue approximation is adequate only for (a) sufficiently lean flames, or, (b) an incorrect approximation omitting the kinetic energy term in the equation of energy balance for richer flames.

5. Discussion of Results.

5.1. Free Radical Curves; Applicability of the Kinetic Steady-State Approximation; Comparison With Other Calculations.

Consider an intermediate, α, whose net rate is given as a sum of rates for forward and reverse reactions

$$R_\alpha = \sum_i (R^f_{\alpha,i} - R^r_{\alpha,i}) . \qquad (13)$$

Since the kinetic steady-state approximation

$$R_\alpha = 0 \qquad (14)$$

has been frequently used to determine x_α, a convenient measure of the adequacy of the approximation is given by a relative deviation, r_α, defined as [3a]

$$r_\alpha = R / R^f_{\alpha,i} \qquad (15)$$

Graph (1) shows that r_0 is of the order of unity for most of the flame so that the kinetic steady-state is not a useful approximation for calculations which are at all sensitive to the profile $x_0(T)$. von Kármán and Penner [18] conjectured that the approximation would be useful in calculating burning velocities. Since there is evidence that flame speeds are comparatively insensitive, their suggestion seems to be useful for rough approximations. Thus, previous calculations on an idealized system showed that M varied by only a factor of about 0.75 with changes in kinetic and diffusion parameters which removed any approximation to the kinetic steady-state (cf. Section 5.6). The assumption that a similar result holds for the ozone flame suggests that, for a fixed set of parameters, the use of the steady-state approximation might give a result of the right order of magnitude even if it grossly distorts profiles.

The existence of a single internal maximum in an intermediate mol-fraction has been attributed to the kinetic steady-state approximation * +. Since

*When von Kármán and Penner [18] interpreted the existence of a maximum in terms of the kinetic steady-state approximation, they contrasted their suggestion with Hirschfelder and Curtiss' [22] interpretation. However, the contrast was based on an incomplete paraphrase which omitted the words in italics: "The reason for this is that the free radicals, in this case oxygen atoms, are essentially in equilibrium with fuel molecules in the region of the hot boundary. This is the significance of setting $K_1=0$." In Hirschfelder and Curtiss' notation, K_1 is the net rate of O atom production, so that $K_1=0$ is just the kinetic steady-state approximation.

+See Westenberg and Fristrom [16], p.598 for comments on experimental studies which have shown maxima in radical concentrations and for references to the literature.

Graph (2) for $x_O(\tau)$ shows such a maximum in the absence of the kinetic steady-state, this interpretation must be abandoned. However, another one which predicts a single internal maximum for a wide class of intermediates [3] does apply. Furthermore, if

$$t = (T - T_{max}) / T_{max}$$

$$\mathcal{Z} = \left[M\, C_{O_3} / \lambda(T_{max}) \right] Z, \text{ where } \mathcal{Z}=0 \text{ is an arbitrary origin,} \qquad (16)$$

then Graphs (2) of $x_O(\tau)$, (3) of $x_O(\mathcal{Z})$, and (4) of dt/dZ show that the previous conjecture [3] for such intermediates applies to the O atom in the ozone flame: despite the steeper τ gradient on the hot side of the maximum, the larger $\mathcal{Z}$ gradient lies on the cold side (due to the rapid increase in dt/dZ in the region of rapid chemical reaction).

These results on the significance of the deviations from the kinetic steady-state differ qualitatively from the assumptions of earlier studies [23,19] and the conclusions of a third [20]. The extremely large deviations reported here would have been somewhat lower in the region about the hot boundary if the older specific rate for O atom recombination had been used. In the earlier study the recombination rate was determined from Eq.(7) using the dissociation rate calculated with the pre-exponential factor for the simple bimolecular collision theory. Subsequent experiments have shown that dissociation reactions have abnormally large pre-exponential factors *. Thus the specific recombination rate used was too low by a factor of the order of 100 at 1250° and of the order of 1000 at 400° +. To obtain a lower bound on the effect of this difference, $R_O' = R_O + 2\,R_4^f$ can be computed using the data of this study. At a temperature 120° off the hot boundary, use of R_O' rather than R_O would give a relative deviation of -0.15 instead of -0.80.

However, this decrease does not alter the qualitative difference which can not be due to the difference between the specific rates and transport coefficients adopted in this study and those assumed in previous investigations. This conclusion was deduced from

PS_1 : a local solution at the hot boundary in the form of a twentieth order power series constructed with the earlier set of parameters. (17)

PS_1 predicted the same qualitative result found in this study. It is not x_O, but x_{O_3} which approximately obeys the steady-state over a wide temperature interval about the hot boundary:

$$T \geq 1217 \; (\tau \geq 0.88) : r_{O_3} \leq 0.01$$
$$T \geq 1167 \; (\tau \geq 0.83) : r_{O_3} \leq 0.033 . \qquad (18)$$

---

* Br_2 can be taken as a typical example [24].

+ The sign of the temperature coefficient was also wrong since the estimate was made before experiments established the negative temperature coefficient for recombination rates.

Although the net production rates of O and of O_3 are related by the equation

$$R_{O_3} = R_O - 2(R_1 + R_4) \tag{19}$$

and $R_O \geq 100 R_{O_3}$ through a temperature range of over 100°, two of these studies equated R_O to zero and left R_{O_3} be non-zero. von Kármán and Penner made this approximation when they were attempting to simplify the ozone equations in their study of flame speeds. They argued that R_1 would be negligible compared with other reactions except in a temperature range about the hot boundary which they felt would be unimportant for the calculation of flame speeds. Sandri made the same approximation in his calculations [19]. According to the results of this study, omission of R_1 alters R_{O_3} by orders of magnitude over this region. While it is true that previous studies of an idealized system [3] would support the contention that any change which left R_{O_3} comparatively small could be expected to be without significant effect, it does not necessarily follow that this could be expected for a drastic alteration in R_{O_3} unless the temperature range itself were a negligible fraction of the whole. Unfortunately, this approximation also gives an erroneous estimate of the size of the temperature region. In any case, it should not be made in any study of flame structure and processes.

In the third study, a Taylor series approximation using second derivatives was used to predict values at $T = T_{max} - 2°$. Tangent integration with 2 degree intervals starting from these values gave solution curves which oscillated violently. After a change to much larger values for G_{O_3} and x_{O_3} gave solution curves which were smooth and more reasonable, the oscillations in the earlier solution were attributed to the "much too small" values of G_{O_3} and x_{O_3} given by the Taylor series. This explanation does not appear to be correct since: (a) Inspection of R_1 showed that use of second derivatives gave starting values certain to about one decimal, which were not off in magnitude; (b) This study has shown that the ozone differential equations in the neighborhood of the solution determined by the hot boundary conditions are so mathematically unstable [4] that the curves are sensitive to the last of eight digits carried in usual computers. Therefore, they require special methods of solution (see Section 4). The introduction of the larger values of G_{O_3} and x_{O_3} avoided the unstable region in which G_O and x_O are increasing and x_{O_3} approximately follows a kinetic steady-state. Thus these larger values were responsible for the report that x_O has a maximum within two degrees of the hot boundary. For the remainder of the flame, x_O was calculated not from the kinetic steady-state approximation but from the equation

$$d[x_O/x_O^{ss}]/dT = 0 \rightarrow d\,x_O/dT = [x_O/x_O^{ss}]\, d\,x_O^{ss}/dT \tag{20}$$

x_O^{ss}: the value of x_O given by the kinetic steady-state approximation.

The present study shows that this would not be useful approximation for a solution determined by the hot boundary conditions. In the neighborhood of the hot boundary, a kinetic steady-state is a better approximation by two orders of magnitude for x_{O_3} than for x_O. Thus for such a solution, Eq. (20) replaces the larger

d $[x_O/x_O^{ss}]/dT$ by zero rather than the smaller d $[x_{O_3}/x_{O_3}^{ss}]/dT$.

The previous studies agree within about 13% on predicted flame speeds (cf. Section 5.6). Although it may be that the assumptions and approximations as discussed above did not greatly affect the calculated flame speed, this could only be proven by repeating the present calculations for the older parameters (cf. Section 5.6).

The following considerations suggested that it would be worth-while to determine how a change in the specific rate for free-radical recombination would affect the calculated M. Table 7 shows that radical recombination provides one of the most important terms in R_O, the net rate of O atom production, until R_O becomes positive. As this occurs, R_{O_3}, and therefore G_{O_3}, begin a much more rapid rise to provide the major change in G_{O_3}. Therefore, it seemed possible that a change in recombination rate might significantly affect the temperature at which R_O becomes positive. The resulting shift in the temperature at which G_{O_3} begins its rapid rise would change M. This suggested that if there is any flame in which recombination rates have a marked effect upon burning velocities, ozone might be one.

The tests were performed using somewhat different free-radical diffusion coefficients (cf. Section 5.5). Two different calculations were made with the specific rates of Section 3:

M	$G_{O_3}(Z_c)$	$P \equiv M\, G_{O_3}(Z_c)$	
0.07736	0.7097	0.05490	(21)
0.149	0.3979	0.05918	

According to Section 5.6 the product P can be approximated roughly as a linear function of $G_{O_3}(Z_c)$. A straight line through the data of Eq. (21) gave

$$P = 0.05958 \qquad M = 0.1617. \tag{22}$$

A third calculation with doubled rates for atom recombination and dissociation and the same value of M gave:

$$M = 0.149 \qquad G_{O_3}(Z_c) = 0.3986 \qquad P = 0.05939. \tag{23}$$

The assumption that d P/d $G_{O_3}(Z_c)$ would be about the same for the data of Eqs. (21,23) gave

$$P = 0.05981 \qquad M = 0.1623. \tag{24}$$

Thus a two fold increase in the recombination rate gave only a 0.4% increase in M. Therefore, the sensitivity to free-radical recombination and

Table 7

Rates of Reactions

T	τ	R_1^f	R_1^r	R_2^f	$2R_4^f$	R_O	R_{O_3}
(+3)+1.231	0.8914	(-3)+1.207	(-3)+1.287	(-5)+8.929	(-4)+8.644	(-3)-1.034	(-6)-8.592
(+3)+1.205	0.8667	(-3)+1.534	(-3)+1.678	(-4)+1.643	(-3)+1.409	(-3)-1.718	(-5)-1.979
(+3)+1.168	0.8308	(-3)+2.040	(-3)+2.329	(-4)+3.569	(-3)+2.550	(-3)-3.196	(-5)-6.799
(+3)+1.159	0.8222	(-3)+2.196	(-3)+2.502	(-4)+4.304	(-3)+2.899	(-3)-3.636	(-4)-1.247
(+3)+1.151	0.8148	(-3)+2.407	(-3)+2.655	(-4)+5.195	(-3)+3.224	(-3)-3.992	(-4)-2.714
(+3)+1.135	0.7999	(-3)+3.702	(-3)+2.975	(-4)+9.647	(-3)+3.941	(-3)-4.178	(-3)-1.692
(+3)+1.128	0.7925	(-3)+5.560	(-3)+3.136	(-3)+1.587	(-3)+4.324	(-3)-3.488	(-3)-4.011
(+3)+1.120	0.7851	(-3)+9.208	(-3)+3.293	(-3)+2.871	(-3)+4.705	(-3)-1.661	(-3)-8.786
(+3)+1.104	0.7703	(-2)+2.611	(-3)+3.555	(-3)+9.519	(-3)+5.350	(-3)+7.688	(-2)-3.208
(+3)+1.089	0.7554	(-2)+5.843	(-3)+3.690	(-2)+2.400	(-3)+5.637	(-2)+2.511	(-2)-7.874
(+3)+1.066	0.7332	(-1)+1.159	(-3)+3.674	(-2)+5.383	(-3)+5.428	(-2)+5.300	(-1)-1.661
(+3)+1.035	0.7035	(-1)+1.693	(-3)+3.[illegible]	(-2)+8.804	(-3)+4.676	(-2)+7.156	(-1)-2.535
(+3)+1.031	0.6998	(-1)+1.853	(-3)+3.194	(-2)+9.[illegible]	(-3)+3.793	(-2)+6.781	(-1)-2.933
(+2)+9.596	0.6319	(-1)+1.679	(-3)+2.841	(-1)+1.204	(-3)+2.639	(-2)+4.176	(-1)-2.855
(+2)+9.030	0.5775	(-1)+1.164	(-3)+2.386	(-1)+1.118	(-3)+1.843	(-4)+3.423	(-1)-2.258
(+2)+8.927	0.5678	(-1)+1.065	(-3)+2.309	(-1)+1.066	(-3)+1.698	(-3)-6.187	(-1)-2.128
(+2)+8.411	0.5182	(-2)+6.236	(-3)+1.953	(-2)+6.958	(-3)+1.112	(-2)-3.026	(-1)-1.500
(+2)+7.688	0.4490	(-2)+2.301	(-3)+1.536	(-2)+6.115	(-4)+5.964	(-2)-4.027	(-2)-8.263
(+2)+7.069	0.3897	(-3)+7.617	(-3)+1.248	(-2)+4.044	(-4)+3.412	(-2)-3.441	(-2)-4.680
(+2)+6.449	0.3303	(-3)+1.905	(-3)+1.016	(-2)+2.472	(-4)+1.910	(-2)-2.403	(-2)-2.561
(+2)+5.417	0.2315	(-5)+8.085	(-4)+7.204	(-3)+8.763	(-5)+6.696	(-3)-9.470	(-3)-8.124

Legend: The reactions are defined by Eq. (4). R_O and R_{O_3} are the net rates of production of O and of O_3 respectively. $R_O = R_1 - R_2 - 2R_4$, $R_{O_3} = -R_1 - R_2$. The number $(\pm Z) \pm Y.YY$ denotes $(\pm Y.YY) \times 10^{\pm Z}$.

dissociation rates appears to be of the same order for the ozone system and for a previously studied free-radical system [28a]. In the latter flame a 300 fold decrease in the free-radical specific rates increased M by a factor of about 1.3. Inspection of the calculations suggests that the difference in the direction of the shift can be attributed to the fact that an increase in free-radical rates* in ozone disturbs the kinetic steady-state approximation for O_3 in the region about the hot boundary.

5.2 Energy Transfer; Constant Specific Enthalpy Approximation.

For consideration of the relative contribution which various physical processes make to energy transfer, the terms in the energy balance equation (1c) will be regrouped. Since the equation assumes an asymptotic approach to thermal and diffusion equilibrium as $Z \to +\infty$, the energy conservation can be conveniently expressed in the form

$$M \sum_i H_i G_i/m_i - \lambda\, dT/dZ = \lim_{Z\to\infty} M \sum_i H_i G_i/m_i$$

$$= \lim_{Z\to\infty} M\,(H/m) \qquad (25)$$

$$H = \sum_i H_i x_i = \text{enthalpy/mol}$$

$$m = \sum_i m_i x_i = \text{mean molecular weight.}$$

The first term in Eq. (25) can be written as the sum of a term due to diffusion and a convection term due to the mass average gas velocity:

$$M\,(H/m) + n \sum_i H_i x_i V_i - \lambda\, dT/dZ$$

$$= \lim_{Z\to\infty} M\,(H/m) \qquad (26)$$

V_i : the diffusion velocity of species i.

In order to show the relative importance of the three processes in dimensionless units, the following ratios have been graphed:

$$RDIFF \equiv \frac{\text{Diffusion Term}}{\text{Conduction Term}} = \frac{n \sum_i H_i x_i V_i}{\lambda\, dT/dZ} \qquad (27)$$

$$RCONV = \frac{\text{Convection Term}}{\text{Conduction Term}} \qquad \frac{M\,[H/m]}{\lambda\, dT/dZ}$$

---

* In this system, Reaction (1) is the idealized analogue of a free-radical dissociation-recombination reaction.

Since dT/dZ approaches zero as $Z \to Z_{cold}$ and has a limiting value of zero as $Z \to \infty$, it is apparent that RCONV must increase as $Z \to Z_{cold}$ and must approach infinity as $Z \to +\infty$. In contrast with the idealized flame previously studied, for which convection was the least important process, Graph 5 shows that convection is the most important process throughout the entire flame and is over a factor of 10 more important throughout the hottest region until G_{O_3} has attained between 0.4 and 0.5 of its limiting cold boundary value. Hirschfelder[29] has shown that when the approximations of Eqs. (1b, 1c) are used, the enthalpy per gram is constant $\longleftrightarrow$ all Lewis numbers are unity. Thus the processes of diffusion and thermal conduction are of equal importance $\longleftrightarrow$ RDIFF = 1 $\longleftrightarrow$ the specific enthalpy is constant $\longleftrightarrow$ all Lewis numbers are unity. Thermal conduction will be the more important process $\longleftrightarrow$ RDIFF < 1 $\longleftrightarrow$ $H \neq \lim_{Z\to\infty} H$. Graph 6 of RDIFF shows the quantitative effect of non-unit Lewis numbers upon the relative importance of the two processes. The ratio has the same qualitative variation found in an idealized system for "light" free-radicals (those whose binary diffusion coefficients are larger than the coefficients for major component pairs)[3]: diffusion is the more important process in the hotter region ($\tau > 0.75$) and thermal conduction is the more important for ($\tau < 0.75$).

The suggestion has been made that the constant specific enthalpy approximation might be used to determine one of the mol-fractions. This approximation has been applied specifically to the ozone flame by von Kármán and Penner[28]. Let

$$\alpha' : \text{ be the species such that } H_{\alpha'} x_{\alpha'} \text{ is the largest term in } H/m = m^{-1} \sum H_\alpha x_\alpha \,. \tag{28}$$

Then, at this point the ratio

$$RH \equiv \frac{(H/m) - \lim_{Z\to\infty} (H/m)}{\lim_{Z\to\infty} (H/m)} \tag{29}$$

Shows the relative error in $x_{\alpha'}$ that would be made if this approximation were used. For this ozone flame, Graph 7 shows the variation in the error which is never greater than eight per cent. However, if this approximation were used in any theoretical calculation, the effect on the integral curves might be greater than the effect at one arbitrary point.

5.3 Heat Release by Radical Recombination.

To test the suggestion[27] that, since radicals are highly energetic species they might serve as an important means of energy transport by diffusing toward the cold boundary and recombining, the relative contribution free-radical recombination makes to the total volume rate of heat release due to chemical reaction

$$HREL \equiv \frac{2R_4 (H_O - 2H_{O_2})}{R_1 (H_{O_3} - H_O - H_{O_2}) + R_2 (H_O + H_{O_3} - 2H_{O_2}) + 2R_4 (H_O - 2H_{O_2})} \,, \tag{30}$$

is given by Graph 8.

Contrary to this suggestion, the contribution of the main combusion reaction in the colder region is more important by an order of magnitude. This contrasts strikingly with the fact that the fraction contributed by radical recombination $\geq 1/2$ for sufficiently hot T ($\tau \geq 0.77$).

For the ozone flame, HREL is qualitatively different than a previously studied idealized flame [3]. In the latter flame Reaction (1) is the analogue of the recombination-dissociation reaction. It contributes much less than a few percent of the total volume rate of heat release. Whereas in the ozone system, dissociation is completely negligible and the contribution is always positive, in the idealized system the contribution is both positive and negative. This is qualitatively the same as the contribution of the Br - Br_2 reaction in the H_2 - Br_2 system.

5.4. Spatial Separation of Processes.

There are both experimental and theoretical reasons for examining the spatial separation of processes in the ozone flame. Theoretically, study of the relative importance of processes in the neighborhood of the hot boundary might suggest useful alternative models. Experimentally, studies of the methane-oxygen system have shown that the adiabatic model (which is used in theoretical studies) is rather good for that system: the calculated and corrected experimental flame temperatures differ by only 10° [28a].

What is of particular interest here is that the methane-oxygen flame has a rather marked separation into three spatial regions [28a]: (1) a low temperature region, commonly expected in flames, in which there is comparatively little chemical reaction but a marked temperature rise due to energy transport; (2) an intermediate temperature region dominated by one sequence of reactions; (3) a higher temperature region extending to the maximum flame temperature dominated by a different sequence of reactions. The Table 7 of reaction rates and the Graph 9 of τ ($\mathcal{Y}$) [cf. Eq. 16] shows the separation of the ozone flame into the first two regions. The separation into two different kinetic regions will now be demonstrated. When the temperature is still 200° ($T = 1143°$) below its limiting hot boundary value, the fuel mol-fraction has decreased to 10^{-3} of its maximum value which occurs at the cold boundary. Conversely, x_c is still 0.87 of its maximum value. Both are, of course, orders of magnitude greater than those for complete thermodynamic equilibrium.

Inspection of the graphs (10,11,2) for the mol-fractions and fractional mass-flow rates shows the greater importance of changes for O atom in this region.

In terms of reaction kinetics, $-R_O > -R_{O_3} > 0$ and R_O/R_{O_3} increases rapidly with increasing T until it reaches a value of over 100 [cf. Table 7]. Thus, in this region the net rate of free-radical production is more important. Table 7 of reaction rates shows the importance of recombination to the net production. For example, at $T = 1143°$, recombination contributes 0.8% of the total (negative) net rate of production. This recalls Fristrom's [29] observation that recombination reactions must be important in the high temperature region of the methane-oxygen flame. The Section 5.3 on heat release has already shown that O recombination is the dominant source of heat release by chemical reactions in this region.

Just as R_O dominates R_{O_3} in kinetics, G_O dominates G_{O_3} by two orders of magnitude so that free-radical mass-flow makes a more important contribution to energy conservation than fuel mass-flow does.

As Section 5.5 shows, there is an approach to diffusion equilibrium prior to thermal equilibrium. Conversely, there is no approach to chemical equilibrium prior to thermal equilibrium. Both x_O and x_{O_3} increase rapidly with respect to thermal equilibrium values, although not so rapidly as in a previous study [20]. Thus at a temperature one degree below the hot boundary temperature, x_O and x_{O_3} are 77 and 79 times greater, respectively, than their equilibrium values.

5.5 The Role of Diffusion.

To provide a basis for estimating the significance of diffusion throughout the flame, two different sets of graphs are given: (1) the ratios (v_i/v) of the average speed for a particle of type i to the mass average speed (Graph 12); (2) the ratios of V_i/M of the actual diffusion velocity to the total mass flow rate, M (Graph 13). Although Section 5.4 shows that there is no approach to chemical equilibrium before thermal equilibrium, there is a prior approach to diffusion equilibrium $(v_i/v \simeq 1)$. Conversely, at certain lower temperatures, diffusion contributes more than the average mass flow to the motion of both O_3 and of O. Thus v_i/v attains values of 2.75 and -2.5 for O_3 and O respectively.

von Kármán and Penner's approximate equation for the burning velocity predicts that it will vary as the inverse square root of the ozone-oxygen molecule binary diffusion coefficient [16b] *. By accident, there has also been a test of the significance of the oxygen atom binary diffusion coefficients. A key-punch error in one run, and a duplication error in a second altered their temperature dependence so that they were decreased twenty-five percent and more in the x_O diffusion equation in the region of most rapid chemical reaction. This gave an estimated M of 0.1617 [cf. Eq. (22)] compared with M = 0.1812 [cf. Eq. (34)] for the diffusion coefficients of Section 3.

5.6 Comparison with Experiment and Other Calculations.

The sole experimental data on the ozone flame are burning velocities determined for several mixtures. Streng and Grosse [12] report a burning velocity of 52.2 cm./sec. for the ozone-oxygen mixture considered here. This corresponds to an experimental value for the total mass-flow rate of

$$M_{exp} = 0.07736. \tag{31}$$

The M assumed in the calculations reported here

$$M_{use} = 0.177 \text{ gm.-cm.}^{-2}/\text{sec.} \tag{32}$$

gave

$$C_{O_3}(Z_{cold}) = 0.3759.$$

---

* His a_1, defined by his Eq. (41) is inversely proportional to D_{O_2,O_3}.

Previous studies by the author have shown that for a three component flame, the product of M G_{fuel} (Z_c) varies slowly with G_{fuel} (Z_c) and can be roughly approximated as a linear function. Therefore, a theoretical value corresponding to the experimental G_{O_3} at the cold boundary was estimated by passing a straight line through two different calculated values:

$$M\, G_{O_3}\,(Z_c) = 0.06653 - 0.03086\,(G_{O_3} - 0.3789). \tag{33}$$

This gave

$$M_{the} = 0.1812. \tag{34}$$

Since Professor Grosse feels that this discrepancy greatly exceeds the likely experimental error [30], it is necessary to consider possible sources of the disagreement. Results of previous calculations on an idealization of a free-radical flame can be used to suggest probable sources of error [26,3]. For an appropriate choice of dimensionless variables, it was found that M could be combined with other parameters to form a dimensionless constant, μ^*, which varied rather slowly with certain parameters:

$$\mu^* = \frac{(m^*)^2 \lambda\,(T_{max}) \times}{M^2 C^*}$$

m^*, C^*: The molecular weight and constant pressure heat capacity for a species, 3, where M is adjusted to make G_3 (Z) satisfy its cold boundary condition. (35)

k^* : any multiplicative factor in the specific rate for one of the most important reactions in the net rate of production of 3.

Thus for 13 and 15-fold variations in the two binary diffusion coefficients involving free-radicals and a 300 fold variation in the ratio of the specific rates for the main combusion reaction to those for the free-radical reaction, μ^* varied only by a factor of 1.8. This suggests that the large ratio M_{the}/M_{exp} should be attributed to either too high a value for one or more of the following quantities: (a) $\lambda\,(T_{max})$, and, therefore, λ (T); (b) the specific rates of reactions which contribute most to $d\,G_{O_2}/dT$ in the region of most rapid chemical reaction. For the ozone flame, the two most important reactions in the temperature domain responsible for most of the rise in G_{O_3} are: (1) R_1^f at the higher temperatures within this region; (2) R_2^f at the lower. (Note that because of the failure of the kinetic steady-state, R_1^f and R_2^f are not directly related). Although further experimental work would be required to choose between the alternatives, it seems less likely that the thermal conductivity is off by over a factor of two. It is worth noting that the activation energy for both R_1^f and R_2^f are subject to considerable uncertainty. For example, the ratio of the (1) specific rate assumed here to the one proposed by Benson and Axworthy [31] is

$$2.9 \exp[-350/T]. \tag{36}$$

At T = 1000°, a temperature in the range where R_1^f makes a large contribution, this ratio is approximately two. Correction of Benson and Axworthy's parameters for (2)

to take account of their use of an older equilibrium constant gave a higher activation energy than the one used in this report [5f]. Apparently this was due to their use of graphical instead of least squares data analysis [56]. Conversely, flow system studies gave a lower value which would predict a somewhat lower specific rate at flame temperatures.

Previous theoretical studies predicted burning velocities for a mixture of similar composition

$$x_{O_3}(Z_{cold}) = 0.25 \qquad (37)$$

for which Lewis and von Elbe reported a burning velocity of 55 cm.-sec.$^{-1}$ [32]. The results, depending upon the value assumed for the reduced diffusion coefficient range from 47 or 51 [20] to 42 or 46 [18]. There is much better agreement between their calculations and experiment than between the results presented here and experiment.

As shown in Section 5.1, it is not certain that the calculated speeds are correct for the parameters assumed. If they are correct, inspection of Eq. (35) shows that the discrepancy between them and the present results is not related in a simple fashion to the difference in parameters since: (1) The values for the thermal conductivity of the gas mixture used in the two studies are within several percent of each other; (2) According to preceding discussion in this section, the two reactions which are responsible for most of the change in G_{O_3} (which determines M) are R_1^f and R_2^f. Whereas a decrease in either would decrease the theoretical M, the ratios of specific rates in the present study to those used in the earlier work are:

	Reaction	f_1	f_2	
T =	1230°	9.9	0.045	
	872°	13.1	0.07	(38)
	397°	15.8	0.36	

5.7 Test of the Significance of the Kinetic Energy Term in the Equation of Energy Balance.

Previously, heuristic argument has been given to support the contention that kinetic energy of over all gas flow can be an important term in the energy balance equation even when viscosity makes no significant contribution. The argument suggested that the former term would be most important where there was the greatest cancellation in the usual terms of the equation of energy balance, i.e., in the neighborhood of the hot boundary [4]. Therefore, as a check upon the importance of kinetic energy, a thirtieth order power series was constructed including those terms. The series sums are:

$$(T-T_{max}) = -0.1125\ T_{max}$$

	without K.E.	with K.E.	% Error	
G_{O_3}	1.9409×10^{-4}	1.9959×10^{-4}	2.8	
x_{O_3}	1.1540×10^{-4}	1.1835×10^{-4}	2.5	(39)
G_O	1.0307×10^{-2}	1.0936×10^{-2}	3.0	
x_O	1.9129×10^{-2}	1.9990×10^{-2}	2.8	

Although these values suggest that the kinetic energy term does not make an important contribution to this flame, calculations on richer ozone flames with higher maximum temperatures (to be included in a later paper) show that it changes the eigenvalue character of the problem.

5.8 Significance of Theoretical Flame Calculations.

As Sandri [33] observed, it is simpler to measure burning velocities than to make theoretical calculations. He argued that the calculations should be used as a means of studying chemical kinetics by comparing theoretical and experimental velocities for appropriate models. The discussion of Sections 5.1, 5.6 illustrates the facts that flame speeds are not particularly sensitive to many parts of a kinetic scheme and that such a comparison could be useful only if the transport coefficients and all but one specific rate which contributed markedly to the rate of consumption of a major fuel component were reasonably well known. However, theoretical calculations could be very useful when the greater detail given by experimental studies of temperature and composition profiles are known. For major components, these have been determined for the methane-ozygen system [34]. Work on determining free-radical profiles is in progress [35]. Theoretical calculations would obviate the use of approximations in the diffusion equations made in analyzing current experimental studies and the uncertainty from double differentiation of experimental data [36].

Alternatively, they can be used to develop a general understanding of the relation between fuel properties and the comparative importance of various processes. For the particular case of ozone, it seems unlikely that uncertainties in the parameters will qualitatively alter any of the results presented here. This conclusion is founded on a comparison of: (a) [illegible] calculations discussed here; (b) unreported calculations using different specific rates for reactions (1) and (2) which were 6 fold larger for (1) and 25 fold larger for (2) at the hot boundary; (c) unreported calculations for various assumed values of K_1; (d) unreported calculations on richer ozone mixtures.

6. Summary of Major Conclusions.

The major conclusions will be summarized according to sections for convenient reference.

Section 4. A single eigenvalue approximation appears to be adequate for the 28 mole percent ozone flame. Two eigenvalues must be used for sufficiently rich ozone mixtures burning at higher temperatures.

Section 5.1.

(a) It seems that the kinetic mechanism may give burning velocities accurate within a factor of about 2 and generally better. Since x_0 does not follow a semblance of the approximation in this (and a fortiori in higher temperature ozone flames), the approximation should not be used in calculating any property at all sensitive to $x_0(\dot{m})$.

(b) It is not x_0 but $x_{0.1}$ which approximately satisfies a kinetic steady-state condition in a temperature interval of over 175° about the hot boundary.

(c) The existance of a single internal maximum should not be interpreted in

terms of the kinetic steady-state approximation. An alternative approximation applies.

(d) Radical recombination in this ozone flame plays an important role but only for temperatures within about 300° of the hot boundary.

(e) von Kármán and Penner underestimated the temperature range over which R_1^r : $M+O_2+O \rightarrow M+O_3$ would be important. It exceeds R_1^r : $M+O_3 \rightarrow O_2+O+M$ over a temperature range of about 200°. The effect of this upon the flame velocity is uncertain.

Sections 5.1 and 5.6. The qualitative differences between the results reported here and those of earlier studies is due to the removing of certain earlier approximations.

Section 5.2.

(a) Convection is the dominant process at all temperatures. Diffusion is more important than conduction at higher temperatures, less at lower.

(b) The specific enthalpy varies over a range of ±8%.

Section 5.3. The rate of heat release per unit volume due to radical recombination is over half the total rate for a temperature interval of over 200° about the hot boundary. Contrary to a previous suggestion, it becomes negligible in the cooler part of the flame. Radicals which diffuse there from the hotter regions are effective primarily in R_2^r : $O+O_3 \rightarrow 2\ O_2$.

Section 5.4. The spatial separation of kinetic processes is reminiscent of the separation found experimentally in the methane-oxygen flame. There is no approach to chemical before thermal equilibrium.

Section 5.5. There is an approach to diffusion equilibrium before thermal (and chemical) equilibrium. The magnitude of the diffusion velocity exceeds the mass average speed for $T <$ ca. 1020° for O and from about T = 910° to T = 1130° for O_3.

Section 5.6. The theoretical M is too large by over a factor of 2. The most likely major sources of the error are too high values at flame temperatures of the rate of R_1^r : $O_3+M \rightarrow O_2+O+M$, or of R_2^r : $O_3+O \rightarrow 2\ O_2$, or both.

Section 5.7. The kinetic energy of overall gas flow does not appear to be very important for this ozone flame. Conversely, it can not be ignored for sufficiently rich ozone flames where it changes the character of the eigen-value problem.

REFERENCES

1. Hirschfelder, J. O., Curtiss, C. F., and Bird, R. B.: Molecular Theory of Gases and Liquids, John Wiley and Sons, New York (1954), Chapter 11.

2. Klein, G.: Phil. Trans. Roy. Soc. (London) A249, 389-457 (1959).

3. Campbell, E. S., Heinen, F. J., and Schalit, L. M.: Submitted for publication. (a)[Sect. 4, Eq. 29].

4. Campbell, E. S., Heinen, F. J., and Schalit, L. M.: Submitted for publication.

5. Campbell, E. S. and Nudelman, C.: Reaction Kinetics, Thermodynamics, and Transport Properties in the Ozone-oxygen System. AFOSR TN-60-502. (1960); (a) Table IX, p. 14; (b) Table XIII, p. 76; (c) pp. 57,77; (d) p. 90; (e) pp. 90, 91; (f) pp.90-94; (g) Tables III, V, pp. 7,8.

6. Hirschfelder, J. O., Curtiss, C. F., and Campbell, D. E.: J. Phys. Chem. 57, 403-14 (1953).

7. Campbell, E. S. and Fristrom, R. M.: Chem. Rev. 58, 173-234 (1958); cf. p. 182-4.

8. Rink, J. P., Knight, H. T., Duff, R. E.: J. Chem. Phys. 34, 1942-7 (1961).

9. Camac, M., Vaughan, A.: Avco Everett Research Laboratory Research Report 84, AFBMD-TR-60-22; J. Chem. Phys. 34, 460-470 (1961).

10. Byron, S. R.; J. Chem. Phys. 30, 1380-1382 (1959).

11. Wray, K. L.: J. Chem. Phys. 37, 1254-63 (1962).

12. Streng, A. G. and Grosse, A. V.: Sixth Symposium (International) on Combustion, Reinhold Publishing Corp., New York (1957), pp. 265-72, cf. p. 269.

13. Campbell, E. S., Buehler, R., Hirschfelder, J. O., and Hughes, D.: J. Assoc. Compt. Mach. 8, 374-83 (1961); (a) p. 383.

14. Schalit, L. M.: Ph.D. Thesis "Deviation from the Kinetic Steady-State Approximation in a Free-radical Flame", New York University, October, 1961; (a) cf. p. 158; (b) pp. 150-158, 160.

15. Campbell, E. S.: To be submitted for publication.

16. Westenberg, A. A. and Fristrom, R. M.: J. Phys. Chem. 64, 591-601 (1961) cf. p. 598.

17. Heinen, F. J.: Ph.D. Thesis, New York University, August 1962.

18. von Kármán, T. and Penner, S. S.: Selected Combustion Problems I (Agard), Butterworths Scientific Publications (1954), pp. 5-41; (a) cf. p. 40; (b) Eq. (107).

19. Sandri, R.: Can. J. Chem., 34, 324-30 (1960).

20. Hirschfelder, J. O., Curtiss, C. F., Campbell, D. E.: J. Phys. Chem., 57, 403-14 (1953).

21. Ninth Symposium on Combustion, Academic Press, New York (1963), p. 80, (comment by J. F. Wehner).

22. Hirschfelder, J. O., Curtiss, C. F. and Campbell, D. E.: University of Wisconsin, CM-724, Nov. 24, 1952, cf. p. 35.

23. von Kármán, T., Millán, G., Penner, S.S.: Sixth Symposium (International) on Combustion, Reinhold Publishing Corp., New York (1957), pp. 1-11, cf. pp. 6,7.

24. Palmer, H. B. and Hornig, D. F.: J. Chem. Phys. 28, 98-105 (1957).

25. Hirschfelder, J. O.: Phys. Fluids, 3, 309 (1960).

26. Campbell, E. S., Heinen, F. J., and Schalit, L.M.: Ninth Symposium on Combustion, Academic Press, New York (1963), pp. 72-80, (a) cf. pp. 75-77.

27. Bartholomé, E.: Z. Elektrochem. 54, 169-73 (1950).

28. Fristrom, R. M., Grunfelder, C., and Favin, S.: J. Phys. Chem., 65, 580-90 (1961), (a) cf. p. 590.

29. Westenberg, A. A. and Fristrom, R. M.: J. Phys. Chem. 64, 591-601 (1961), cf. p. 597.

30. Private communication.

31. Benson, S. W. and Axworthy, A. E.: J. Chem. Phys. 26, 1718-26 (1957).

32. Lewis, B. and von Elbe, G.: J. Chem. Phys. 2, 283-90 (1934).

33. Sandri, R.: Canadian J. Chem. 34, 313-23 (1956).

34. Fristrom, R.M., Grunfelder, G., and Favin, S.: J. Phys. Chem. 65, 580-90 (1961).

35. Private communication from R.M. Fristrom and J. F. Wehner.

36. Westerberg, A. A. and Fristrom, R.M.: J. Phys. Chem. 64, 1393-98 (1960).

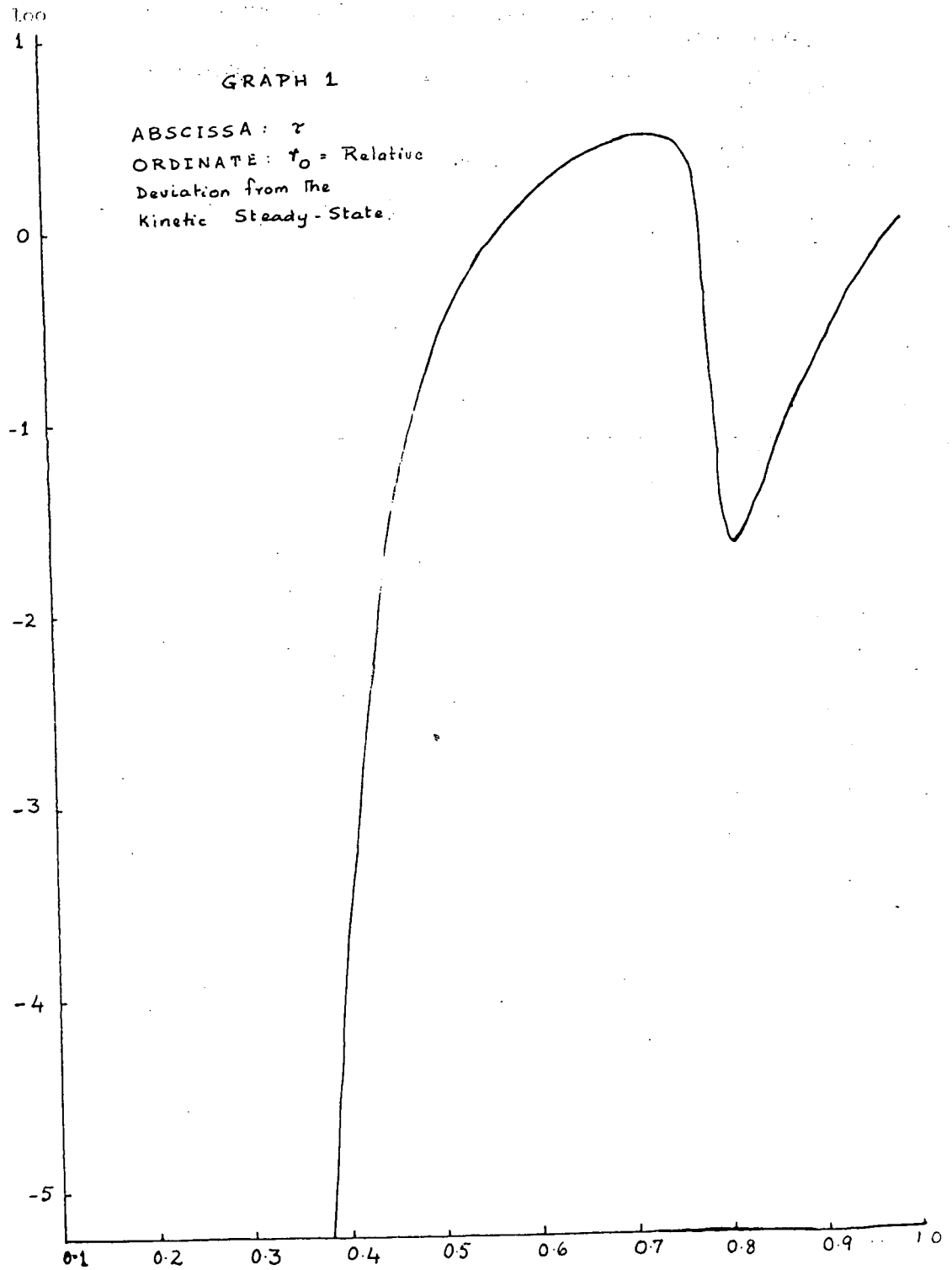
GRAPH 1
ABSCISSA : τ
ORDINATE : f_0 = Relative Deviation from the Kinetic Steady-State.
1
0
-1
-2
-3
-4
-5
0·1
0·2
0·3
0·4
0·5
0·6
0·7
0·8
0·9
1·0

GRAPH 2

ABSCISSA : τ

ORDINATE : $X_0 \times 10^4$

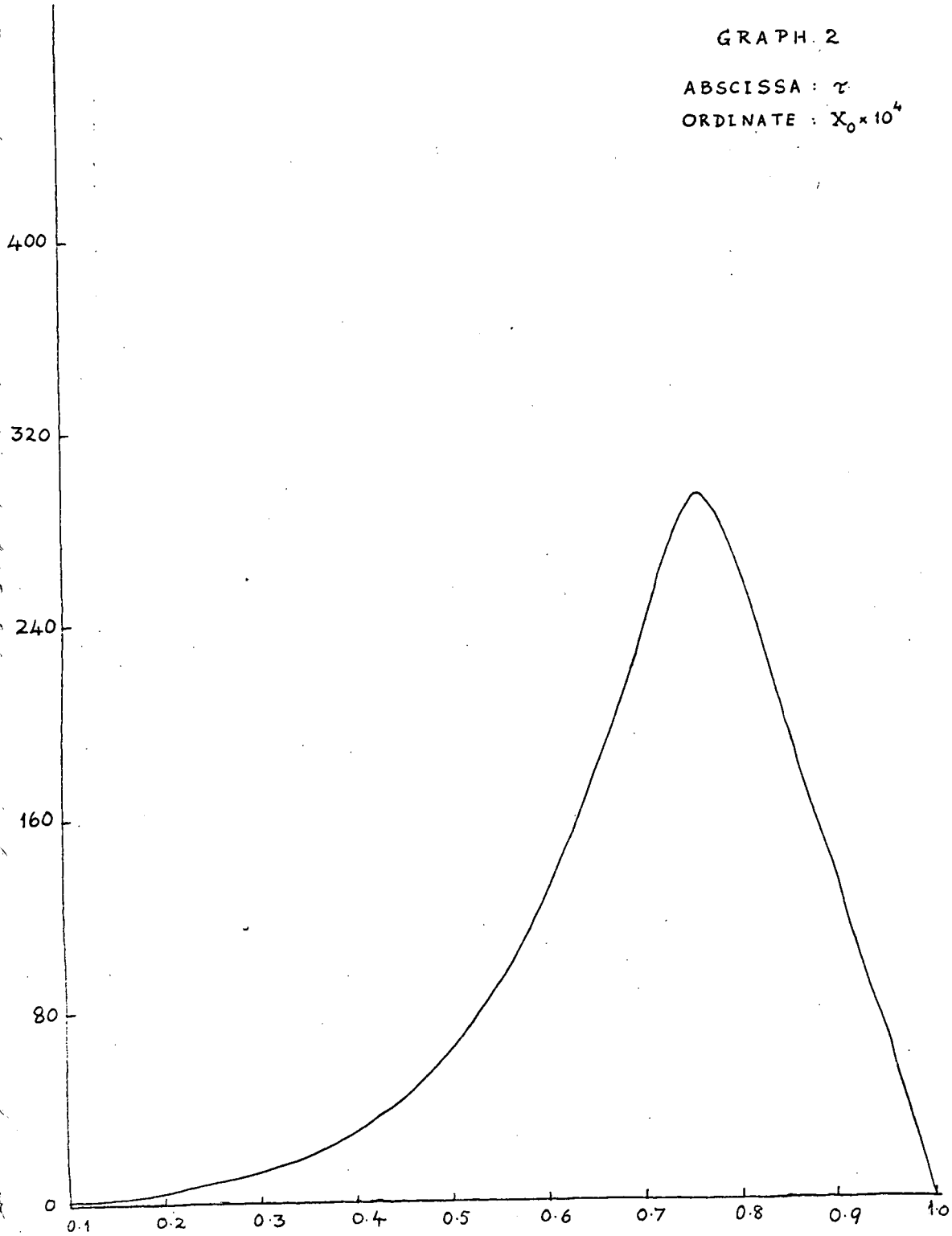

GRAPH 3

ABSCISSA: Reduced Distance,
$\zeta = [M C_{O_3} / \lambda(T_{max})] z$:
for an arbitrary origin.

ORDINATE: $X_O \times 10^4$

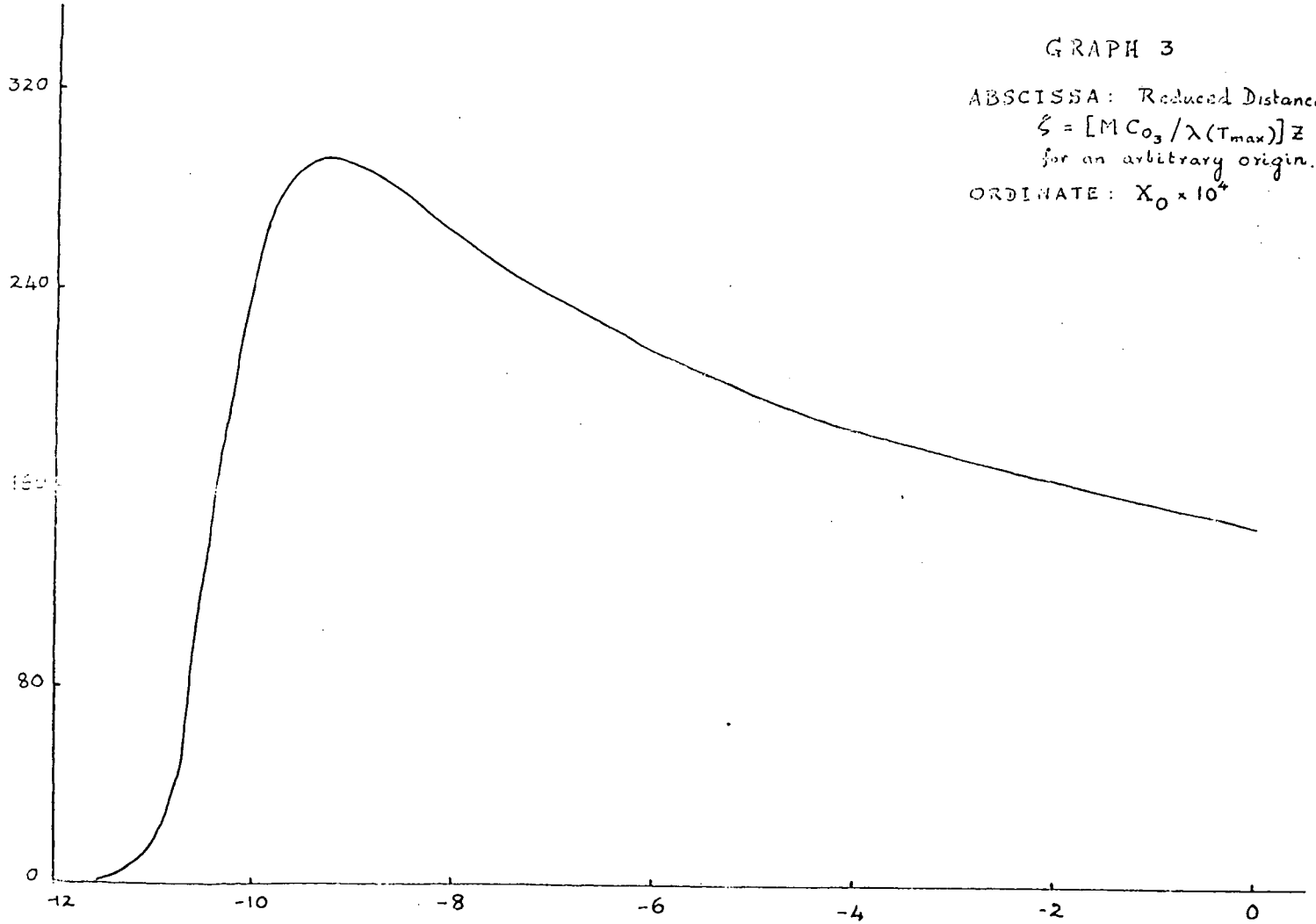

GRAPH 4

ABSCISSA : τ

ORDINATE : $dt/d\tau$,

$t = (T - T_{max})/T_{max}$

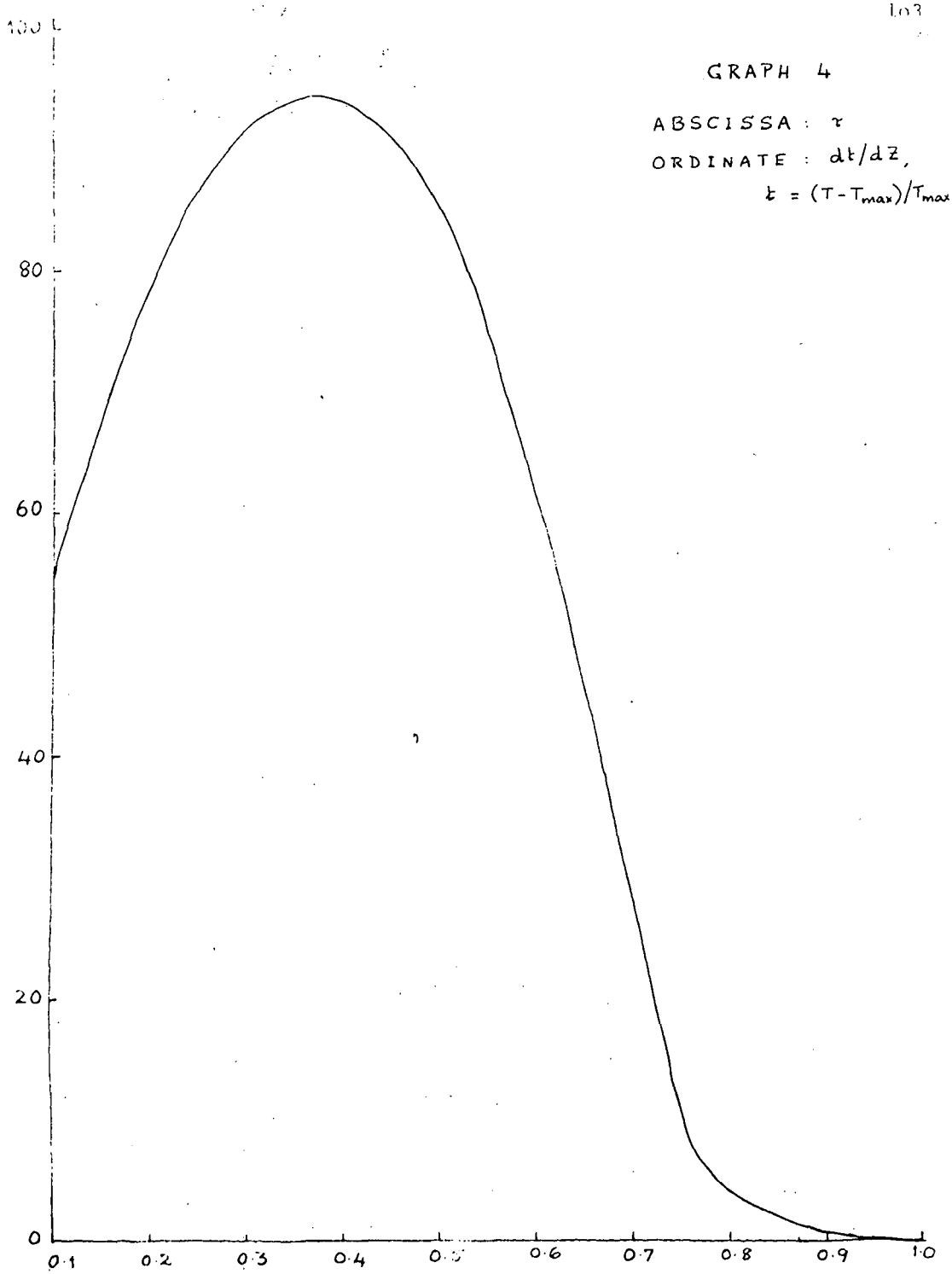

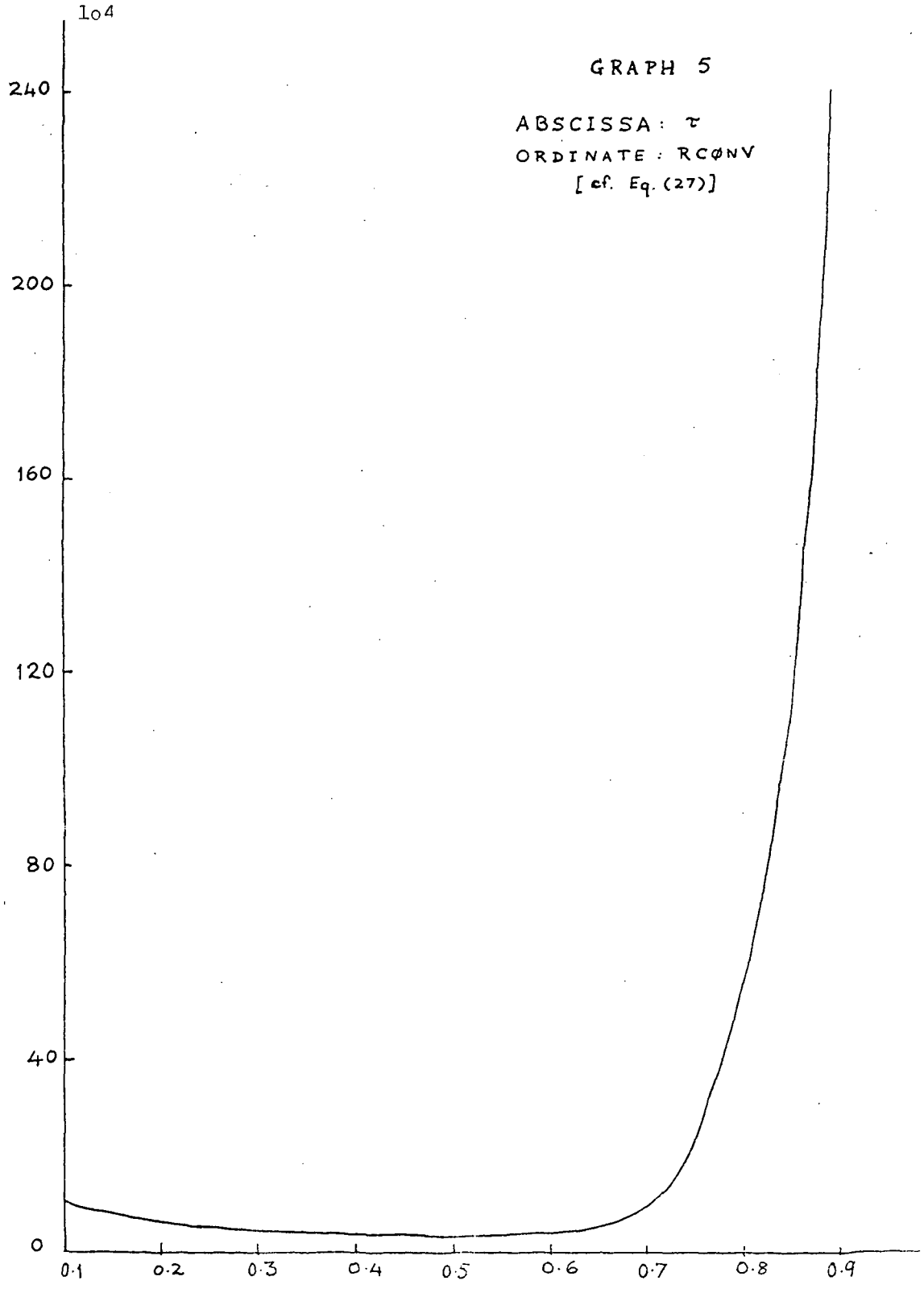
1o4
GRAPH 5
ABSCISSA : τ
ORDINATE : RCØNV
[cf. Eq. (27)]
240
200
160
120
80
40
0
0·1
0·2
0·3
0·4
0·5
0·6
0·7
0·8
0·9

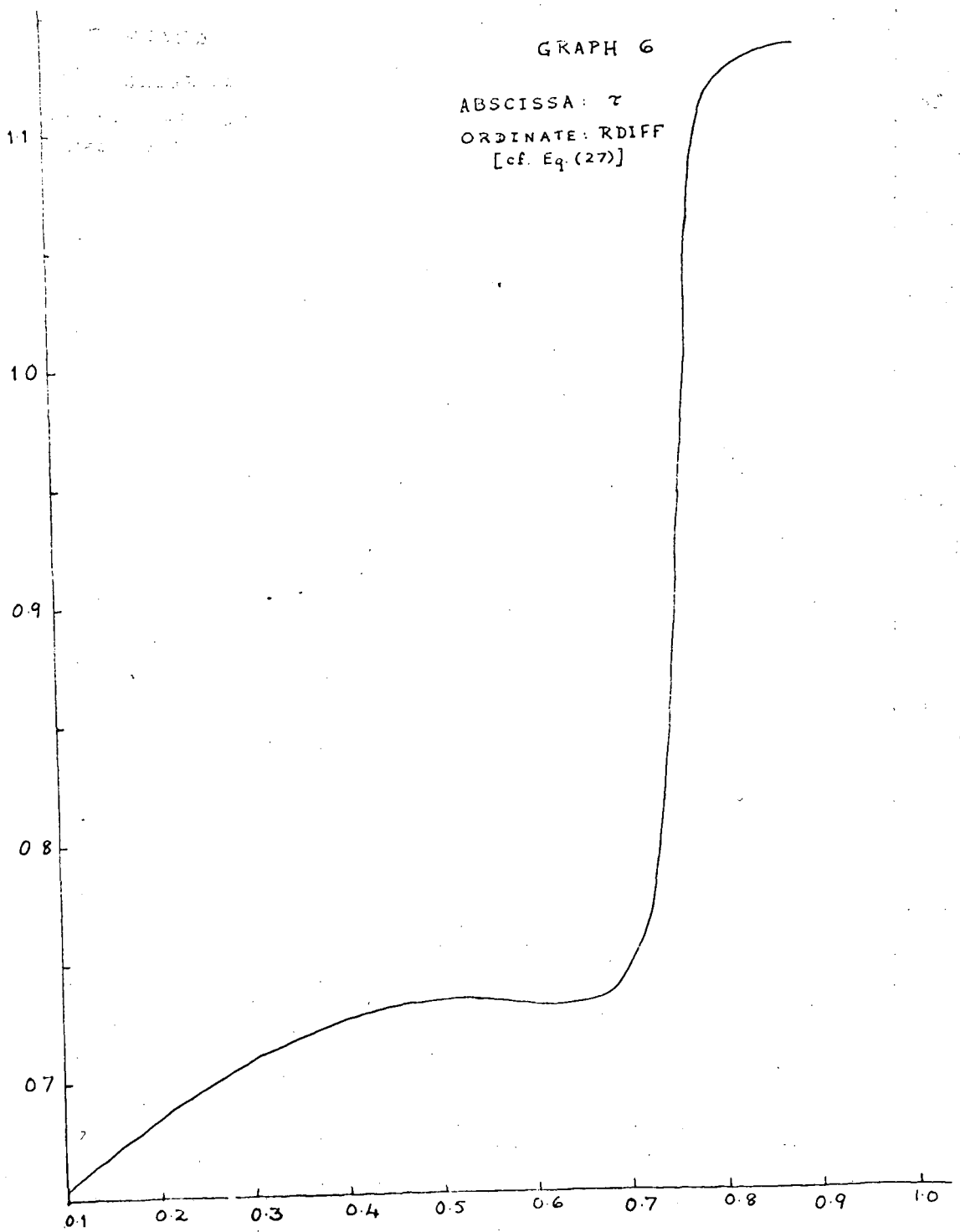
GRAPH 6
ABSCISSA: τ
ORDINATE: RDIFF
[cf. Eq. (27)]
1.1
1.0
0.9
0.8
0.7
0.1
0.2
0.3
0.4
0.5
0.6
0.7
0.8
0.9
1.0

GRAPH 7

ABSCISSA: τ

ORDINATE: RH

[cf. Eq. (29)]

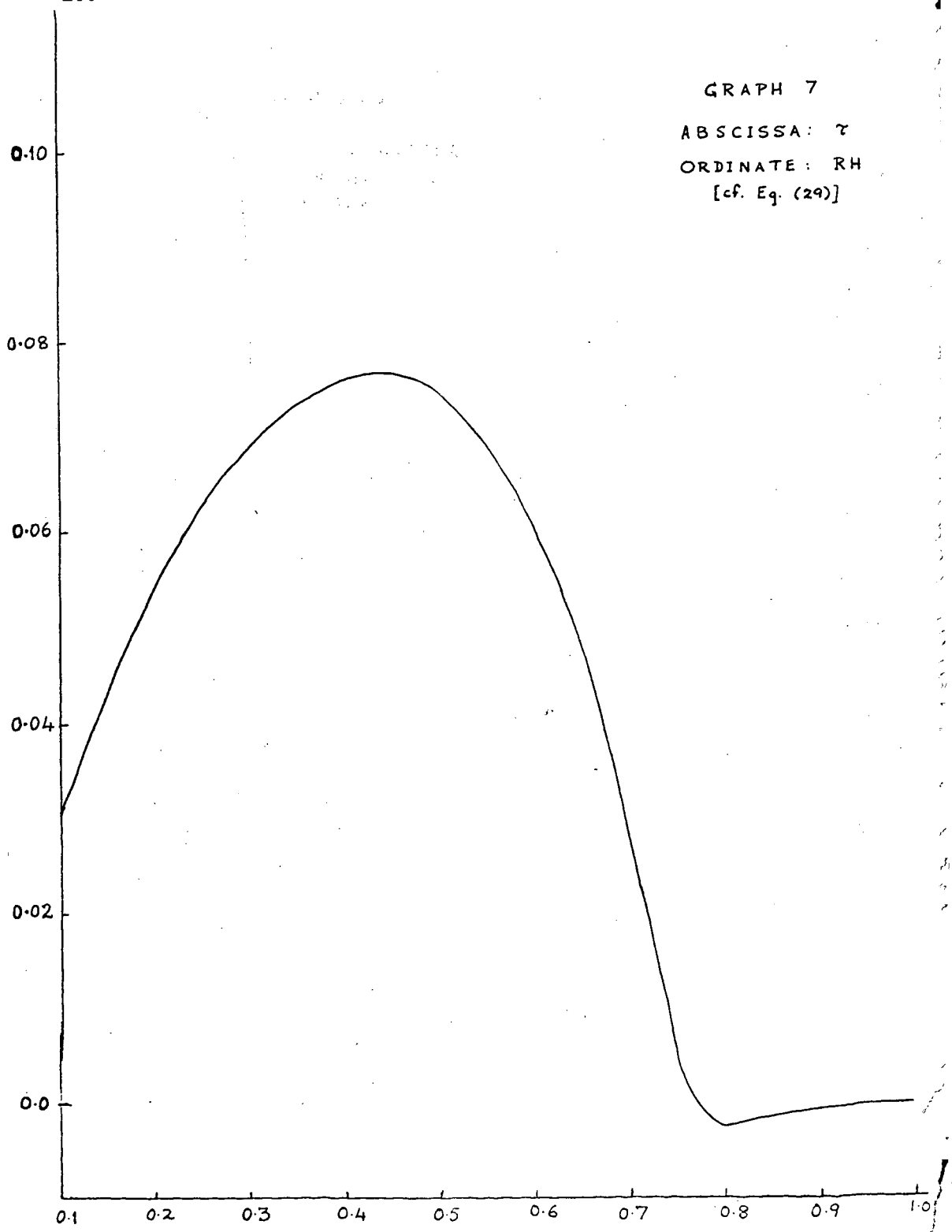

GRAPH 8

ABSCISSA : τ

ORDINATE : HREL

[cf. Eq. (30)]

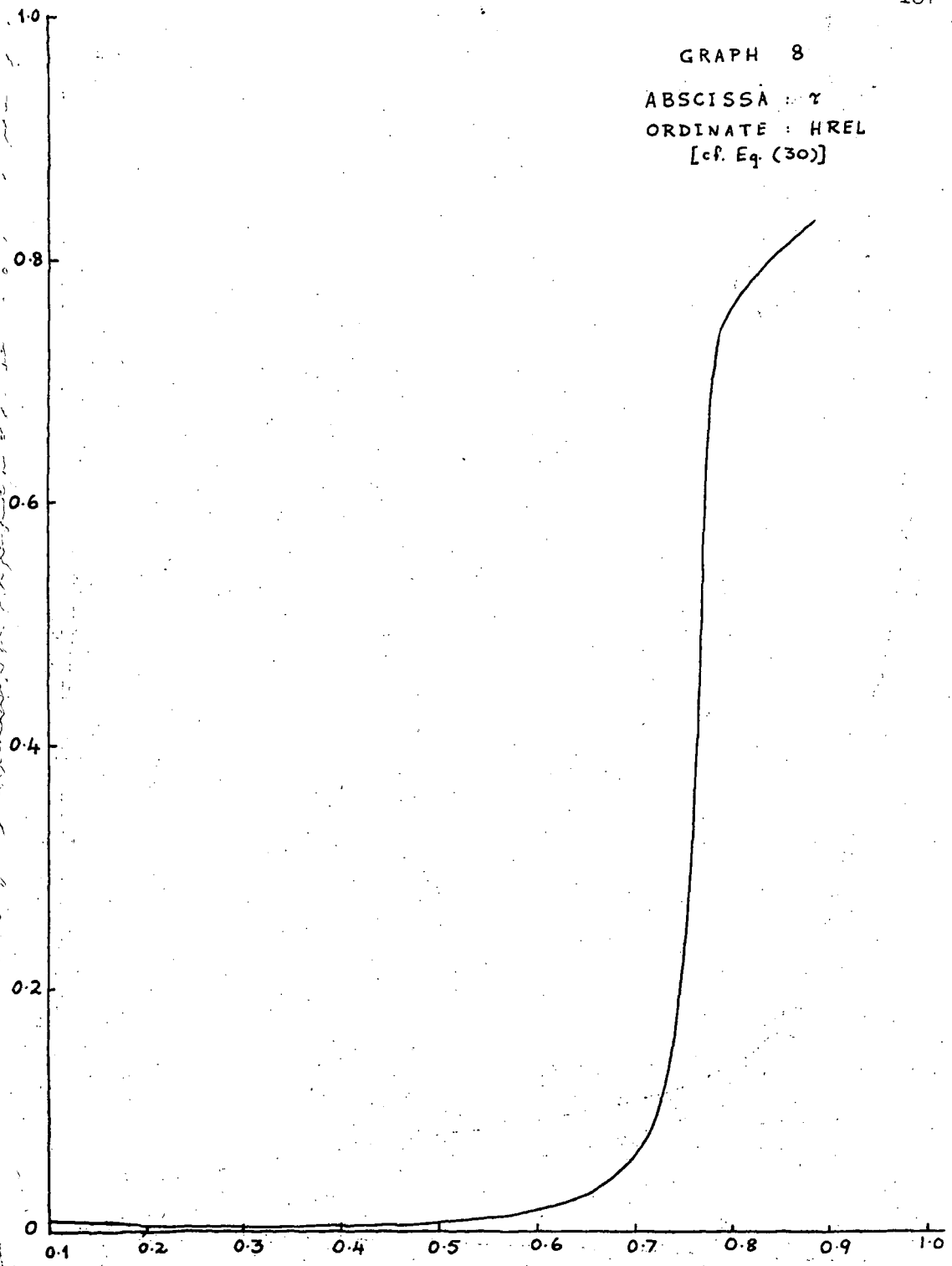

GRAPH 9

ABSCISSA: Reduced Distance,
$\zeta = [M C_{O_3} / \lambda (\tau_{max})] z$

ORDINATE : τ

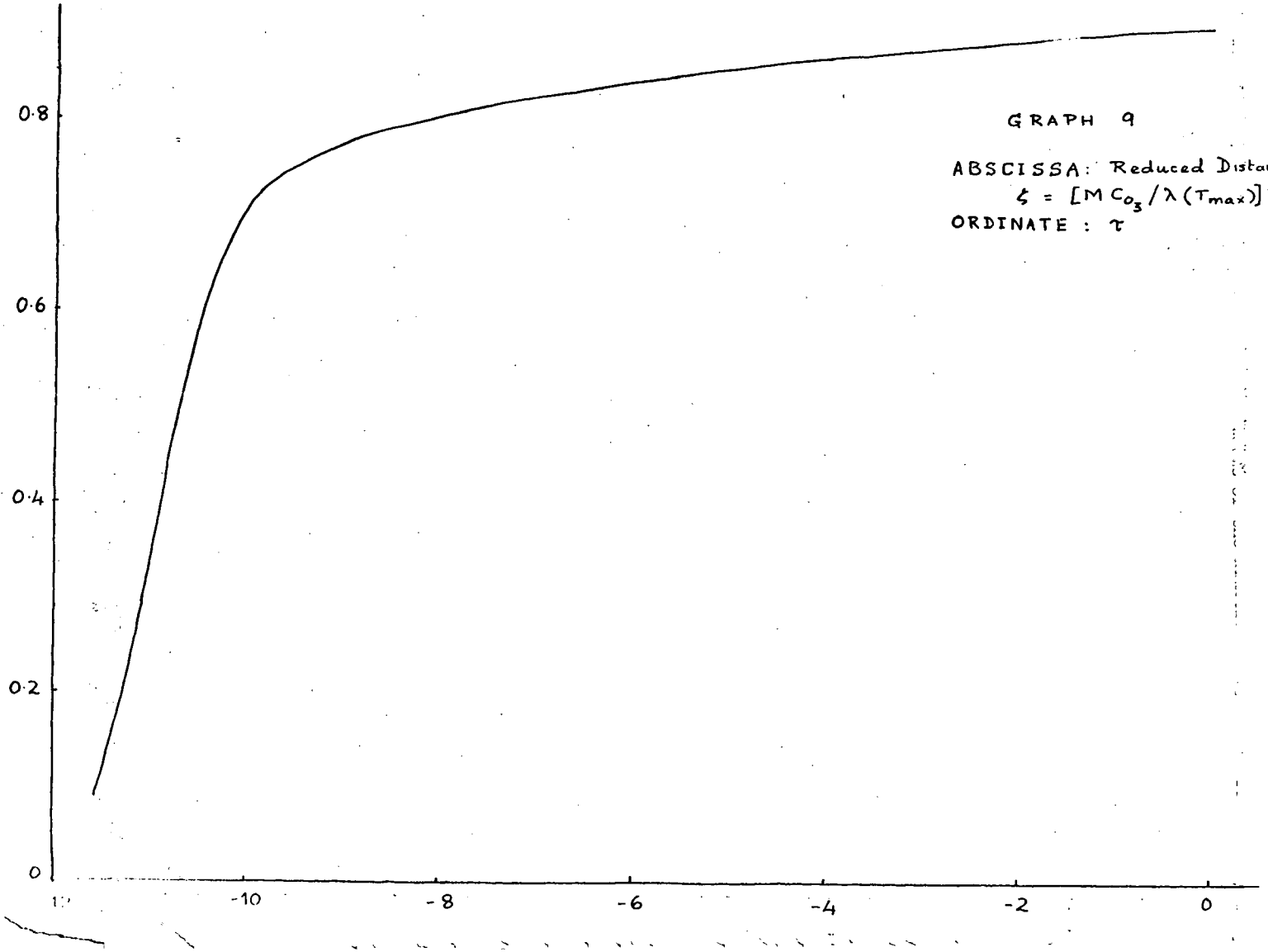

GRAPH 10

ABSCISSA: τ

ORDINATE:

$G_{O_3} \times 10^3$ ——————

$X_{O_3} \times 10^3$ —·—·—·—

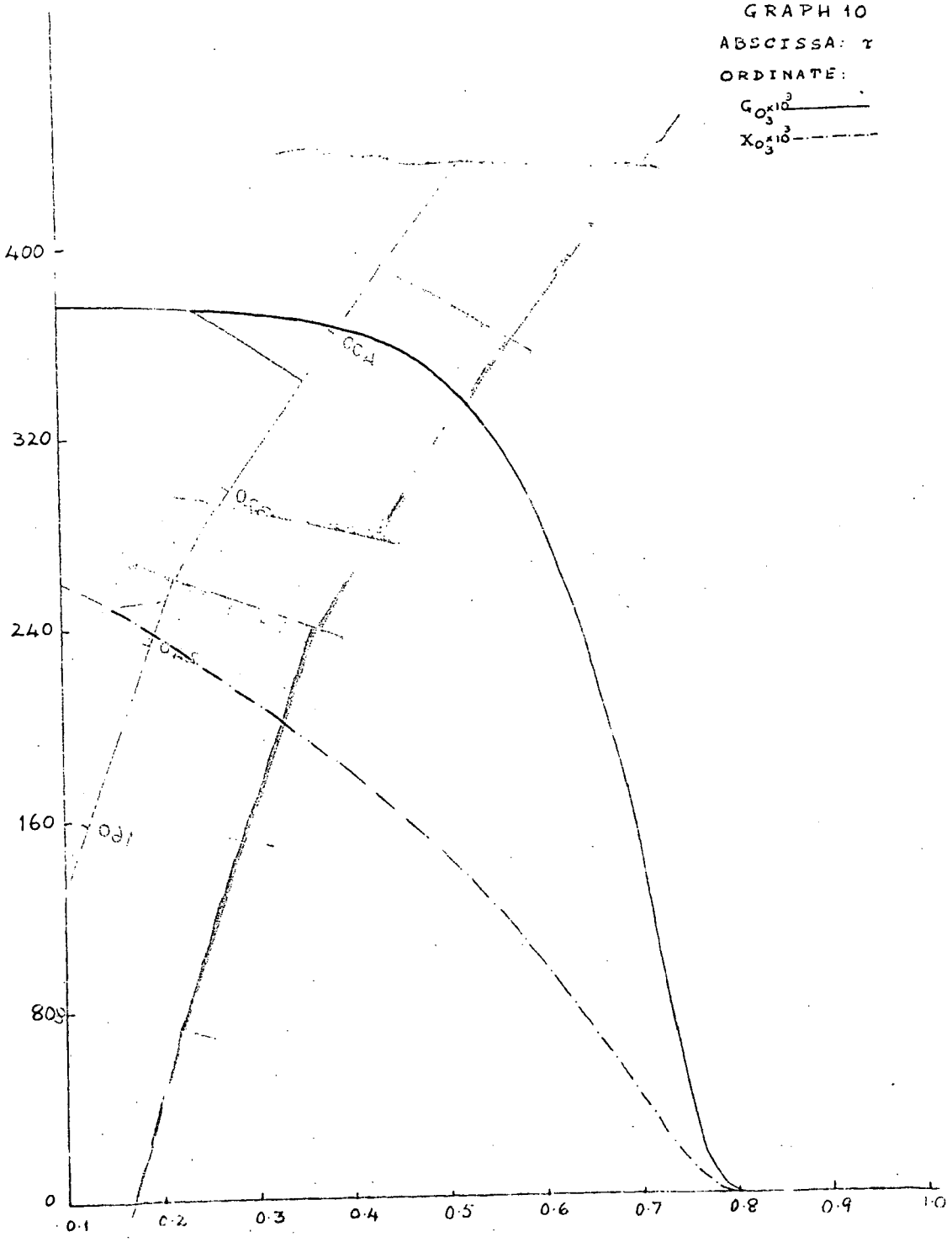

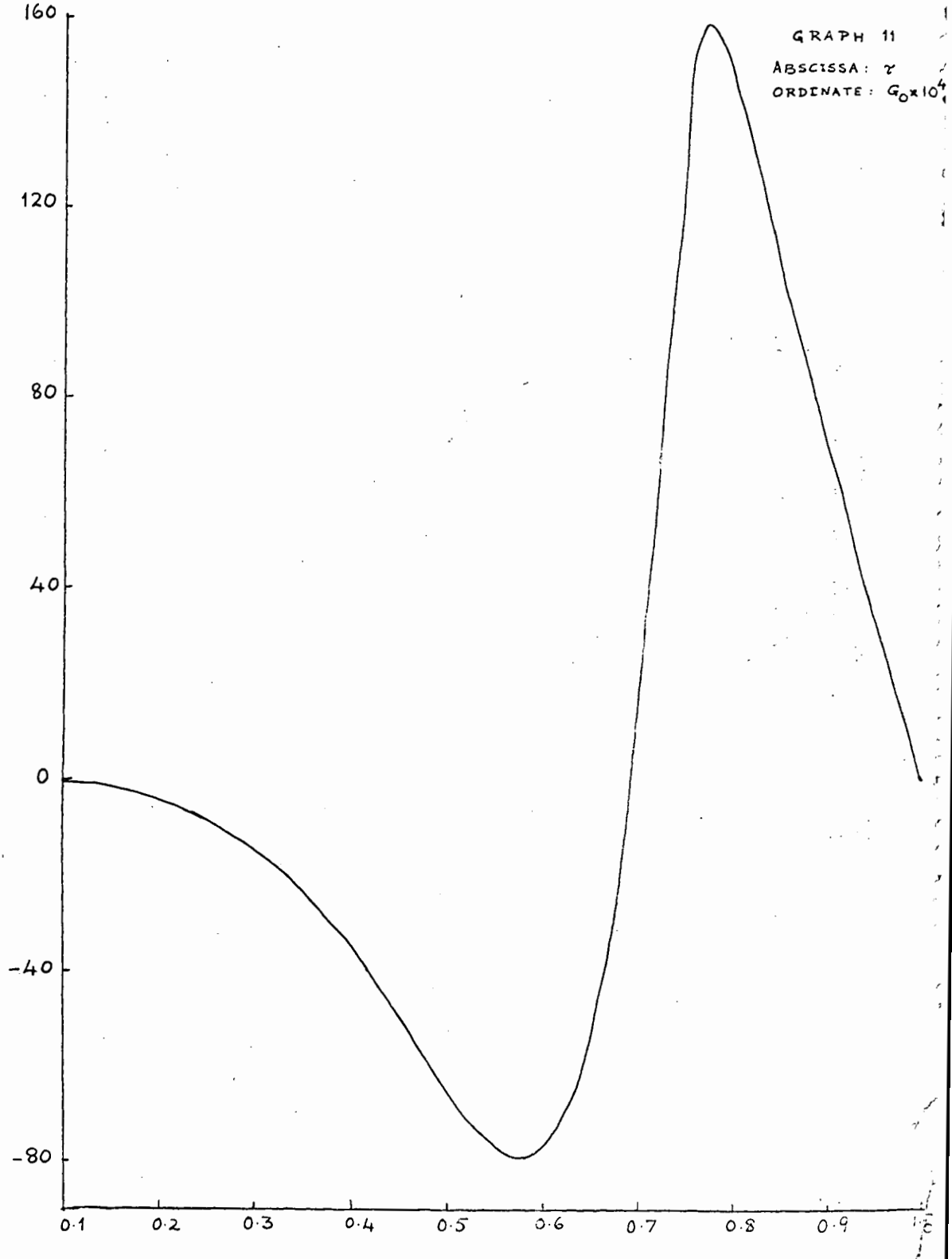
GRAPH 11
ABSCISSA : γ
ORDINATE : $G_0 \times 10^4$
160
120
80
40
0
-40
-80
0·1
0·2
0·3
0·4
0·5
0·6
0·7
0·8
0·9
1·0

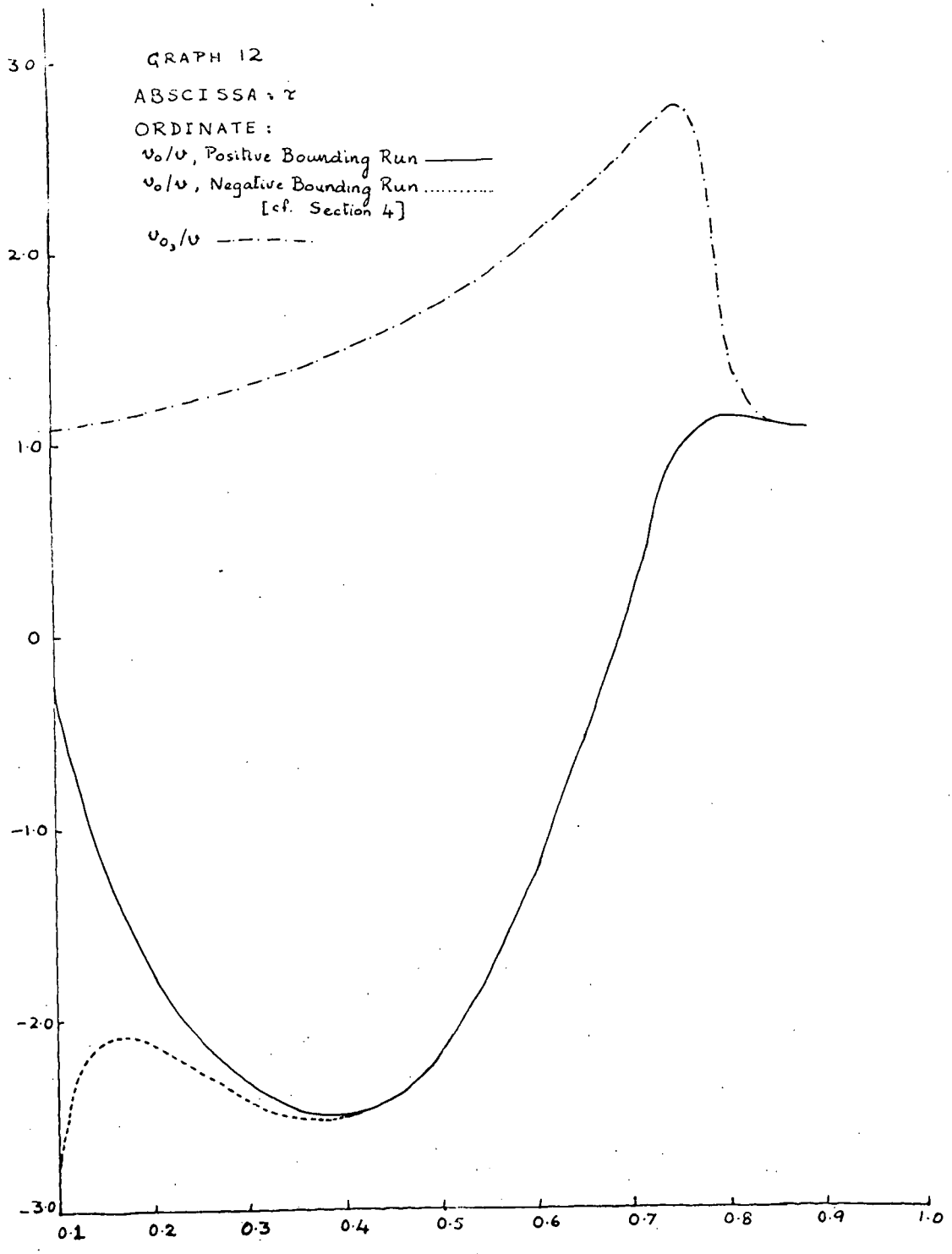
GRAPH 12
ABSCISSA : τ
ORDINATE :
v_o/v, Positive Bounding Run
v_o/v, Negative Bounding Run
[cf. Section 4]
v_{o_3}/v
3·0
2·0
1·0
0
-1·0
-2·0
-3·0
0·1
0·2
0·3
0·4
0·5
0·6
0·7
0·8
0·9
1·0

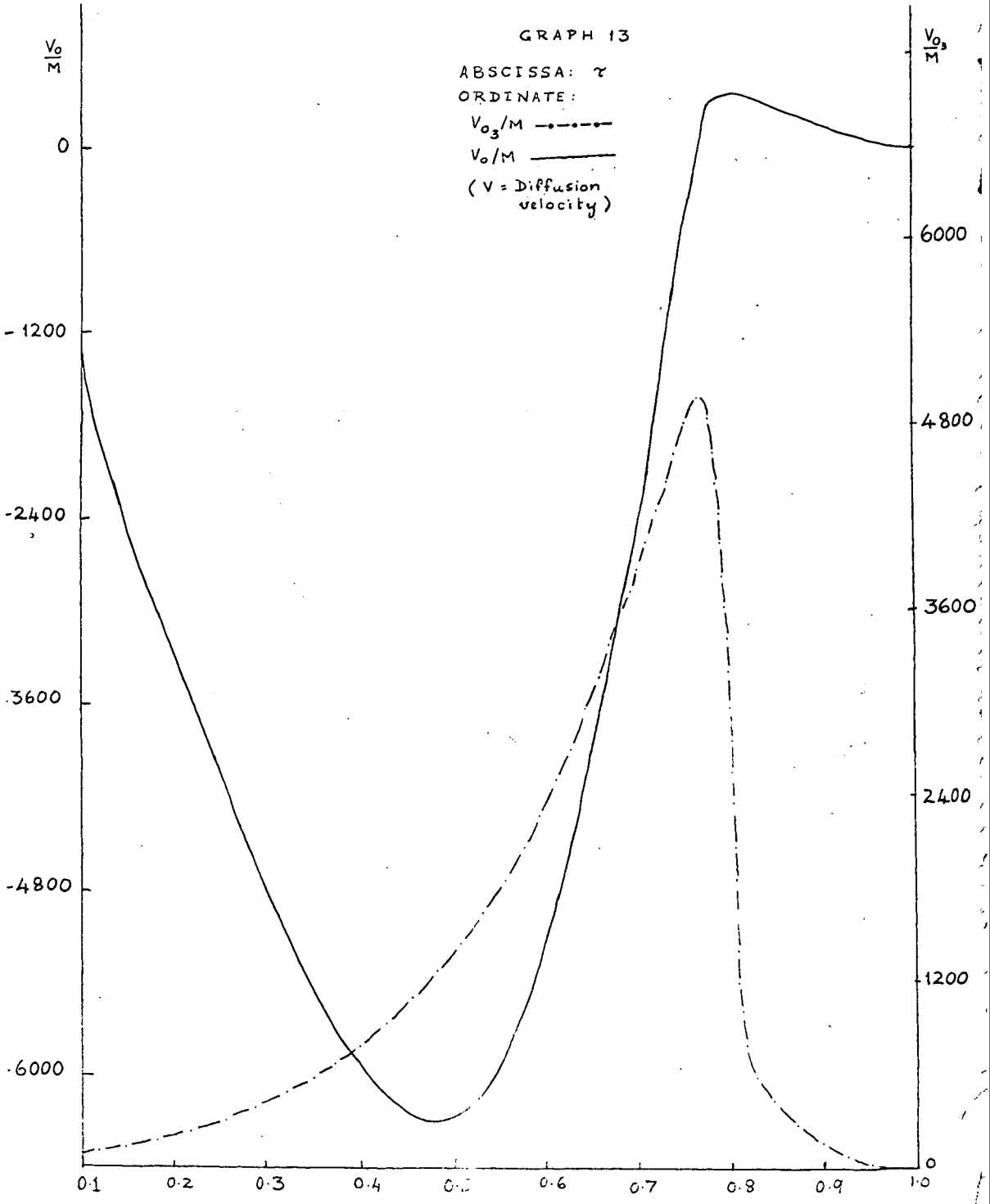
GRAPH 13
ABSCISSA: τ
ORDINATE:
V_{O_3}/M
V_O/M
(V = Diffusion velocity)
$\frac{V_O}{M}$
$\frac{V_{O_3}}{M}$
0
-1200
-2400
-3600
-4800
-6000
6000
4800
3600
2400
1200
0
0·1
0·2
0·3
0·4
0·5
0·6
0·7
0·8
0·9
1·0

Kinetic Studies of Hydroxyl Radicals in Shock Waves. IV Recombination Rates in Rich Hydrogen-Oxygen Mixtures

Garry L. Schott and Paul F. Bird

University of California, Los Alamos Scientific Laboratory
Los Alamos, New Mexico

Previous work[1,2,3] in rich hydrogen-oxygen-diluent flames has shown that in the final stage of the combustion reaction, several reversible reaction steps are maintained substantially in equilibrium, while net progress is achieved by the removal of excess species through three-body recombination reactions. The reversible reactions couple the recombination paths, so that each recombination reaction has the same degree of nonequilibrium (ratio of equilibrium constant to the quotient of the activities of products and reactants), and a single measurement serves to determine the chemical composition. Kinetics studies in such flames[3,4] have shown that the important recombination reactions are:

$$H + H + M \xrightarrow{k_1} H_2 + M \qquad (1)$$

$$H + OH + M \xrightarrow{k_2} H_2O + M \qquad (2)$$

and have provided values of the rate coefficients k_1 and k_2 under flame conditions.

Observations on this reaction system in shocked gas mixtures have been reported in earlier papers of the present series,[5,6,7] and have indicated establishment of equilibrium conditions in the reversible reaction steps promptly at the end of the induction period. This paper reports measurements of the kinetics of the slow disappearance of OH following its maximum concentration in shocked H_2-O_2-Ar mixtures.

EXPERIMENTAL METHODS

Basic shock wave techniques and the ultraviolet line absorption method of determining OH concentration have been discussed in Part I[5]. However, many modifications of apparatus and procedures have been incorporated in the present work, and it is appropriate to present the methods used in this investigation.

The dimensions of the circular shock tube were: internal diameter, 10 cm throughout; driver chamber length, 192 cm; test chamber length, 373 cm. Its construction was of brass, and the interior surface of the test chamber was plated with nickel to decrease its porosity. Single and multiple layer brass shim stock diaphragms were used. Evacuation of the test chamber was accomplished through a side port located 13 cm from the diaphragm position. Final evacuation was done with an NRC B-2 oil diffusion-ejection booster pump backed by a Kinney KC 5 mechanical pump. Vacuum measurements in the test chamber were made with a CVC Philips gauge connected to a side port midway along its length.

Shock velocity measurement was made by a series of five deposited platinum resistor gauges. These gauges were 1 mm by 6 mm and had resistances between 30 and 200 Ω. They were flush mounted with the shorter dimension disposed axially

at intervals of 60.00, 50.00, 30.00, and 29.94 cm, beginning 198 cm from the diaphragm. The gauge outputs were amplified, shaped by 2D21 thyratrons, echoed after 6.25 μsec, mixed with 10 μsec timing marks, and presented on an oscilloscope raster[8] operating at 100 μsec/line. A modified Tektronix 545 instrument was used.

The quartz windows for the light beam used in measuring OH concentrations were located 1.3 cm downstream from the fourth velocity gauge, some 34 cm from the end of the shock tube. This setup allowed several hundred microseconds for observation of the moving gas behind the incident shock wave before the arrival of the reflected wave from the end plate or the hydrogen driver gas from upstream.

The optical train from the flash discharge lamp to the photomultiplier detector was mounted independently of the shock tube. The flash lamp was operated in the way described in Part I[5]. The lamp itself differed, however, in that the H_2O vapor pressure was regulated at 0.9 mm Hg by $NaC_2H_3O_2 \cdot 3H_2O + NaC_2H_3O_2$ at 0°C. At this working pressure the luminosity was much freer of spurious fluctuations in intensity than at higher pressures, and its intensity was only slightly diminished. A 2.5 cm focal length spherical lens immediately in front of the lamp focused the luminous region inside the toroidal anode crudely at the monochromator entrance slit 70 cm away, providing condensation of the beam in the (vertical) direction along the 2 mm by 10 mm collimating slits on either side of the shock tube windows. The luminous region itself was substantially as wide as the slits. At the monochromator entrance slit a crude f = 1.0 cm cylindrical lens was used with its axis parallel to the slit to condense the beam onto the entrance slit and provide for filling the width of the grating. The 1P28 photomultiplier detector was placed immediately outside the exit slit of the monochromator.

The anode resistor used was 22 K Ω, and 4 ft of RG-71 cable delivered the signal to the input terminal of a type L preamplifier in a Tektronix type 545 oscilloscope. Thus the electronic response time was about 2 μsec, which approximately matches the time inhomogeneity in the gas sample within the 2 mm width of the beam. Faster response can be achieved, but for recombination rate measurements over periods like 10^{-4} seconds it is unnecessary, and reduction in statistical noise is achieved by relaxing the time resolution.

The oscilloscope photographs contained, in addition to the light transmission record, a base line of zero photoelectric signal, and in displaced positions, a trace bearing timing marks and a trace of the unabsorbed photoelectric signal from a separate flashing of the lamp. This monitor trace was synchronized with the lamp firing in the same way as in the experimental trace. It was needed because the lamp signal, while reproducible in shape, was not quite constant over the time of the experiment.

The JACO model 8200 monochromator was operated in an air thermostat at 36 ± 1°C. The first order spectrum was used with the entrance slit width 0.050 mm and the exit slit width 0.570 mm. The instrument was calibrated with a low pressure mercury discharge spectrum and set to transmit (ideally uniformly) between $3088.7 \leq \lambda_{air} \leq 3097.3$Å, with transmission decreasing linearly to zero at 3087.9Å $\geq \lambda_{air}$ and 3098.1Å $\leq \lambda_{air}$. Precision of the calibration and thermal stability are estimated at ±0.3Å. Photographic spectra made with film held against the exit slit confirmed the isolation of the lines[9] between $R_2 20$ (λ_{air} = 3089.0Å) and $Q_2 8$ (λ_{air} = 3096.8Å).

Experimental gas mixtures were prepared manometrically from commercial cylinder gases in a thoroughly evacuated glass-lined (domestic hot water) tank and heated from beneath to be mixed by diffusion and convection for at least 24 hours before use. Mass spectrographic analysis of each batch confirmed the absence of unintended components beyond traces of N_2 and CO_2.

DATA REDUCTION

The raw data obtained in each experiment consist primarily of the recorded initial conditions, the shock velocity data contained in the photograph from the raster oscilloscope, and the OH concentration data contained in the oscilloscope photograph of the photoelectric signal. Prior to any chemical kinetics analysis these data are reduced to the apparent OH concentration as a function of time under particular conditions of temperature, pressure, and concentrations of other species. These preliminary data reduction procedures are discussed first.

Shock Velocity

Evaluation of the shock wave velocity from the gauge positions and shock arrival times was done by adjusting each time for small differences in circuitry response (corrections of a few tenths of a microsecond), fitting the five x,t data points to the quadratic expression $t = \underline{a} + \underline{b}x + \underline{c}x^2$, and evaluating $(dt/dx)^{-1}$ at the observation window position. Except in shots at 15 and 20 cm Hg initial pressure, $\underline{c}$ was invariably positive, and the average attenuation of the shock velocity was about 1% per meter (0.1% per tube diameter). The heavier diaphragms used for the higher pressure shots apparently opened more slowly and sometimes caused the shock velocity to reach its maximum further downstream[10]. From least squares treatment, the indicated uncertainty in $\underline{b}$, which is most of the uncertainty in dt/dx, was usually a few tenths of a percent. In a few cases it was as great as 1%, indicating irregular behavior of the shocks and/or the detection system.

Hugoniot Calculations

Solution of the Rankine-Hugoniot equations was carried out by means of a computer code[11] to obtain the temperature, density, and composition behind each shock wave as functions of the initial conditions, the shock velocity, and the progress of chemical reaction. The computations for equilibrium conditions were obtained straightforwardly by the general method of Brinkley[12] which is incorporated in the shock equations code. The restricted equilibrium computations for selected extents of recombination less than the final equilibrium extent were made by arbitrarily constraining[13] the number of moles per original mole of material in the system. The species Ar, H_2, O_2, H_2O, OH, H, and O were considered in the computations. Ideal gas thermodynamic functions for H_2, O_2, H_2O, OH, and O were obtained from the JANAF tables[14] and formulated for interpolation in the polynomial form used previously in this[11] and other[15] laboratories. Ar and H were treated as calorically perfect and the coefficients were evaluated accordingly.

Determination of [OH]

The calibration curve relating absorbance and OH concentration used in the earlier work was an empirical one based on observations of equilibrium gases in shock waves. For the present work, a much more refined method has been developed. It is a semi-empirical method based in part on absorbance measurements in equilibrium shocked gas, but it makes use of the fundamental molecular properties of OH to extend the calibration to regimes of OH concentration, temperature, and pressure where equilibrium observations could not be made.

The calibration program consists of three parts: (1) experimental determination of the spectral intensity distribution of our OH line source, (2) formulation of the absorption spectrum of OH on the basis of theory and integrated absorption coefficients derived from independent experiments, and (3) numerical synthesis of the response of thermal absorber to the lamp spectrum in order to account, within existing uncertainty in the absorption spectrum parameters, for the experimentally determined absorbance of equilibrium mixtures. The details of these steps are being reported separately; the methods used and their application to the old, higher

pressure lamp spectrum are described elsewhere[16]. The principal features of the calibration are summarized as follows. The line shapes and relative intensities in the lamp spectrum were determined from high dispersion photographic spectrograms made by repeated flashes. The source spectrum and the absorber spectrum were each described in the computations by superposition of lines having combined Doppler and Lorentz broadening[17]. The line strengths given by Dieke and Crosswhite[9] as modified by Learner[18] were used. The values of the transition probability coefficient, F, and the pressure broadening parameter, a, (as defined in the literature[19]) found to describe suitably the measured equilibrium absorbances were $F = 3.50 \times 10^{-4}$ and $a = 335\ P(atm)/T(^{\circ}K)$. These values are in reasonable agreement with those reported elsewhere[19,20]. Perhaps the present calibration is not significantly more accurate than the old empirical one in the regime where the latter was determined, but the extension to other regimes is superior, and the whole calibration is on a much firmer basis.

The computer program generates the absorbance ($-\log_{10}$ of the fractional transmission) of the incident spectrum for a specified absorber temperature, pressure, and optical density (product of OH concentration and path length). Points covering the ranges of these parameters involved in the experiments were assembled and a numerical interpolation scheme was used to derive the OH concentration for a series of absorbance values during each experiment. For this purpose an average temperature and pressure for each experiment was obtained as the mean of the values computed for partial equilibrium conditions with zero recombination and complete equilibrium conditions. The absorbance for each optical density in the table was first interpolated to the appropriate temperature and then the appropriate pressure. Finally the several measured absorbances were interpolated to optical densities and hence OH concentrations. A quadratic interpolation formula was used in each step, with two of the three values of the independent variable bracketing the desired value.

Rate Equation

The rate equation for the disappearance of OH in a reacting mixture of H_2, O_2, H_2O, OH, H, and O is developed for conditions of variable density shock wave flow in a manner which incorporates the recombination mechanism, reactions (1) and (2), and anticipates the insertion of partial equilibrium relationships among the several species. Let us define the mole number of each species, n_i, by the relationship

$$\rho n_i = [I] \tag{3}$$

where ρ is the density in grams per liter and [I] is the concentration of species I in moles per liter. We then identify the partial derivative with respect to time $(\partial[I]/\partial t)_\rho = \rho dn_i/dt$ as the net volumetric rate of chemical production of species I[21].

Now it has been shown that[1,2,22] in the system being considered, equating the total volumetric rate of production of all species to the combined chemical recombination rate from all paths, R_{recomb}, leads to

$$\rho d(n_H + n_{OH} + 2n_O + 2n_{O_2})/dt = -2\ R_{recomb}. \tag{4}$$

To formulate n_H, n_O, and n_{O_2}, and their derivatives in terms of the measured [OH], we proceed as follows. Let

$$[OH] = \alpha\ [H]. \tag{5}$$

Then

$$n_{OH} = \alpha\ n_H \tag{6}$$

and

$$\rho dn_H/dt = (\rho/\alpha)dn_{OH}/dt - (\rho n_{OH}/\alpha^2)d\alpha/dt. \tag{7}$$

Similarly let

$$[O] + [O_2] = \beta\,[OH]^2, \tag{8}$$

so that

$$n_O + n_{O_2} = \beta\rho n_{OH}^2 \tag{9}$$

and

$$\rho d(n_O + n_{O_2})/dt = 2\beta\rho^2 n_{OH} dn_{OH}/dt + \rho^2 n_{OH}^2 d\beta/dt + \beta\rho\, n_{OH}^2 d\rho/dt. \tag{10}$$

The scale of time, t, experienced by an element of shocked gas is converted to the scale τ at an observation point stationary with respect to the unshocked gas by

$$dt = (\rho/\rho_o)\, d\tau \tag{11}$$

where ρ_o is the density of the unshocked gas.

The variables ρ, α, and β are considered as functions of the independent variable [OH]. Then from the definition, equation (3), it follows that

$$\rho dn_{OH}/dt = d[OH]/dt\,(1 - d\ln\rho/d\ln[OH]) \tag{12}$$

Finally, for conditions in which the recombination mechanism consists of reactions (1) and (2) and all dissociation rates are negligible, we express the total recombination rate, R_{recomb}, in terms of concentrations and conventional rate coefficients by

$$R_{recomb} = k_1\,[M_1][H]^2 + k_2\,[M_2][H][OH] \tag{13}$$

where $[M_1]$ and $[M_2]$ are the total gas concentrations acting as third bodies in recombination reactions (1) and (2).

Then substitution of equations (5) - (13) into equation (4) and rearrangement of terms leads to

$$\alpha d(1/[OH])/d\tau = 2(\rho/\rho_o)\, k_1\,[M_1]\left(1 + \frac{\alpha k_2[M_2]}{k_1[M_1]}\right)$$

$$\{\,(1 + \alpha + 4\alpha\beta[OH])(1 - d\ln\rho/d\ln[OH]) - d\ln\alpha/d\ln[OH]$$

$$+ 2\alpha\beta[OH](d\ln\beta/d\ln[OH] + d\ln\rho/d\ln[OH])\,\}^{-1}. \tag{14}$$

For convenience we now refer to the factor 2 and the complicated expression in braces on the right hand side of equation (14) as A, and for lack of information to the contrary, identify the third body concentrations $[M_1]$ and $[M_2]$ with the total gas concentration, [M]. Thus the rate coefficients are referred to the experimental gas mixture, and we re-write the rate equation as

$$\alpha d(1/[OH])/d\tau = A\,(\rho/\rho_o)\,[M](k_1 + \alpha k_2) \tag{15}$$

Equation (15) has been cast in this form in anticipation of finding the disappearance of OH to be effectively second order in OH and of determining the slope of an approximately linear plot of 1/[OH] versus τ from each experiment.

RESULTS

Experiments have been done with three different gas mixtures, whose compositions are given below:

Mixture Designation	$\%H_2$	$\%O_2$	%Ar
R-1	4.03	1.00	94.97
R-2	2.02	0.50	97.48
R-3	8.07	1.00	90.93

The results of thirty-one experiments in the temperature range $1400° \leq T \leq 2000°K$ are assembled in Table I. In these experiments, the plots from which $d(1/[OH])/d\tau$ was determined were approximately straight over the entire interval plotted, which in most cases was from about 50 μsec to about 500 μsec after passage of the shock front. During this period [OH] fell from the values given in column 3 to those given in column 4. Column 5 contains the slopes derived from the plots. Columns 6 and 7 contain the values of [OH] and temperature computed from the initial data and shock velocity for each experiment on the basis of equilibrium with respect to all reactions except dissociation-recombination reactions and no change in the total mole number $n = \Sigma n_i$, from the value n_o in the unshocked gas mixture. Implicit in these computations are the relationships:

$$\alpha = [OH]/[H] = K_{18}[H_2O]/[H_2] \tag{16}$$

and

$$\beta = ([O] + [O_2])/[OH]^2 = K_{19}/[H_2O] + K_{20}/[H_2] \tag{17}$$

where K_{18}, K_{19}, and K_{20} are the equilibrium constants for the reactions

$$H + H_2O \rightleftarrows OH + H_2 \tag{18}$$

$$OH + OH \rightleftarrows H_2O + O \tag{19}$$

and

$$OH + OH \rightleftarrows H_2 + O_2 \tag{20}$$

Complete conversion of the initial O_2 to H_2O with no production of OH, H, or O corresponds to final values of n/n_o of 0.990 in mixtures R-1 and R-3 and 0.995 in mixture R-2, and computations show that [OH] varies approximately linearly with n/n_o.

To interpret $d(1/[OH])/d\tau$ by equation (15) for conditions prevailing early in the recombination reaction, computations were made of partial equilibrium conditions with $n/n_o = 1.000$ and $n/n_o = 0.999$. The values of [M], α, (ρ/ρ_o), and β [OH] were taken as the means of these two computations, and the logarithmic derivatives which appear in the factor A were approximated from the finite differences between these two computations. [M] and α so evaluated are listed in columns 8 and 9 of Table I. (ρ/ρ_o) was invariably between 3.2 and 3.6. The factor A varied systematically from 1.7 to 1.0 as α varied from 0.01 to 0.1.

The derived values of $k_1 + \alpha k_2$ given in the last column of Table I were obtained from the measured slopes in column 5 by multiplication by the factor $\alpha\rho_o / \rho[M]A$. The following values of k_1 and k_2/k_1 have been derived by linear least squares fitting of the entire set of values of $k_1 + \alpha k_2$ in Table I and the indicated subsets thereof.

Group of Experiments				k_1	k_2/k_1
T range (°K)	[M] range mole/liter x 10^3	Mixtures	No.	liter^{2}mole^{-2}sec^{-1} x 10^{-8}	
1400-2000	8-36	All	31	6.6	7.1
1400-1700	8-36	All	17	6.1	11.4
1700-2000	9-30	All	14	5.9	8.5
1400-1700	8-10	R-1,R-3	6	5.6	17.8
1400-1700	17-19	R-1,R-3	7	6.1	9.5
1700-2000	9-10	R-1,R-3	6	6.6	7.7
1700-2000	17-19	R-1,R-3	4	4.9	14.0

We conclude that k_1 in an atmosphere consisting primarily of argon is $6 \pm 1 \times 10^8$ liter^{2}mole^{-2}sec^{-1} between 1400° and 2000°K, and that $k_2/k_1 = 10 \pm 5$ under these same conditions. No variation of either k_1 or k_2/k_1 with temperature can be established. When the points are plotted, a small trend toward lower apparent rate coefficients at higher values of [M] or [OH] is shown between the groups of points in mixtures R-1 and R-3 with [M] $\approx 9 \times 10^{-3}$ mole/liter and [M] $\approx 18 \times 10^{-3}$ mole/liter. However, this trend is not consistently borne out by the few experiments at still higher densities or the rather scattered data from mixture R-2. Such a trend may or may not be due to a small systematic error in the OH absorption spectrum calibration.

To be sure, significant departure of α from the assumed partial equilibrium value of K_{18} $[H_2O]/[H_2]$ would lead to serious error in the rate coefficients deduced. However, the available data[23] on the rates of the bimolecular reaction paths by which this equilibrium is approached indicate that α does not depart from its ideal value by more than one percent under the conditions of the present experiments. Departure of [O] and $[O_2]$ from their assumed equilibrium relationship to [OH] would be less serious in the rich mixtures studied here.

The composition of the gas acting as the third body in the present work differs greatly from that which has been used in any of the other studies in this system, and the rate coefficients determined cannot be compared in detail. The values found here are generally lower than those reported[3,4] in mixtures composed primarily of H_2, N_2, and H_2O. Within our own experiments, the only component of [M] to vary appreciably and systematically as α was varied is $[H_2]$, which was about eight times as large (after formation of H_2O, H, and OH) in the experiments with mixture R-3 as in those with mixture R-2. If H_2 were markedly more efficient than Ar in catalyzing reactions (1) and (2), the apparent rate coefficients at lower α would be increased, producing higher k_1 values and lower k_2/k_1 values. Other workers[3,4] have not found evidence for marked efficiency of H_2 as third body.

GASDYNAMIC INSTABILITY

Nine additional experiments were attempted at temperatures between 1100° and 1300°K. These yielded apparent rate coefficients which scattered between 50% and 200% of those found above 1400°K. In several of these experiments, particularly those at higher densities, there were undulations of the OH absorption record and other indications of spin-like instability in the flow behind the shock wave. Investigation of this behavior is outside the scope of the present paper. However it may well be that such instabilities are in fact present in the higher temperature experiments, but their scale is evidently fine enough not to disrupt the kinetics dramatically.

Table I

Summary of Experimental Results

Concentrations are in moles/liter, times in seconds, temperatures in °K, and velocities in km/sec.

Mix	Shock Velocity (obs'd.)	$[OH] \times 10^6$ (obs'd.) initial	final	$\frac{d(1/[OH])}{d\tau} \times 10^{-9}$	$[OH] \times 10^6$ (calc'd.)	T (calc'd.)	$[M] \times 10^3$ (calc'd.)	$\alpha \times 10^2$ (calc'd.)	$(k_1 + \alpha k_2) \times 10^{-8}$
R-1	1.226	5.2	2.5	.80	6.64	1546	8.84	4.49	10.5
R-1	1.232	5.1	2.2	.68	6.87	1560	8.87	4.65	9.3
R-1	1.251	7.2	2.4	.75	7.56	1599	8.92	5.13	11.3
R-1	1.396	14.2	4.5	.42	13.78	1921	9.31	9.71	12.1
R-1	1.408	13.0	3.5	.37	14.35	1949	9.34	10.15	11.4
R-1	1.417	16.9	4.1	.37	14.81	1972	9.36	10.50	11.8
R-1	1.200	6.9	1.8	1.47	11.57	1494	17.52	3.89	8.4
R-1	1.223	11.0	1.2	1.39	13.12	1541	17.67	4.43	9.0
R-1	1.275	14.0	1.4	1.05	16.97	1651	17.99	5.79	9.0
R-1	1.293	17.1	2.2	1.09	18.40	1689	18.09	6.31	10.2
R-1	1.385	26.7	2.9	.88	26.54	1896	18.58	9.33	12.3
R-1	1.388	28.2	2.9	.74	26.80	1903	18.59	9.42	10.4
R-1	1.196	13.4	0.6	3.23	22.58	1485	34.99	3.80	9.0
R-2	1.209	3.4	2.1	.65	3.27	1543	8.79	4.42	7.0
R-2	1.345	6.6	2.8	.55	6.04	1844	9.15	8.52	12.4
R-2	1.362	6.4	3.5	.28	6.44	1885	9.19	9.14	6.8
R-2	1.381	13.6	2.5	.64	13.80	1931	18.46	9.86	8.6
R-2	1.184	5.9	0.5	3.53	8.21	1490	25.21	3.81	11.1
R-3	1.247	1.8	0.6	2.31	2.20	1525	8.97	1.26	6.2
R-3	1.253	2.1	0.7	2.76	2.28	1537	8.99	1.31	7.6
R-3	1.279	2.4	0.7	2.35	2.69	1589	9.07	1.53	7.3
R-3	1.408	3.9	1.1	1.56	5.32	1863	9.43	2.97	8.2
R-3	1.409	4.6	1.4	1.37	5.35	1866	9.44	2.99	7.3
R-3	1.417	4.9	1.3	1.63	5.55	1884	9.46	3.10	8.9
R-3	1.185	2.2	0.3	7.84	2.85	1405	17.53	.835	7.8
R-3	1.212	2.7	0.4	5.64	3.47	1457	17.72	1.01	6.4
R-3	1.217	2.7	0.4	4.91	3.59	1466	17.75	1.04	5.7
R-3	1.396	6.9	1.1	2.66	10.09	1838	18.81	2.82	6.7
R-3	1.399	7.2	1.0	2.74	10.21	1843	18.82	2.85	7.0
R-3	1.348	8.7	0.4	4.63	12.79	1733	29.92	2.23	6.0
R-3	1.229	4.7	0.4	11.1	7.76	1488	35.65	1.12	6.8

ACKNOWLEDGMENTS

The authors acknowledge gratefully the participation of Mr. John G. Williamson and Mr. James L. Young in the performance of the experiments and Mr. Michael P. Eastman in the measurement of the photographic records.

REFERENCES

1. Bulewicz, James, and Sugden, Proc. Roy. Soc. (London) A235, 89 (1956).
2. W. E. Kaskan, Combust. Flame 2, 229 (1958).
3. Dixon-Lewis, Sutton, and Williams, Discussions Faraday Soc. 33, 205 (1962).
4. E. M. Bulewicz and T. M. Sugden, Trans. Faraday Soc. 54, 1855 (1958).
5. Bauer, Schott, and Duff, J. Chem. Phys. 28, 1089 (1958).
6. G. L. Schott and J. L. Kinsey, J. Chem. Phys. 29, 1177 (1958).
7. G. L. Schott, J. Chem. Phys. 32, 710 (1960).
8. H. T. Knight and R. E. Duff, Rev. Sci. Instr. 26, 257 (1955).
9. G. H. Dieke and H. M. Crosswhite, J. Quant. Spectr. Radiative Transfer 2, 97 (1962).
10. D. R. White, "Influence of Diaphragm Opening Time on Shock-Tube Flows", General Electric Research Laboratory Report No. 58 RL 1999, June, 1958.
11. Bird, Duff, and Schott, Los Alamos Scientific Laboratory Report LA 2980, 1964.
12. S. R. Brinkley, Jr., J. Chem. Phys. 15, 107 (1947).
13. G. L. Schott, J. Chem. Phys., accepted for publication, 1964.
14. JANAF Interim Thermochemical Tables, The Dow Chemical Company, Midland, Michigan, December, 1960, and Supplements through December, 1962.
15. Eschenroeder, Boyer, and Hall, Phys. Fluids 5, 615 (1962).
16. P. F. Bird, "Absorbance of the OH Radical in a Specific Wavelength Interval near 3090Å", Thesis, University of New Mexico, Department of Physics, 1961.
17. S. S. Penner, "Quantitative Molecular Spectroscopy and Gas Emissivities", Addison-Wesley, Reading, Massachusetts, 1959, Sections 3-5 and 4-4.
18. R. C. M. Learner, Proc. Roy. Soc. (London) A269, 311 (1962).
19. T. Carrington, J. Chem. Phys. 31, 1243 (1959).
20. W. E. Kaskan, J. Chem. Phys. 31, 944 (1959).
21. S. S. Penner, "Chemistry Problems in Jet Propulsion", Pergamon Press, New York, 1957, Section 72.
22. W. E. Kaskan and G. L. Schott, Combust. Flame 6, 73 (1962).
23. F. Kaufman and F. P. Del Greco, Ninth Symposium (International) on Combustion, Academic Press, New York, 1963, page 659.

RATE AND MECHANISM OF THE HOMOGENEOUS D/H SUBSTITUTION REACTION BETWEEN C_2H_2 and D_2, as STUDIED IN A SHOCK TUBE

Kenji Kuratani and S. H. Bauer

Department of Chemistry, Cornell University
Ithaca, New York

INTRODUCTION

One of the most intriguing facts which came to our attention during the course of our shock tube studies is the occurance of unsuspected reactions which take place at high temperatures, but under conditions which heretofore had been assumed to be insufficiently severe for appreciable reactions to occur. One example, discussed in detail in this paper, is the reaction between acetylene and hydrogen at temperatures up to 1700°K. When one mixes acetylene and hydrogen at these temperatures no change in the concentration of the acetylene can be detected for as long as one millisecond. During this interval, each acetylene molecule is subjected to an enormous number of collisions with argon (the ambient gas), acetylene and hydrogen molecules. That the acetylene and hydrogen are actually involved in an extensive association reaction, but that the acetylene is rapidly replenished by the reverse processes, becomes evident when deuterium is used in place of hydrogen. The mechanism derived from our studies have given us an insight to possible structures of the transition states of acetylene and of ethylene. The following special features of shocks of operation are thereby demonstrated:

(a) the samples are heated very rapidly and homogeneously, and
(b) it is possible to follow in time a sequence of steps for a selected reaction.

EXPERIMENTAL

The Shock Tube

The studies described below were conducted in a stainless steel shock tube, 6" in diameter, for which the driver section was 8 feet long and the driven section 22 feet long. Observations were made by recording the infrared emission at selected wave lengths for incident shocks. The windows were located 18 feet downstream from the diaphragm. Shock speeds were measured with platinum strip thermal detectors and displayed on a raster; the pressure profile was monitored at the window position with a rapid-response Kistler piezo-electric gauge. Mylar diaphragms in a variety of thicknesses were used and in all cases were ruptured by exceeding their yield pressures. The experimental section of the shock tube was pumped down with a diffusion pump to pressures of the order of 1×10^{-4} mm mercury; the leak rate was less than 1 micron per minute. Shocks were run between 2 to 3 minutes after filling the tube with pre-mixed gas samples.

The Optics

Infrared transmitting windows of calcium fluoride were mounted flush with the inner walls of the shock tube. These are 2" in length and 10mm in width. The monochromator is a modified Perkin-Elmer instrument in which a 83 x 83mm B and L grating, 150 lines per mm, blazed at 6μ for the 1st order, had been inserted. A gold-doped germanium detector, liquid nitrogen cooled, was mounted at the focus on a Cassegrain mirror system, which served to reduce the image of the exit slit by a factor of 6. External mirrors focused

a Nernst glower at the center of the shock tube. The image was then transferred by off-axis paraboloids and flat mirrors to the entrance slit of the monochromator. The glower was used for alignment of the optics and wave length calibration of the monochromator. In the parallel ray portion of the external optics a 150 cps sector and various test cells can be inserted. When used in this configuration the detector output was registered by a tuned amplifier and pen recorder. To limit the transit time for the shocked gas various masks were inserted in front of the mirrors. For a signal/noise ratio of 15 to 1, the spectral resolution of this system as calibrated with HBr lines was found to be:

At 3195 cm^{-1}, with slits 0.4~0.8 mm : 11.4 cm^{-1}/mm slit

2555 cm^{-1}, with slits 0.5~0.7 mm : 7.3 cm^{-1}/ mm slit

The design features of this system have been described[1] as constructed performance proved superior to that anticipated in the design.

The Samples

Various mixtures of acetylene, deuterium and argon were mixed in glass-lined tanks of 200 liter capacity and allowed to remain at room temperature several days before use. The deuterium was the best available commercial grade and was used without purification. The acetylene was washed thoroughly with concentrated sulphuric acid to remove the acetone. The shock tube was cleaned after each run. Since the reflected shock temperatures were considerably higher than those needed for the incident shock exchange experiments the acetylene was extensively pyrolyzed by the reflected shocks. Much carbon soot had to be removed from the tube walls and the windows after each run.

Selection of the Analytical Frequencies for Acetylene

To select the optimum analytical frequencies at which the unsubstituted and deuterated acetylenes emit at these elevated temperatures and to determine the extent of their mutual interference theoretical intensity envelopes were computed for the various bands, based on the reported rotational constants for the ground and first excited vibrational states of acetylene[2a, b, c, d]. These are illustrated in Figure 1. For estimating the concentration of acetylene present we selected the frequency 3195 cm^{-1}, at which the contribution by C_2H_2 exceeds by a factor of 5 that due to C_2HD. At 2555 cm^{-1} the relative contribution due to C_2HD is largest.

Quantitative calibrations were obtained at these selected frequencies. Note that at t = 0 (immediately after passage of the shock) all the acetylene is present as C_2H_2; whereas at a sufficiently long time, when the sample had attained equilibrium under shock conditions, its composition may be computed from the known equilibrium constants for the isotope exchange reaction. Thus, at t = 0,

$$I_0 = g\left[\epsilon\,(C_2H_2)\cdot c_o(C_2H_2)\right]\chi_{3195}$$

in which g represents the geometric factor of the optical and detecting system, c_o is the initial concentration of the C_2H_2 (in moles/l) and ϵ represents the emissivity of the gas at the shock temperature. Furthermore, at equilibrium ($t \to \infty$),

$$I_\infty = g\left[\epsilon(C_2H_2)\cdot c_\infty\,(C_2H_2) + \epsilon\,(C_2HD)\cdot c_\infty\,(C_2HD)\right]\chi_{3195}$$

Note that at 3195 cm^{-1} the contribution to the emission by the fully deuterated acetylene is negligible. In the above equations it was assumed that the concentrations are sufficiently low so that no correction for self absorption need be made, ~~for self absorption~~. One can then

obtain the ratio I_∞/I_o, and since the ratios of the concentrations of the species may be computed, the ratio $\epsilon(C_2HD)/\epsilon(C_2H_2)$ may be evaluated.

$$\frac{I_\infty}{I_o} = \frac{c_\infty(C_2H_2)}{c_o(C_2H_2)} + \frac{\epsilon(C_2HD)}{\epsilon(C_2H_2)} \quad \frac{c_\infty(C_2HD)}{c_o(C_2H_2)}$$

Typical data are given in Table I.

The ratio of emissivity coefficients at 2555 cm^{-1} were obtained by a similar procedure. In this case however one cannot measure I_o since at $t = 0$ no C_2HD is present and the emissivity increases relatively slowly from $I = 0$ at $t = 0$. In part, this is due to the finite time for vibrational relaxation of this mode, and the resolving time of our detector-amplifier system. Instead we must use I_o', which is the emission intensity measured under the identical experimental conditions for a mixture of $C_2H_2 + H_2$.

$$I_\infty(C_2H_2 + D_2) = g\left[\epsilon(C_2H_2)\cdot c_\infty(C_2H_2) + \epsilon(C_2HD)\cdot c_\infty(C_2HD)\right]\chi_{2555}$$

$$I_o'(C_2H_2 + H_2) = g\left[\epsilon(C_2H_2)\cdot c_o(C_2H_2)\right]\chi_{2555}$$

$$\frac{I_\infty(C_2H_2 + D_2)}{I_o'(C_2H_2 + H_2)} = \frac{c_\infty(C_2H_2)}{c_o(C_2H_2)} + \frac{\epsilon(C_2HD)}{\epsilon(C_2H_2)} \quad \frac{c_\infty(C_2HD)}{c_o(C_2H_2)}$$

The results are included in Table I. Hence, the emission intensity recorded at each of the frequencies is related to the corresponding concentrations by:

$$I\,(3195) \propto \left[c(C_2H_2) + 0.48\ c\ (C_2HD)\right]$$

$$I\,(2555) \propto \left[c(C_2H_2) + 3.10\ c\ (C_2HD)\right]$$

Calculation of Shock Parameters

The gas temperature behind the incident shock (T_2) and the gas density ratio cross the shock front (ρ_2/ρ_1) were computed from the measured shock velocities and the known enthalpies of the gaseous mixtures. The initial temperature wasassumed to be 298°K. No correction was made for the very small enthalpy change due to the isotopic substitution. It was observed that the shock speed attenuated slightly during its passage down the tube; the measured values were extrapolated to provide the shock velocity at the plane of observation.

THE KINETIC DATA

Kinetics of the decrease in C_2H_2(as measured by the emission intensity at 3195 cm^{-1})

When a mixture of acetylene,hydrogen and argon is shock heated to a temperature in the range 1300°K to 1700°K the emission intensity rises sharply to a level which depends on the concentration of C_2H_2, due to the compression by the shock and the vibrational excitation of acetylene to the 1st level. This emission remains constant over the period

of observation. Further, when deuterium and argon are shock heated under the same conditions no appreciable emission is observed. However, a mixture of acetylene, deuterium and argon produces a sharp rise in emission which slowly decreases with time. We propose that this decrease is due to the conversion of some of the acetylene to deuteroacetylene. To a first approximation (to be corrected later), the emitted intensity is proportional to the product of a geometrical factor, the sensitivity of the recording system, and the instantaneous concentration of the acetylene. Let ρ_2^o represent the gas density immediately after passage of the shock. Then one may write

$$\frac{\rho_2^o}{I_o}\,\frac{dI}{dt} = \frac{d\cdot\rho(C_2H_2)}{dt} + \frac{\epsilon(C_2HD)}{\epsilon(C_2H_2)}\,\frac{d\cdot\rho(C_2HD)}{dt}$$

for the rate of change in emission with time only. Note that in the analysis given below the initial reaction rates were considered, as derived from the initial slopes of the emission intensities as recorded by the oscilloscope. The time scale observed on the oscilloscope trace must be multiplied by the density ratio across the shock front (ρ_2/ρ_1) to convert the "laboratory" reaction rate to particle time. The initial reaction rate constant is then defined by the equation:

$$R_o \equiv \frac{\rho_2^o}{I_o}\,\frac{\Delta I}{\Delta t}_o = k\,(C_2H_2)_o^n\,(D_2)_o^m\,(Ar)_o^\ell\,.$$

To establish the reaction order for this exchange with respect to D_2, values of R_o were plotted against $1/T$ for a series of shocks in which the initial C_2H_2 and Ar were almost constant but $(D_2)_o$ differed by a factor of two, see Figure 2. The difference in rates over the temperature range covered is equal to $m \log 2$, so that $m = 1$ is experimentally determined.

To establish the order of the reaction with respect to the acetylene, the observed values of $R_o/\rho_2^o(D_2)$ were plotted against the reciprocal of the absolute temperature: see Figure 3. In this graph three reference temperatures were selected, centered at regions for which there were significant numbers of points. Effective rate constants at different temperatures were reduced to the nearest reference temperature by reading rates parallel to the average slope. Then the logarithms of these reduced values of $R_o/\rho_2^o(D)$ were individually plotted (for T_1, T_2, T_3) against the logarithm of the density of acetylene: see Figure 4. The slopes vary somewhat with temperature; they are respectively,

$$n = 0.29 \pm 0.01 \quad \text{at} \quad 1350°K$$
$$= 0.20 \pm 0.03 \quad \text{at} \quad 1455°K$$
$$= 0.23 \pm 0.03 \quad \text{at} \quad 1612°K$$

We have adopted the average $n = 0.24$.

The overall order for the exchange reaction as measured by the rate of disappearance of the C_2H_2 was then obtained from a series of experiments corrected to a single temperature, in which the total pressure was changed by a factor of 5, while maintaining the composition of the mixture constant. In these experiments the concentration of each component may be expressed in terms of a single variable which could be the density of the acetylene. The slope of a logarithmic plot of the initial rates against the logarithm of the initial acetylene

density thus gives the total order. The result of six runs in which the acetylene density varied from 0.53×10^{-3} to 2.51×10^{-3} gave at $T = 1455°K$ a value for $(n + m + \ell) = 1.20 \pm 0.05$. Since it was established above that $m = 1.0$ and $n = 0.24$ it follows that $\ell = 0$; that is, the argon concentration does not affect the initial rate of disappearance of the acetylene. The rate constant k_H as evaluated on the basis of the equation

$$R_o = k_H (C_2H_2)_0^{0.24} (D_2)_0^{1.0} (Ar)_0^0$$

was plotted against the reciprocal of the absolute temperature: see Figure 5. The deduced activation energy is $E_H = 33.8 \pm 0.4$ kcal/mole, and the corresponding log $A = 7.9$, for the rate of disappearance of acetylene due to reaction with deuterium, in the temperature range 1200° to 1700°K.

Kinetics of Production of C_2HD (as measured by emission at 2555 cm^{-1})

The procedure for measuring the growth in concentration of C_2HD during shock and deduction of the corresponding rate law was essentially the same as that described above for the disappearance of C_2H_2. In this case there was a small additional complexity. The acetylene originally present in the shocked gas produced a large emission at zero time. This showed up as a step function with a finite rise time, due to the combined effect of the vibrational relaxation of the C_2H_2, the resolving time of the recording system, and the particle passage time as the shock sped by the calcium fluoride windows. Below 1600°K this emitted intensity showed a rapid initial rise covering a period of about 20 microseconds, followed by an almost linear slower increase due to the production of C_2HD by the exchange reaction. Above this temperature the inflection point could not be easily detected; hence the data cited below were restricted to runs made below 1600°K. Again it was established that the order of the reaction was unity with respect to the initial deuterium concentration. As tested previously, $R_o/\rho_2^0 (D_2)$ values were plotted against the reciprocal temperature and the points were corrected to the reference temperature of 1470°K. The reduced $R_o/\rho_2^0(D_2)$ were then replotted against the density of acetylene. The slope of this curve gave for the order of the reaction with respect to acetylene $n = 0.24 \pm 0.04$, checking the value deduced for the rate of disappearance of C_2H_2. Another plot provided a value for the total order, which proved to be 1.24 ± 0.07. Thus we have demonstrated that the rate of appearance of C_2HD and the rate of disappearance of C_2H_2, under the conditions of our experiment follow the same functional dependence on the initial concentrations of reactants. A plot of the reduced rate constant against the reciprocal of the temperature is shown in Figure 6. The activation energy is $E = 29.3 \pm 1.1$ kcal/mole and the corresponding log $A = 7.5$. The limits of error quoted for E_H and E_D are based on the internal consistency of each set of runs; we consider these activation energies to be equal within their absolute limits of error.

Corrected Values for the Rate Constants

In the preceding paragraphs it was demonstrated that the functional dependencies of the rate of depletion of C_2H_2 and the rate of formation of C_2HD on the initial concentrations of the reactants and on the temperature are equal. It is now possible to correct the apparent rates, deduced directly from the changes of the emission intensities at 3195 cm^{-1} and 2555 cm^{-1}, to obtain absolute rates, by noting the relative contributions of each species to the intensities recorded at these frequencies:

$$-k_H (C_2H_2)^{0.24} (D_2) = -\frac{dC_2H_2}{dt} + \left[\frac{\epsilon(C_2HD)}{\epsilon(C_2H_2)}\right]_{3195} \frac{dC_2HD}{dt} = -\frac{dC_2H_2}{dt} + 0.48\,\frac{dC_2HD}{dt}$$

$$+k_D(C_2H_4)^{0.24}(D_2) = -\frac{dC_2H_2}{dt} + \left[\frac{\epsilon(C_2HD)}{\epsilon(C_2H_2)}\right]_{2555} \frac{dC_2HD}{dt} = -\frac{dC_2H_2}{dt} + 3.10\,\frac{dC_2HD}{dt}$$

On rearranging terms:

$$-\frac{dC_2H_2}{dt} = k_{C_2H_2}(C_2H_2)^{0.24}(D_2) = \frac{3.10\,k_H + 0.48\,k_D}{3.10 - 0.48}(C_2H_2)^{0.24}(D_2)$$

$$+\frac{dC_2HD}{dt} = k_{C_2HD}(C_2H_4)^{0.24}(D_2) = \frac{k_H + k_D}{3.10 - 0.48}(C_2H_2)^{0.24}(D_2)$$

Specifically, at 1470°K,

$$k_{C_2H_2} = 1.17 \times 10^3 \quad (\text{liter/mole})^{0.24}\ \text{sec}^{-1}$$

$$k_{C_2HD} = 0.82 \times 10^3 \quad (\text{liter/mole})^{0.24}\ \text{sec}^{-1}$$

We thus find that the rate of increase of C_2HD is almost equal to 2/3 of the rate of decrease in the C_2H_2. Since the acetylene is removed only by the isotopic exchange reaction (as demonstrated by the fact that C_2H_2 plus H_2 does not show a decrease in the emission at 3195 cm^{-1}), it follows that the remaining 1/3 of the C_2H_2 leads to the production of C_2D_2. The rate of production of C_2D_2 is then roughly 1/2 of that of C_2HD.

To substantiate this conclusion we cite rough analytical data obtained in a single-pulse experiment based on a sample composition and temperature pulse comparable to that used for the infrared runs. Mass spectrometric analysis of a shocked mixture of $C_2H_2 + D_2$ showed:

(a) The amount of H_2 generated was definitely less but comparable to that of HD.
(b) The decrease in the amount of C_2H_2 was larger than the amount of C_2HD generated.
(c) No methane or ethylene was produced.

A few preliminary IR runs at 2350 cm^{-1} showed that emission due to C_2D_2 did rise following shock heating of a mixture of acetylene and deuterium. However, this experiment was not completed and no quantitative data on the rate of production of C_2D_2 were obtained by the infrared technique.

The weighted average of the energies of activation obtained from the ln k vs 1/T plots (using internal consistency as the basis for weighting E_H and E_D) is 32.7 ± 1 kcal/mole. This leads to:

$$k_{C_2H_2} = 8.5 \times 10^7 \exp(-32700/RT), \quad (\text{liter/mole})^{0.24}\ \text{sec}^{-1}$$

$$k_{C_2HD} = 6.0 \times 10^7 \exp(-32700/RT), \quad (\text{liter/mole})^{0.24}\ \text{sec}^{-1}$$

Typical sets of data are summarized in Table II. These are but examples of the large number of shocks run. The values given are for the 3195 cm^{-1} band.

DISCUSSION OF MECHANISM

A thorough search of the literature has yet to be completed. To date we found only one report on a gas phase study of the $(C_2H_2 + D_2)$ reaction. Coats and Anderson[3] heated equimolar mixtures of the two gases in 25 ml bulbs for 2 - 10 minutes to temperatures 500° - 900°C, at a total initial pressure of 300 mm Hg. The reaction bulbs were allowed to cool to room temperature and their contents were analyzed. In view of the diversity of products produced (ranging from methane to benzene, toluene and carbon deposits) heterogeneous steps evidently played prominent roles in these conversions. Their product distribution suggested that free radical reactions as well as molecular processes had occured. There are, of course, numerous reports on the rates and mechanisms of D/H substitution in hydrocarbons as catalyzed by a variety of surfaces, and as induced by radiations which generate atoms. In the latter, the primary attack is an atomic displacement or an abstraction.

The pyrolysis of acetylene in shock tubes has been investigated[4]. In this laboratory shock tube studies of the homogeneous substitution reactions between $(NH_3 + D_2)$[5], $(H_2S + D_2)$[5], and $(HCl + D_2)$[6] have been completed. For these systems the rate laws are significant different in that they show an overall second order dependence, in constrast to the overall 1.24 order dependence deduced for $(C_2H_2 + D_2)$. The observation that the activation energy is low (~33 kcal/mole) and that the rate depends on the first power of the deuterium concentration argues against all the chain reactions we have been able to devise. Indeed, the observed rates are much too high to be consistent with the known or estimated homogeneous rates of dissociation of D_2[7] and of $C_2H_2 \rightarrow C_2H + H$. Finally, the fact that the rate of production of C_2D_2 is about half of that of C_2HD suggests that these species are derived from the same transition state, which we designate $C_2H_2D_2^*$. The following mechanism is consistent with all the observations.

We postulate the occurance of two types of unstable intermediates:
(a) $C_2H_2 \cdot D_2$, which is a molecular complex between acetylene and deuterium, and which is particularly sensitive to dissociation by collision with another acetylene; and
(b) $C_2H_2D_2^*$, which is an electromcally excited ethylene, with V_d symmetry, approximately 3 e.v. above the ground state $[E_A + \Delta H_{hydrog}(C_2H_2) \approx 3\ \text{e.v.}]$. Species in this state have a much greater probability for dissociation than for interval conversion to stable etheylene. The formal rate expression is based on the sequence:

$$C_2H_2 + D_2 \underset{k_1}{\overset{k_{-1}}{\rightleftharpoons}} C_2H_2 \cdot D_2$$

$$C_2H_2 \cdot D_2 + C_2H_2 \underset{k_2}{\overset{k_{-2}}{\rightleftharpoons}} 2\,C_2H_2 + D_2$$

$$C_2H_2 \cdot D_2 \underset{k_3}{\overset{k_{-3}}{\rightleftharpoons}} C_2H_2D_2^*$$

$$C_2H_2D_2^* \xrightarrow{2k_{-3}} C_2HD \cdot HD \xrightarrow{k_{-1}} C_2HD + HD$$

$$\Big| \; k_2(C_2H_2)$$

$$C_2H_2D_2^* \xrightarrow{k_{-3}} C_2D_2 \cdot H_2 \xrightarrow{k_{-1}} C_2D_2 + H_2$$

$$\Big| \; k_2(C_2H_2)$$

The production of $C_2H_2 \cdot D_2$ via (-2) may be neglected because it is a three body process; it appears that Ar is not an effective third body for (1), and hence is correspondingly ineffective for (-1). Also, during the initial stages of the reaction, the reverse steps involving C_2HD and C_2D_2 are negligible. Schematically, the sequence of structures is diagramed in Figure 7.

On applying the steady state condition to the transient species $C_2HD \cdot HD$, $C_2H_2D_2^*$ and $C_2H_2 \cdot D_2$, one readily derives:

$$\frac{d(C_2HD)}{dt} = \frac{k_1 k_3 \alpha}{2 k_2} \; \frac{(D_2)(C_2H_2)}{1 + \alpha (C_2H_2)}$$

$$\text{where } \alpha = \frac{k_2}{k_{-1} + \frac{3}{4} k_3}$$

For the initial rate of production of C_2D_2 a similar expression follows, but the coefficient is $k_1 k_3 / 4 k_2$. For the initial rate of depletion of C_2H_2 the identical functional dependence is obtained, with the coefficient $3 k_1 k_3 \alpha / 4 k_2$. The measure rate constant is thus identified with

$$\frac{3}{4} \; \frac{k_1 k_3 (C_2H_2)^{.76}}{k_{-1} + \frac{3}{4} k_3 + k_2 (C_2H_2)}$$

It is evident that the net power dependence of $d(C_2H_2)/dt$ on the acetylene concentration could range from unity to zero, depending on the magnitude of $\alpha (C_2H_2)$ relative to unity; that is, on the relative efficiency for depletion of $C_2H_2 \cdot D_2$ via collisions with C_2H_2 compared with that by decomposition and rearrangement. Note that α is temperature dependent. Even though many shocks were run we found that a sufficient range in acetylene concentrations had not been covered to permit us to evaluate . The rather low activation energy observed is accounted for, as is also the ratio of products produced.

ACKNOWLEDGEMENTS

This work was supported by a grant from NASA (NsG-116-61), to whom grateful acknowledgement is made.

REFERENCES

1. A Survey of Methods for Chemical Analysis of Transient Species of Microsecond Resolution, S. H. Bauer, N. C. Rol, and J. H. Kiefer, Physical Chemistry in Aerodynamics and Space Flight, Ed. A. L. Meyerson and A. C. Harrison, Pergamon Press, NY., 1961 (p. 118).

2. a) M. T. Christensen, et al, Proc. Roy. Soc., A238, 15 (1957)
   b) H. C. Allen, et al, J. Amer. Chem. Soc., 78, 3034 (1956)
   c) J. Overend and H. W. Thompson, Proc. Roy. Soc., A234, 3061 (1956); A232, 291 (1955)

3. F. H. Coats and R. C. Anderson, AFOSR TN-56-491 (AD 110-305) University of Texas, Oct. 1956 under AF18(600)-430, Chem. 50-1.

4. a) C. F. Aten and E. F. Greene, Dis. Farad. Soc., 22 162 (1956)
   b) S. S. Penner et al, AGAR Dograph No. 61
   Fundamental Data Obtained from Shock Tube Experiments
   Ed. A. Ferri, Pergamon Press, NY., p219, p. 183 (1961)
   c) J. N. Bradley, Shock Waves in Chemistry and Physics, John Wiley and Sons, Inc., New York, 1962, p. 128, 267, 321, 325

5. Assa Lifshitz, Chava Lifshitz and S. H. Bauer, unpublished

6. C. Sadowski, S. K. Addecott and S. H. Bauer, unpublished

7. J. P. Rink, J. Chem. Phys., 36 1398 (1962)

TABLE I. Experimental Determination of the Ratios of ϵ's

	at 3195 cm^{-1}			at 2555 cm^{-1}	
	(α)	(β)		(γ)	(δ)
$\frac{I_\infty}{I_o}$	0.225	0.315	I_∞ ($C_2H_2 + D_2$)	25.4	27.0
			I_o ($C_2H_2 + H_2$)	14.0	15.0
$\frac{c_\infty(C_2H_2)}{c_o(C_2H_2)}$	0.053	0.111		0.25	0.25
$\frac{c_\infty(C_2HD)}{c_o(C_2H_2)}$	0.352	0.440		0.50	0.50
$\frac{\epsilon(C_2HD)}{\epsilon(C_2H_2)}$	0.49	0.465		3.14	3.10
Ave.	< 0.48 >			< 3.12>	

(α) Average of 4 runs with $\frac{c_o(C_2H_2)}{c_o(D_2)} = 3.333$, at 1600 - 1700°K

(β) Average of 4 runs with $= 2.00$, at 1550 - 1650°K

(γ) At about 1670°K

(o) At about 1720°K

TABLE II: Typical Data for the 3195 cm^{-1} Band

Run No.	465	397	404	410	405	458	451	430	424
$C_2H_2/D_2/Ar$	10/10/80	10/10/80	10/10/80	5/10/85	5/10/85	3/10/87	3/10/87	10/5/85	10/5/85
p_1(total)	26	82	41.5	80	80	61	61	81	43
$\rho_2^o(C_2H_2)$	0.59×10^{-3}	1.91×10^{-3}	0.99×10^{-3}	0.78×10^{-3}	0.87×10^{-3}	0.34×10^{-3}	0.378×10^{-3}	1.80×10^{-3}	1.01×10^{-3}
$\rho_2^o(D_2)$	0.59×10^{-3}	1.91×10^{-3}	0.99×10^{-3}	1.57×10^{-3}	1.74×10^{-3}	1.14×10^{-3}	1.26×10^{-3}	0.90×10^{-3}	0.51×10^{-3}
T_2 °K	1390	1545	1665	1245	1680	1200	1700	1410	1695
ρ_2/ρ_1	4.19	4.34	4.44	3.65	4.01	3.47	3.83	4.12	4.35
R_o	0.0422	0.545	0.489	0.0306	0.970	0.0111	0.753	0.0900	0.329
$R_o/\rho_2^o(D_2)$	0.715×10^2	2.85×10^2	4.96×10^2	0.195×10^2	5.59×10^2	$0.097_5 \times 10^2$	5.98×10^2	1.00×10^2	6.45×10^2
k_H	0.426×10^3	1.28×10^3	2.61×10^3	0.109×10^3	3.04×10^3	$0.065_5 \times 10^3$	3.94×10^3	0.455×10^3	3.38×10^3

p_1, in mm Hg

ρ_2^o, the corresponding gas density (moles/l) immediately after passage of the shock

$R_o \equiv \frac{\rho_2^o}{I_o} \left(\frac{\Delta I}{\Delta t}\right)_o \left(\frac{\rho_1}{\rho_2}\right)$, in mole liter^{-1} sec^{-1}

$k_H = R_o/\rho_2^o(D_2)\, \rho_2^o(C_2H_2)^{0.24}$, in (l/mole)$^{0.24}$ sec^{-1}

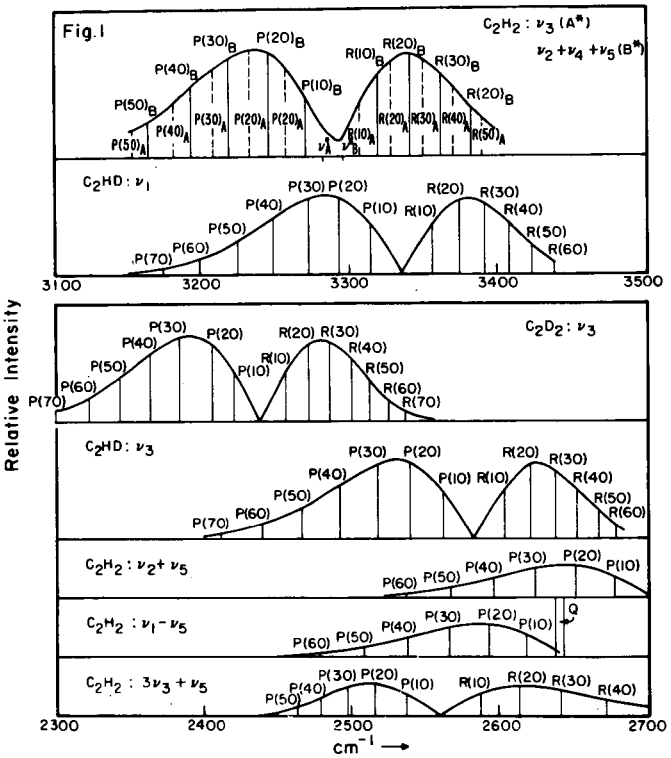

Fig. 1 Theoretical envelopes showing relative emission intensities of acetylene, mono-and dideuteroacetylene at 1700°K.

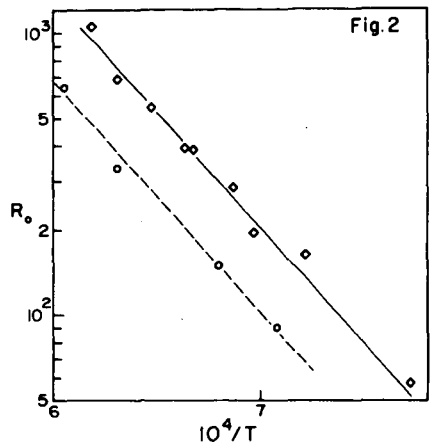

Fig. 2 Logarithmic plot of R_o vs $10^4/T$, for runs with constant $(C_2H_2)_o$, and $(\overline{Ar})^o$, but $(D_2)_o$ differs by a factor of two:

Solid Line: $C_2H_2/D_2/Ar = 10/10/80$

Dashed Line: $C_2H_2/D_2/Ar = 10/5/85$

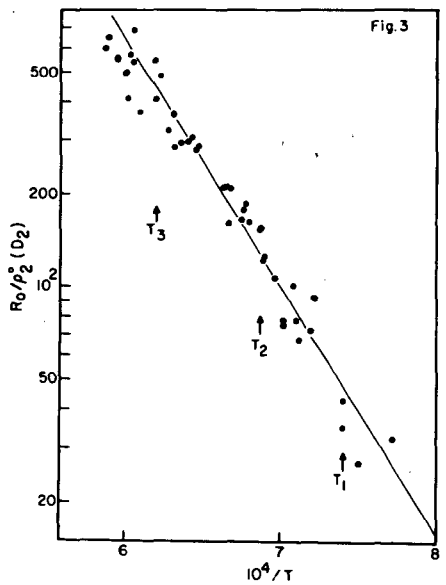

Fig. 3 Logarithmic plot of $R_o/p^o_2(D_2)$ vs 10^4T, for all runs:

$C_2H_2/D_2/Ar$ = 10/10/80; 5/10/85; 3/10/87; 10/5/85

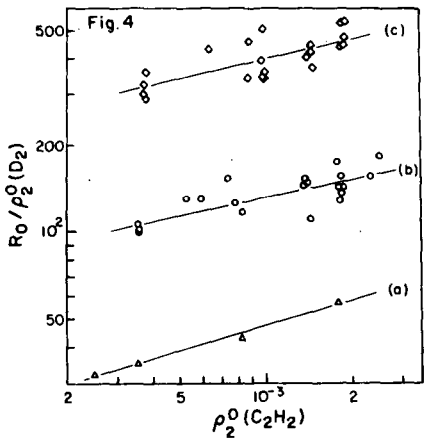

Fig. 4 Logarithmic plots of the reduced values of $R_o/\rho_2^o(D_2)$ vs $\rho(C_2H_2)_o$, corresponding to the temperatures

(a) 1350 °K (b) 1455 °K (c) 1612 °K

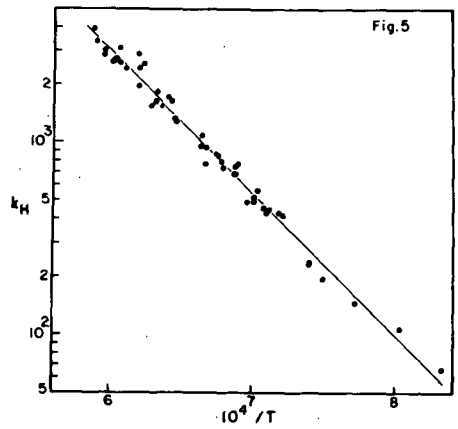

Fig. 5 Plot of the rate constant for the disappearance of C_2H_2, due to reaction with D_2, as measured from the decline in emission intensity at 3195 cm^{-1}, vs the reciprocal temperature.

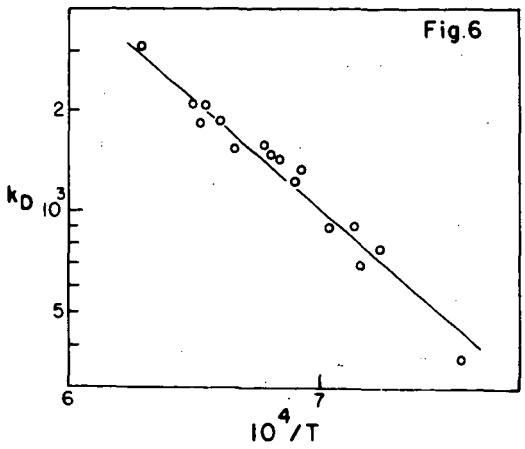

Fig. 6 Plot of the rate constant for the production of C_2HD, as measured from the rise in emission intensity at 2555 cm^{-1}, vs the reciprocal temperature.

FIG. 7

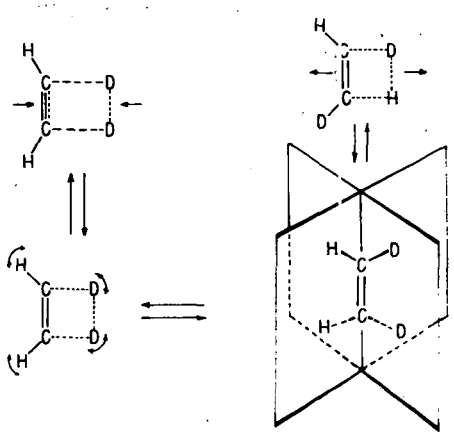

Fig. 7 Proposed sequence of configuration for the H/D exchange.

The Kinetics of Decomposition of Acetylene in the 1500°K Region

Howard B. Palmer and Frank L. Dormish

Department of Fuel Technology, The Pennsylvania State University
University Park, Pa.

Introduction

The thermal decomposition of acetylene is one of the most-studied phenomena in the chemistry of gases. Despite the apparent simplicity of the C_2H_2 molecule, its thermal behavior is exceedingly complex. Within the past ten years, it has been studied in static systems (1, 2, 3), in flow systems (4-8), in shock tubes (9-12), and in flames (13). The temperature range covered in these studies has spanned the region from about 625°K to 2500°K, but with a gap in the 1000°K region that has been studied only very recently (6, 14). Explorations have been made of the product distributions, of the effects of vessel surfaces, of changing surface-to-volume ratios, of adding free radical capturers such as NO, and of adding organic compounds that might participate in the mechanism. The rate of formation and the characteristics of the carbons and polymers formed in the decomposition have been studied extensively.

There is substantial agreement on some aspects of the decomposition. It appears to be settled that at low temperatures, a homogeneous reaction which is second order in $[C_2H_2]$ dominates the behavior. The reaction is a chain and leads to the formation of high molecular weight compounds, with some side products such as H_2, C_2H_4, CH_4, and C_4H_4. The activation energy is approximately 50 kcal and the frequency factor of the uninhibited reaction is very large. Silcocks (3) gives

$$k = 3.72 \times 10^{16} \exp(-50.2 \text{ kcal/RT}) \text{ cc/mole sec.}$$

A heterogeneous reaction is also observed at low temperatures.

Silcocks reports that it is first-order in $[C_2H_2]$, with an activation energy of 42.7 kcal. He gives values of the rate constant at five temperatures.

The situation at high temperatures contains more conflict. It has been difficult to determine the order of the reaction and the activation energy, either with flow systems (8) or in shock tubes. However, if one presumes the reaction order to be integral, the best choice at high temperatures appears to be second-order in acetylene. The rate constants at the highest temperatures (9, 12) disagree by a factor of about 10, but agreement is considerably better at temperatures below 1900°K.

Both Aten and Greene (9) and Minkoff and Tipper (15) agree that the rate constants at high and low temperature can be used to define the rate over the whole range; i.e., they agree that the mechanism remains the same, at least up to and including the rate-determing step. However, Aten and Greene prefer their own high temperature data, while Minkoff and Tipper prefer those of Kistiakowsky and Bradley (12). These choices yield markedly different results, respectively:

$$\text{(data of ref. 9)}\quad k = 10^{12.89}\exp(-39\ \text{kcal/RT})\ \text{cc/mole sec}$$

$$\text{(data of ref. 12)}\quad k = 10^{15.15}\exp(-45.8\ \text{kcal/RT})\ \text{cc/mole sec}$$

Quite aside from questions raised by such a discrepancy, we think it unjustifiable to assume that one is measuring the rate of the same reaction sequence at 2000°K and at 700°K. The low temperature homogeneous reaction is a chain of length (3) on the order of 100 or more. There is no evidence that the reaction at high temperature is a chain. Indeed the only direct experimental evidence (12) of which we are aware indicates that it is essentially a simple sequence of consecutive reactions.

It is clearly important to discover what happens between the lower limit of the shock tube studies, ca. 1400°K, and the upper limit of the studies in vessels, ca. 800°K. This intermediate region is appropriate for studies using flow systems. Anderson and his colleagues (4, 5) have done exactly this, but have concentrated most of their attention upon product distributions and the implications of these regarding the mechanism. Very recently, however, Munson and Anderson (6) have published work from which it is possible to extract rate constant data and we shall discuss these later. Towell and Martin (8) used a flow reactor to study the decomposition over temperatures from about 1200°K to 1450°K. They had difficulty in defining the order of reaction, but their data compare reasonably well with shock tube data if one assumes second order behavior.

The present experiments represent an effort to study the decomposition very carefully at three temperatures, the highest of which overlaps

the shock tube studies. Particular attention has been given to determining the order of reaction and the absolute magnitudes of rate constants at these three temperatures. The work is basically an extension of that performed by Kinney and Slysh (7).

Experimental Procedure

The apparatus was only slightly modified from the arrangement used by Kinney and Slysh (7) and will therefore be described only briefly. It was a flow system operating at ambient pressure. The pyrolysis tube was 5 mm i.d. refractory porcelain, sealed to Pyrex at the ends, and mounted in a furnace capable of attaining 1500°C. C_2H_2 was metered with a capillary flowmeter before being mixed with the helium carrier. Input rates were varied so as to produce mixture compositions ranging from 0.20 to 1.30 mole per cent C_2H_2.

Temperature profiles within the pyrolysis tube were measured with a Pt-Pt:Rh thermocouple for each of three temperature settings and at several flow rates. They were found to be essentially independent of flow velocity, from which it is inferred that the gas temperature was indeed being measured. This conclusion is supported by estimates of the radial temperature distribution in the tube based upon approximate values for the thermal diffusivity of the gas. The estimates show that the temperature at the center of the tube (2.5 mm from the wall) should not differ from the wall temperature by more than a few degrees. Because the furnace was short, the temperature profiles did not possess a plateau region. A typical profile is shown in Fig. 1, together with what we call the "staircase" approximation to it, by means of which it was possible to correct the experimental data to the temperature of an imaginary 5-cm-long hot zone having a constant temperature near the actual temperature peak. It was also convenient to discuss the effect of flow velocity upon the per cent decomposition in terms of the fictitious residence time ("contact time") of the gas in the imaginary hot zone.

Calculations of the extent of decomposition in the hot zone were carried out for each run by an iterative procedure in which an equation for the rate constant was assumed in order to compute the relative contributions from decomposition at each of the temperature levels on the staircase. Most of the decomposition occurred on the top level, which meant that it was quite easy to correct for the other contributions, using rough values for the rate constants in the first trial. From the results of the runs at three different temperature settings, a better expression for the temperature-dependent rate constant was derived and used in the second calculation of corrections. This single iteration was found to yield satisfactory values for rate constants at each of the three hot zone temperature levels (1333°K, 1433°K, and 1528°K). Details of these calculations are presented in reference 16.

The helium used was Matheson "research grade" gas, purity approximately 99.99%. It was passed through a bed of Cu at 400°C for O_2 removal and then through a tower containing Ascarite and Anhydrone to remove CO_2 and H_2O. The C_2H_2, a purified grade of 99.5% minimum purity, was bubbled through concentrated H_2SO_4 to remove acetone before introduction into the helium stream. The mixture of C_2H_2 and He was routed through a dry ice-cooled, glass wool-packed trap before entering a coil of tubing 4 feet in length that served to ensure homogeneity of the mixture that entered the pyrolysis tube.

Beyond the water-cooled exit of the furnace were three traps in series. The first was cooled by dry ice and served principally as a pre-cooler to ensure good trapping efficiency in the subsequent liquid N_2-cooled traps. These traps captured acetylene, diacetylene, vinylacetylene, methyl acetylene, and allene. Hydrogen and methane were not trapped, but were converted to H_2O and CO_2 over CuO filings at 700°C. Vitreous carbon that formed on the tube wall during the run was determined by burning it off with oxygen at 1255°C, running the effluent gas through a CuO trap, and capturing the CO_2 in Ascarite. A very small amount of reddish polymer, deposited just beyond the furnace exit, was the only product ignored. Analyses were performed using vapor chromatography and (for CO_2 and H_2O) by weighing Ascarite and Anhydrone absorption towers.

Results and Discussion

The decomposition has been studied at three temperatures: 1333°K, 1433°K, and 1528°K. These represent the effective hot zone temperatures to which the decomposition data were corrected. Because the emphasis in the present paper is upon the kinetics of decomposition, details of product analyses are not presented here. They were in broad agreement with the results of other investigations (6, 7). A note of special interest is that the more prominent C_4 product at 1333°K was vinylacetylene, but at 1528°K it was diacetylene.

In Table I are summarized the experimental data on the extent of decomposition of C_2H_2 at various nominal contact times. These formed the basis for calculations of rate constants. The order of reaction has been determined at the three hot zone temperatures by examining the extent of decomposition as a function of the initial concentration at fixed flow rate--i.e. at fixed effective contact time in the hot zone. The results appear in Fig. 2, and represent mixed first- and second-order behavior. This may be seen as follows: consider a reaction with rate given by

$$\frac{-dc}{dt} = k_u C + k_b C^2 \qquad (1)$$

Integration yields

$$\left(\frac{C_o}{C}\right) = k_u t + \int_o^t k_b C dt \qquad (2)$$

$$= (k_u + k_b \bar{C})t \qquad (3)$$

where $\bar{C}$ is a mean concentration over the time interval, and will approximately equal $(C_o + C)/2$ when the extent of decomposition is small. When this is the case, Eq. 3 yields

$$(1 - \frac{C}{C_o}) = (k_u + k_b \bar{C})t \qquad (4)$$

Thus for mixed first and second order, a study at fixed time (i.e. fixed flow rate) and small extent of decomposition should show an approximately linear dependence of the extent of decomposition upon the input concentration, with a finite intercept at $C_o = 0$ if there is in fact a first-order contribution. This is the case in Fig. 2.

One can calculate first-order rate constants from the intercepts in Fig. 1. The result for 1528°K is not as reliable as the other two because of the smaller number of points, the long extrapolation to $C_o = 0$, and the larger extent of decomposition. The calculations involve a correction to yield the extent of decomposition in the effective hot zone. This is in principle a multiply iterative procedure, but we found that the correction was sufficiently small that a rough treatment of the data could provide crude rate constants from which corrections could be formed to yield good rate constants in a single iteration, as discussed earlier.

The k_u values obtained are 0.221 sec^{-1} at 1333°K; 0.482 sec^{-1} at 1433°K; and 0.745 sec^{-1} at 1528°K. On an Arrhenius plot, these define a line given by

$$k_u = 4.2 \times 10^3 \exp(-26 \text{ kcal/RT}) sec^{-1}$$

The uncertainties in the numerical values of this expression are surely considerable (but difficult to estimate). Nevertheless it is clear that both the frequency factor and the activation energy rule out a homogeneous unimolecular reaction. If we assume that the reaction is heterogeneous, the rate constant k_{het} will be $k_{het} = k_u(V/S)$, where (V/S) is the volume-to-surface ratio. In our reactor, this ratio was 1.25×10^{-4} liter/cm^2, where the units have been chosen so as to permit easy comparison with the low-temperature results of Silcocks (3). The comparison is shown in Fig. 3. k_{het} is now given by

$$k_{het} = 5.25 \times 10^{-1} \exp(-26 \text{ kcal/RT}) \text{ liter } cm^{-2} sec^{-1}$$

An extension of this line goes through the middle of Silcocks' data. It is tempting to conclude that the heterogeneous reactions are the same, but caution is required because a modest alteration of the parameters in the expression for k_{het} could cause the extension to miss Silcocks' points altogether. There is much more to be explored on the matter of a heterogeneous decomposition. We have noted with interest that the yields of H_2, C_4H_4, and C_4H_2 all move toward zero at $C_o = 0$, and carbon plus CH_4 become virtually the only products. Clearly the mechanism of the surface decomposition must be grossly different from the gaseous process.

Fig. 2 shows that the gaseous decomposition conforms nicely to second-order kinetics, and it is possible to obtain k_b from the slopes. We have preferred to use data on the per cent decomposition as a function of the effective contact time in the hot zone, averaging the rate constants obtained from a number of runs (6 to 8) at the same temperature but at various flow rates and input concentrations. The results have been corrected, in each case, for the first-order contribution. The procedure (16) is tedious and will not be outlined here.

The results for k_b, in units of cc/mole sec, are: $(1.40 \pm 0.10) \times 10^3$ at 1333°K; $(3.42 \pm 0.23) \times 10^3$ at 1433°K; and $(2.49 \pm 0.36) \times 10^4$ at 1528°K. The uncertainties attached to each result are the average absolute deviations of the experimental points.

Figure 4 is an Arrhenius plot of all available data for k_b, ranging from about 650°K to 2500°K. The solid curve will be discussed later. Our data and those of Skinner and Sokolski (11) agree very well, in the sense that their higher-temperature points fall on the best line through our results. However, their values below about 1500°K (not included in the figure) show a change in slope that requires comment at a later point in this discussion. The data of Towell and Martin (8), obtained in reactors very similar to ours, parallel our data well. Agreement would be even better if their results could be readily corrected for the contribution from the heterogeneous decomposition. The results of Aten and Green (9) are in reasonable agreement with ours and with Skinner's but show a smaller slope. The best high temperature line, which we have selected by eye, defines k_b as

$$k_b = 3.2 \times 10^{14} \exp(-50 \text{ kcal/RT}) \text{ cc/mole sec.}$$

The frequency factor seems close to normal, in contrast to that cited earlier for the low-temperature reaction. This does not prove that one is observing an elementary reaction at high temperatures, but suggests that the hot reaction is not a chain. An extrapolation of the best high temperature line falls below the low temperature k_b values by a factor of 10^2 or more.

Thus the question remains: what happens between 800°K and 1400°K? The work of Munson and Anderson (6) contributes much toward an answer. They used a flow reactor of diameter 2.2 cm and, at high concentrations of C_2H_2 (20-21 mole per cent at p_{tot} = 1 atm), covered temperatures from 773°K to 1123°K. They did not obtain rate constants, but they do report the time-dependence of the C_2H_2 concentration at six temperatures. These results are of precision sufficient to permit examination of the reaction order by the usual methods of kinetics. Our analysis shows that the reaction is second-order in $[C_2H_2]$ at 873°K, 923°K, and 973°K, but that the order is not well defined at the higher temperatures. The second-order rate constants at the three lower temperatures are in remarkably good agreement with an extrapolation of low-temperature data.

If one approximates the kinetics at the three higher temperatures (1023°K, 1073°K, and 1123°K) by a first-order expression, the rate constants

so obtained show a temperature coefficient corresponding to an activation energy in the vicinity of 30 kcal. It thus seems quite clear that the kinetics of the decomposition undergo a transition at about 1000°K, and that one cannot make a direct comparison of second-order rate constants at low and high temperatures.

In view of the known complexity of the decomposition, it is not really surprising to find complications in the kinetics; but the behavior does seem extraordinary. An acceptable mechanism must: (a) give second-order kinetics at low temperature, with a rate constant similar to that cited from the results of Silcocks; (b) there must be some sort of transition region at intermediate temperatures; and (c) at high temperatures the reaction must be second-order but now with k_b similar to that cited previously from our data and the shock tube data.

Behavior of this sort can occur in the mechanism presented below. This is offered as a stimulus to further work. It makes no attempt to account in detail for all products, and there is no direct evidence for the steps involved in it. Our comments follow each reaction postulated.

(1) $C_2H_2 + C_2H_2 \rightarrow C_2H_2^* + C_2H_2$.

This represents unimolecular excitation of acetylene to its lowest-lying triplet state. C_2H_2 is shown as the collision partner for the excitation on the presumption that in a mixture of C_2H_2 and a monatomic gas, e.g. He, C_2H_2 will be many times more effective than He because it can possess vibrational energy. The actual change of multiplicity probably occurs most rapidly when the amount of energy to be transferred is not very large (17). Thus a detailed mechanism for reaction 1 would include vibrational excitation. However, because establishment of vibrational equilibrium is probably rapid relative to the rate of reaction 1, one can think of at least one of the C_2H_2 molecules as being highly excited vibrationally without introducing a necessity for modifying the simple equation above.

Minkoff (2) has suggested that the first step is double excitation, $2\ C_2H_2 \rightarrow 2\ C_2H_2^*$. This has the virtue of being spin-allowed, but the energy requirement will be very much greater (roughly double) that for step 1 above; this should weigh more heavily against the double excitation than does the forbiddenness factor (perhaps 10^{-4}) entering into the rate constant of reaction 1.

Reaction 1 will probably have an energy barrier somewhat higher than the singlet-triplet excitation energy, which has been estimated (9) to lie between 42 and 67 kcal above the ground state, using data discussed by Laidler (17).

(2) $C_2H_2^* + C_2H_2 \rightarrow 2\ C_2H_2$,

deactivation of triplet acetylene. By microscopic reversibility, C_2H_2 must be much more effective than He in the deactivation. There will presumably be a small activation energy in the rate constant, and a forbiddenness effect in the pre-exponential factor.

(3) $C_2H_2^* + C_2H_2 \rightarrow C_4H_4^*$.

This is an addition reaction to yield a triplet dimer. The reaction will be in competition with step 2, and will be fast. The rate constant for a reaction that may be comparable, viz, the addition of NO_2 to C_2H_2, has been reported (18) to equal $10^{12.1}$ exp(-15 kcal/RT) cc/mole sec.

(4) $C_4H_4^* + C_2H_2 \rightarrow C_2H_2^* + C_4H_4$,

a chain-transfer reaction that is not simply an exchange of multiplicities because formation of vinylacetylene from $C_4H_4^*$ requires H atom migration. There should be an appreciable but small activation energy. We suspect that in a reaction of this type the collision efficiency ("steric" factor) may be very low.

(5) $C_4H_4^* + C_2H_2 \rightarrow$ products.

This alternative to reaction 4 is thought of as a radical addition reaction leading to stable products such as benzene. It is oversimplified for the sake of allowing a tractable expression for the overall kinetics. That is, it might also be thought of as a deactivation; or it might not end the chain at all, but rather continue it by a subsequent transfer reaction analogous to step 4; or the product might in turn add to C_2H_2. However, observations by Robertson *et al.* (19) of the yield of benzene in C_2H_2 pyrolysis do support the suggestion that a large fraction of the reaction events in step 5 do not lead to a continuation of the chain. It further appears from that work that reaction 5 has a large temperature coefficient. We shall assume that its activation energy is much larger than that for step 4, and that its collision factor is also much larger; in this way it becomes possible for its rate to be less than that of step 4 at low temperature but to exceed it at higher temperatures.

The postulated reaction scheme is terminated at this point. It is of course recognized in doing so that other reactions must occur. The scheme is a simplified version of that discussed by Minkoff and Tipper (15), but with the difference in the singlet-triplet excitation step noted previously.

A steady-state treatment of the scheme yields

$$-d[C_2H_2]/dt = [C_2H_2]^2 k_3(k_1/k_2)\left\{[3 - k_4/(k_4 + k_5)]/[1 + (k_3/k_2)k_5/(k_4 + k_5)]\right\} \quad (4)$$

At low temperatures, we expect $k_4 >>> k_5$. Then

$$-d[C_2H_2]/dt = 2[C_2H_2]^2 k_3(k_1/k_2)[1/(1 + k_3k_5/k_2k_4)] . \quad (5)$$

We expect k_3 to be considerably greater than k_2; but with $k_4 >>> k_5$, the result is

$$-d[C_2H_2]/dt = 2[C_2H_2]^2 k_3(k_1/k_2) \quad (6)$$

At higher temperatures, k_5 will compete with k_4 and the chain length

will be reduced. In the limit that $k_5 >> k_4$, continuing to assume $k_3 >> k_2$, the steady-state treatment yields

$$-d[C_2H_2]/dt = 3k_1[C_2H_2]^2 \quad . \qquad (7)$$

This rate will be substantially less than that given by the previous result, if extended to high temperature. The consequence is that at the temperature where k_5 begins to compete effectively with k_4, an Arrhenius plot of the apparent second-order rate constant should begin to show a decreasing slope. Once the condition, $k_5 >> k_4$, is reached, the slope will rise again to that characteristic of k_1.[5] This seems to conform rather well to the plot in Fig. 4. The transition region for k_4 versus k_5 appears to begin at about 900°K and extends to about 1400°K.

The high-temperature results cited earlier now yield

$$k_1 = 1.1 \times 10^{14} \exp(-50 \text{ kcal/RT}) \text{ cc/mole sec}$$

and, using this k_1, the low-temperature results of Silcocks yield

$$(k_3/k_2) = 1.60 \times 10^{2} \quad .$$

If we require that $(k_4/k_5) = 10(k_3/k_2)$ at 700°K and $(k_4/k_5) = 0.2$ (i.e. $<< 1$) at 1400°K, the temperature dependence of (k_4/k_5) is found to be

$$(k_5/k_4) = 4.2 \times 10^{4} \exp(-25.1 \text{ kcal/RT}) \quad .$$

Employing these three parameters, k_1, (k_3/k_2), and (k_5/k_4), Equation 4 may be used for a computation of the second-order rate constant over the whole temperature range. The result is shown by the solid curve in Fig. 4. The fit seems quite successful, particularly when it is realized that the C_2H_2 disappearance rates reported by Munson and Anderson may have been appreciably enhanced by heterogeneous decomposition on carbon particles formed in their reactant stream. It is not possible to make a correction for this effect; the point is that the k_b values computed from their results are probably too large.

Some comment on the parameters is in order. k_1 has a surprisingly large pre-exponential factor, in view of the violation of spin conservation in reaction 1. However, in a recent study of SO_2 decomposition, Gaydon et al. (20) have found that unimolecular excitation of SO_2 to its lowest triplet state appears to be aided by energy transfer from internal degrees of freedom. This has the effect of raising the pre-exponential factor so as to largely compensate for the forbiddenness of the reaction. The apparent energy of activation is lowered in such a case. In C_2H_2-C_2H_2 collisions, there are many possibilities for energy transfer from internal modes and it is possible to rationalize k_1 on this basis. If the interpretation is correct, then the true activation energy of step 1 probably lies between 55 and 60 kcal, and a simple Arrhenius expression for k_1 is not very realistic. However, refinement of k_1 does not yet seem justifiable.

The (approximate) temperature independence of (k_3/k_2) is about what one would expect on the basis of the earlier discussion of these reactions. The magnitude of the ratio, i.e. 160, is also reasonable.

As for (k_5/k_4), the large ratio of pre-exponential factors is not unexpected, but no particular significance can be attached to the 25 kcal difference in activation energies except to say that it seems consistent with the experimental results of Robertson et al. (19). Beyond this, our ignorance of the details of the postulated steps 4 and 5 is almost total.

A final remark should be made on the report by Skinner and Sokoloski (11) that the rate constant for formation of vinylacetylene below about 1500°K lies above the low-temperature extension of their results for conversion to all products at temperatures above 1500°K (points shown in Fig. 4). If the result is real, it presents a severe complication. We would suggest tentatively that their low yields of vinylacetylene may have led to analytical errors, as indicated to some extent by their difficulty in obtaining a mass balance on reactants plus products.

Conclusions

It is possible to reconcile most low- and high-temperature data in the literature on acetylene pyrolysis by a chain mechanism in which the main chain-ending reaction has a stronger temperature dependence than does one of the chain-carrying reactions. This leads to long chains at low temperatures and essentially non-chain behavior at high temperatures. It seems very probable that the first step in the mechanism is excitation of C_2H_2 to its lowest-lying triplet state, and that one of the chain steps is a spin-exchange reaction.

In systems possessing high surface-to-volume ratios, e.g. in heavily sooting systems, a first-order heterogeneous decomposition reaction, the products of which appear to be principally carbon and CH_4, is expected to dominate the kinetics.

Acknowledgment

We are indebted to the U. S. Atomic Energy Commission for partial support of this work under Contract AT(30-1)-1710.

References

1. G. J. Minkoff, D. M. Newitt, and P. Rutledge, J. Appl. Chem. 1957, 406.
2. G. J. Minkoff, Can. J. Chem. 36, 131 (1958).
3. C. G. Silcocks, Proc. Roy. Soc. A242, 411 (1957).
4. F. C. Stehling, J. D. Frazee, and R. C. Anderson, Sixth Symposium (International) on Combustion, New York, Reinhold (1957), p. 247.
5. F. C. Stehling, J. D. Frazee, and R. C. Anderson, Eighth Symposium (International) on Combustion, Baltimore, Williams and Wilkins (1960), p. 775.
6. M. S. B. Munson and R. C. Anderson, Carbon 1, 51 (1963).
7. C. R. Kinney and R. S. Slysh, Proceedings of the Fourth Carbon Conference, Oxford, Pergamon Press (1960), p. 301.
8. G. D. Towell and J. J. Martin, A.I.Ch.E. Jour. 7, 693 (1961).
9. C. F. Aten and E. F. Greene, Combustion and Flowe 5, 55 (1961).
10. W. J. Hooker, Seventh Symposium (International) on Combustion, London, Butterworths (1959), p. 949.
11. G. B. Skinner and E. M. Sokoloski, J. Phys. Chem. 64, 1952 (1960).
12. J. N. Bradley and G. B. Kistiakowsky, J. Chem. Phys. 35, 264 (1961).
13. J. D. Chase and F. J. Weinberg, Proc. Roy. Soc. A275, 411 (1963).
14. C. F. Cullis, Dept. of Chemical Engineering and Chemical Technology, Imperial College, London; private communication of work in press.
15. G. J. Minkoff and C. F. H. Tipper, Chemistry of Combustion Reactions, London, Butterworths (1962).
16. F. L. Dormish, M. S. Thesis, Dept. of Fuel Technology, The Pennsylvania State University, University Park, Pa., 1962.
17. K. J. Laidler, The Chemical Kinetics of Excited States, Oxford, 1955.
18. J. H. Thomas, Trans. Faraday Soc. 48, 1142 (1952).
19. W. W. Robertson, E. M. Magee, J. Fain, and F. A. Matson, Fifth Symposium (International) on Combustion, New York, Reinhold (1955), p. 628.
20. A. G. Gaydon, G. H. Kimbell, and H. B. Palmer, Proc. Roy. Soc. A276, 461 (1963).

Table I.

Summary of experimental data on the decomposition rate

1333°K#			1433°K#			1528°K#		
c.t.* (sec)	C_o (mole %)	% Dec.	c.t.* (sec)	C_o (mole %)	% Dec.	c.t.* (sec)	C_o (mole %)	% Dec.
0.100	0.58	3.9	0.100	0.50	8.2	0.046	0.50	9.1
0.150	0.57	5.6	0.150	0.22	11.2	0.094	0.50	18.2
0.150	0.81	6.3	0.150	0.27	11.4	0.150	0.50	31.2
0.150	0.96	6.5	0.150	0.52	12.8	0.150	0.69	37.7
0.150	1.02	7.2	0.150	0.97	14.3	0.150	0.78	39.7
0.150	1.28	7.5	0.150	1.25	16.5	0.180	0.50	37.0
0.200	0.52	7.5	0.150	1.30	16.8	0.190	0.50	37.8
			0.200	0.53	18.1			

Hot zone temperature.

* Nominal contact time = (hot zone volume)/(vol. flow rate at hot zone temperature).

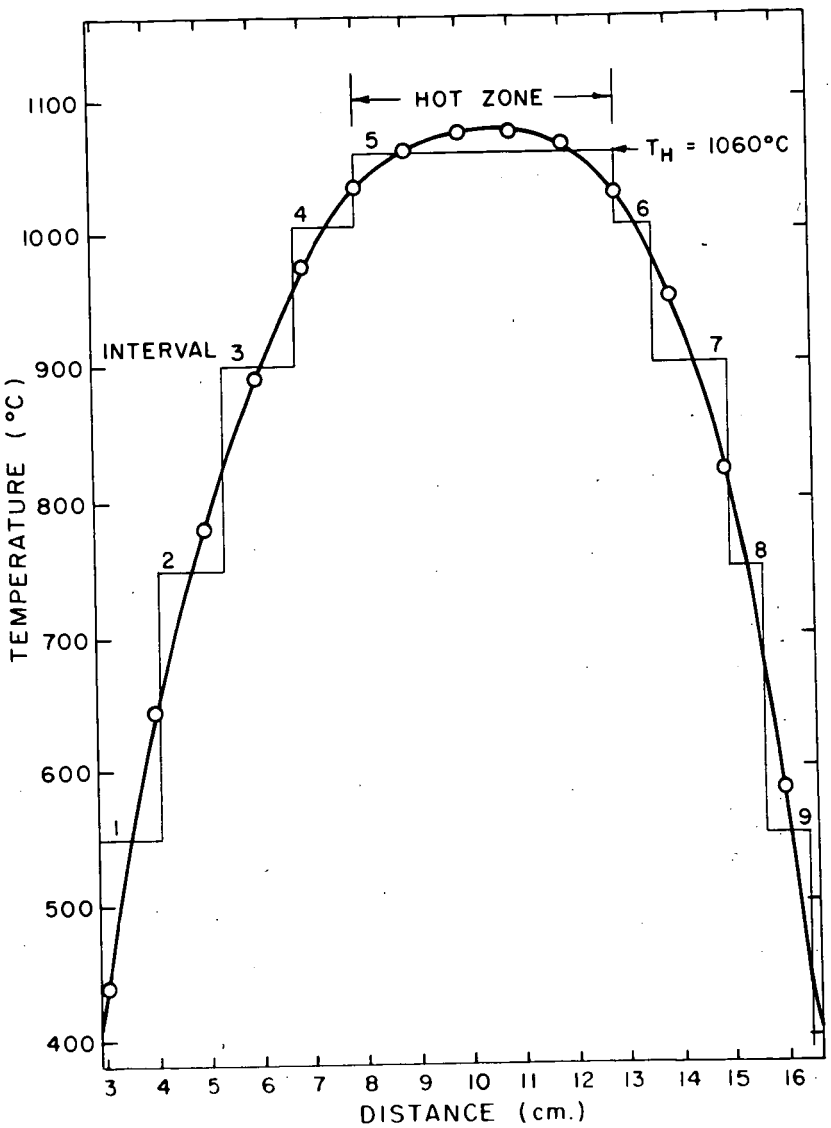

Fig. 1. Temperature profile for the furnace having the hot zone at 1060°C (1333°K). The "staircase" approximation to the profile is illustrated.

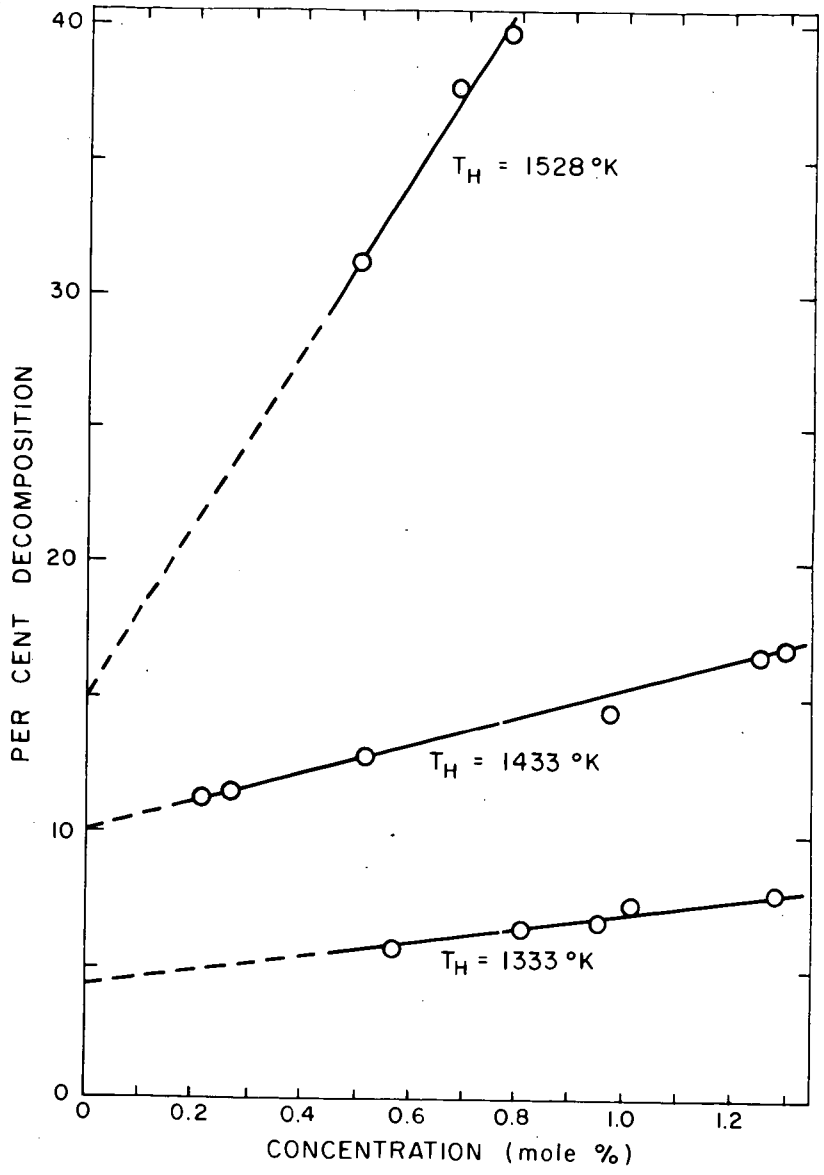

Fig. 2. Effect of change in initial concentration upon extent of decomposition at fixed contact time (0.150 sec).

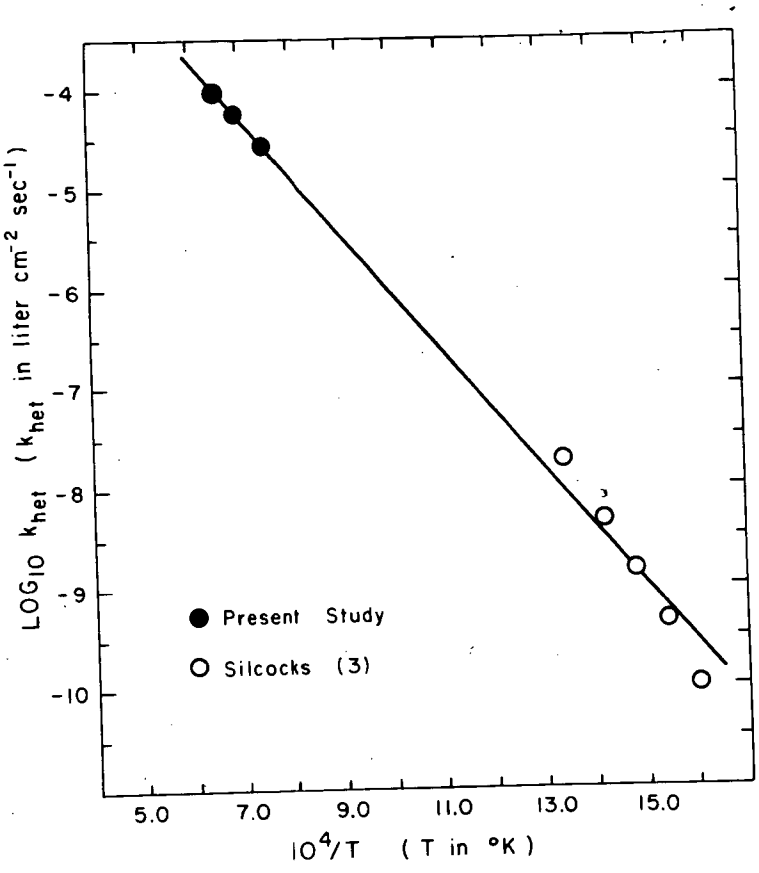

Fig. 3. Arrhenius plot of heterogeneous rate constants for C_2H_2 decomposition from the present work and from Silcocks (3).

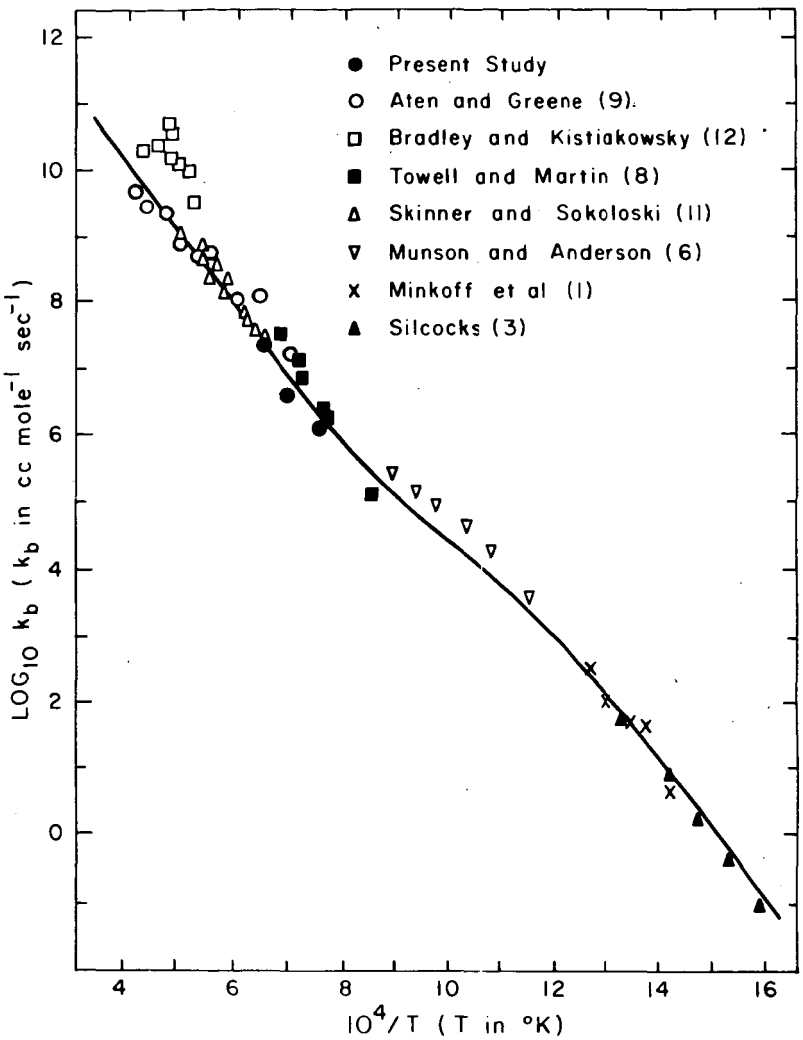

Fig. 4. Arrhenius plot of second-order rate constants for acetylene decomposition from the present work and from the literature.

Shock Tube Study of the Acetylene - Oxygen Reaction

R. F. Stubbeman* and W. C. Gardiner, Jr.

Department of Chemistry, The University of Texas, Austin, Texas

A number of investigations of the high temperature combustion of acetylene have been reported in recent years. The techniques employed have included probe studies of low pressure flames, spectroscopic studies of atomic flames, and various observations on detonation and shock waves in acetylene - oxygen mixtures. We report here a shock tube study of visible continuum emission, ultraviolet emission and OH absorption in incident shock waves through acetylene - oxygen mixtures.

EXPERIMENTAL

The shock tube was constructed of 2" x 4" aluminum tubing. Observations were made through quartz and lucite windows mounted flush with the tube walls. Velocity measurements were made with a series of flush resistance gauges spaced on either side of the observation station. Continuum emission was observed through the lucite window using an interference filter of about 80 A bandwidth centered at 4320 A for wavelength selection and a 1P28 photomultiplier tube for detection. The photomultiplier current pulses were amplified and then converted to logarithmic scale with a high frequency operational amplifier for oscilloscope recording. Ultraviolet emission was observed using a Beckman DU monochromator for wavelength selection and a 1P28 for detection. Absorption studies were made using a light source consisting of a microwave discharge in about 10 mm of argon containing a trace of bismuth vapor. The bismuth resonance line at 3067 A was isolated with the DU monochromator and used for monitoring OH concentration. Sensitivity of the absorption system was calibrated by observations of OH concentration at chemical equilibrium in shocks through H_2-O_2 mixtures. The arrangement of the equipment was such that either OH absorption or ultraviolet emission could be observed simultaneously with the continuum emission, and that the origin of the effects observed in the two measuring systems was identical with maximum error of 3 microseconds. The shock tube was readily evacuated to the 10^{-5} mm range and had an outgassing and leak rate of about 2 microns per hour.

Experimental mixtures were prepared in a conventional mercury-pumped vacuum system. The acetylene concentration was about one percent and oxygen concentrations varied from .34 to 7.3 percent, the remainder being argon diluent. Conventional precautions in purification and mixing were observed. Initial pressure in all experiments was 5 mm. No-reaction temperatures computed from shock velocities covered the range 1500 - 2200 °K.

*Present address: Esso Research and Engineering Company, Linden, N. J.

RESULTS

Both the visible and the ultraviolet radiation appeared as a pulse, following an induction period. The ultraviolet emission, which was observed at 2196 A, was far weaker than the visible emission, but both had essentially the same pulse shape and appeared simultaneously. Hydroxyl radical concentration rose to values above the detectability threshold, about 10^{-8} moles/liter in these experiments, just the emission pulses were returning to baseline.

Induction times defined by appearance of OH could be plotted as log $(O_2)x t_i$ versus 1/T as in the hydrogen - oxygen study of Schott and Kinsey or in earlier studies of the acetylene - oxygen reaction by Kistiakowsky and coworkers. The resulting plot showed that the OH induction times were about 2-3 times longer than induction times previously measured for this reaction using observations of onset of density change due to heat release in reaction, vacuum ultraviolet emission or ionization to define the end of the induction periods.

Time constants for the exponential rise in intensity of the continuum emission were obtained from the linear portions of the logarithmically recorded pulses. These, when plotted in the above form, showed no temperature dependence, in contrast to the strong temperature dependence (activation energy about 20 kcal/mole) found by Kistiakowsky and Richards for the time constants of the vacuum ultraviolet exponential rise.

The lack of temperature dependence for the exponential rise constants led to a very strong temperature dependence of the ratio of continuum emission induction time to decadic time constant, which is a measure of the number of decades of concentration through which the emitting species rises as chain branching reactions proceed. At 1800 °K these values scattered around 30, but at 2100 °K they were down to less than 10.

Peak intensity of the continuum pulses was also strongly dependent on temperature. Between about 1600 °K and 2100 °K this was found to increase by about a factor of 10. Emission was strongest in mixtures near stoichiometric.

A search was made for structure in the ultraviolet emission intensity in the region 2000 - 2200 A. This was done in a series of shocks of nearly constant strength in a lean mixture. The intensity distribution appeared to be uniform.

DISCUSSION

Previous shock tube studies on this reaction indicated that the main reaction sequence of the induction period could be understood in terms of the following branching chain sequence:

$$H + O_2 \rightarrow OH + O$$
$$O + C_2H_2 \rightarrow OH + C_2H$$
$$OH + C_2H_2 \rightarrow H_2O + C_2H$$
$$C_2H + C_2H_2 \rightarrow C_4H_2 + H$$
$$C_2H + O_2 \rightarrow 2\,CO + H.$$

This mechanism was proposed in order to account for the similarity of H_2 - O_2 and C_2H_2 - O_2 induction period behavior and for the appearance of diacetylene in mass spectrometric studies of shocked C_2H_2 - O_2 mixtures. Several features of the high temperature reaction are not accounted for, as for example ionization or the appearance of formaldehyde; this provisional mechanism would have these features considered as side reactions not contributing to the main chain. Any side product whose concentration depends on the concentration of main chain species, however, is a satisfactory disgnostic for the progress of the chain reactions. It was proposed by Hand, for example, that the vacuum ultraviolet radiation observed by Kistiakowsky and Richards was due to excited CO produced by reaction of O with CH produced by oxidation of C_2H. The CO emission, therefore, would be an indirect measure of the chain carrier concentrations at any given time. Likewise, the continuum emission observed in this work comes from electronically excited CO_2, which is produced from reaction of O with CO, and is, therefore, also an indirect measure of chain reaction progress.

Consideration of this reaction sequence shows that OH concentration should become observable when the chain has progressed to the point of giving macroscopic evidence of reaction, i.e. final products or heat evolution. In this work, however, it was found that the OH concentration rises only much later, after most of the final products have been formed. It follows, therefore, that OH is rapidly suppressed against its high rate of production in the chain by other reactions. When the acetylene concentration begins to decrease, this could be

$$OH + CO \rightarrow CO_2 + H.$$

The decay of continuum and ultraviolet radiation appeared to be simultaneous under all conditions, indicating that they probably have a common source. Since one of the reaction partners producing the emitter of the continuum radiation is a stable product, O is the most likely candidate for this role. Its destruction can only be by a final product. A probable pathway is

$$O + H_2O \rightarrow OH + OH.$$

The lack of temperature dependence found for the exponential growth constant is probably complex in origin. It is likely to be due to a counterbalance of the increasing rate of chain center multiplication, as temperature increases, by increased rate of destruction of those particular species leading to the continuum emission, namely O and CO.

Failure to find the CO 4th positive system in the 2000 - 2200 A region is probably due to instrumental limitations.

This work was supported by the U.S. Army Research Office - Durham.

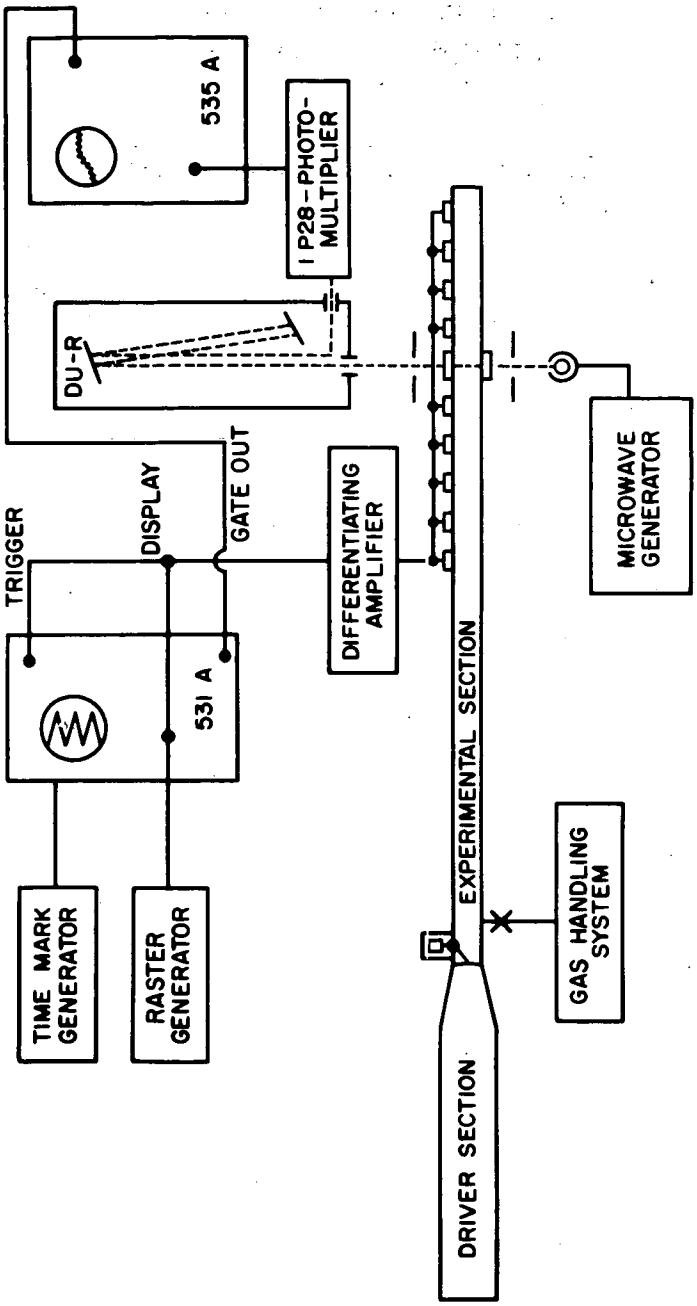

Fig. 1. Block Diagram of Apparatus.

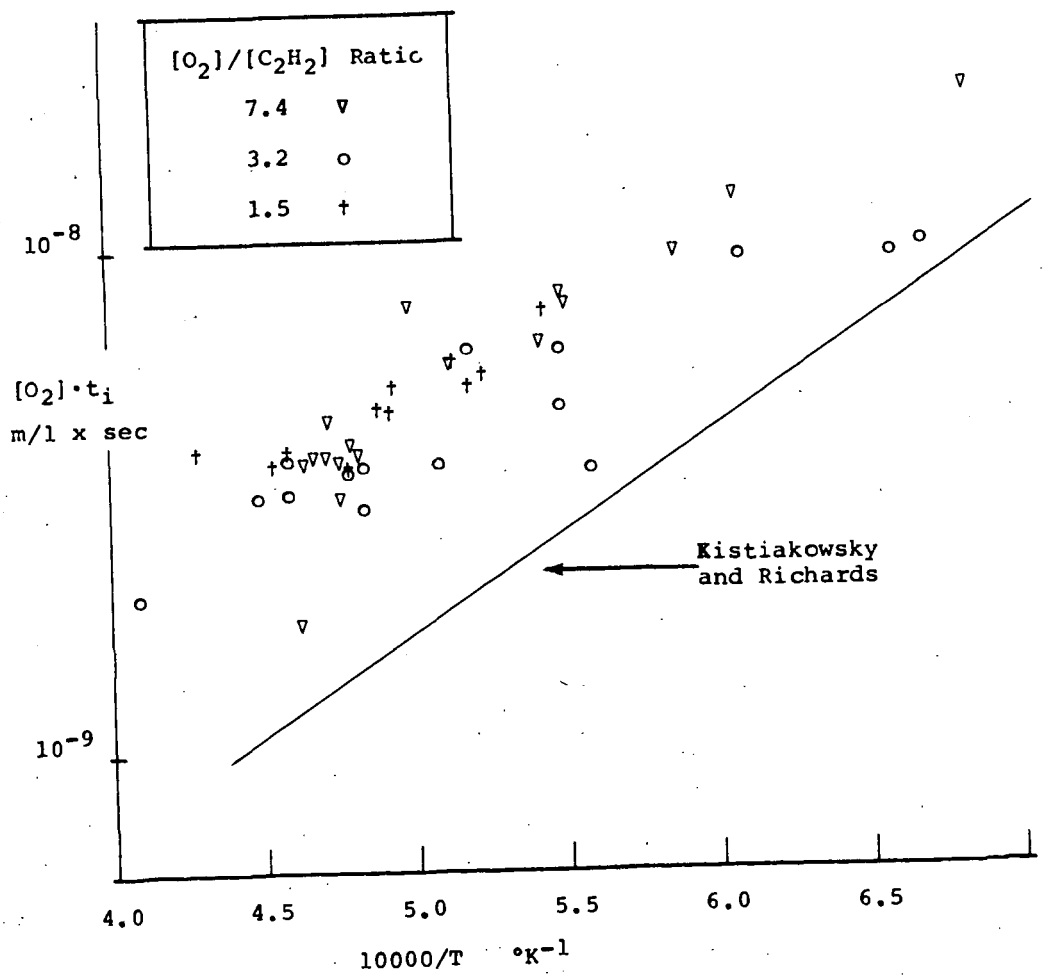

Fig. 2. Induction Times for OH appearance.

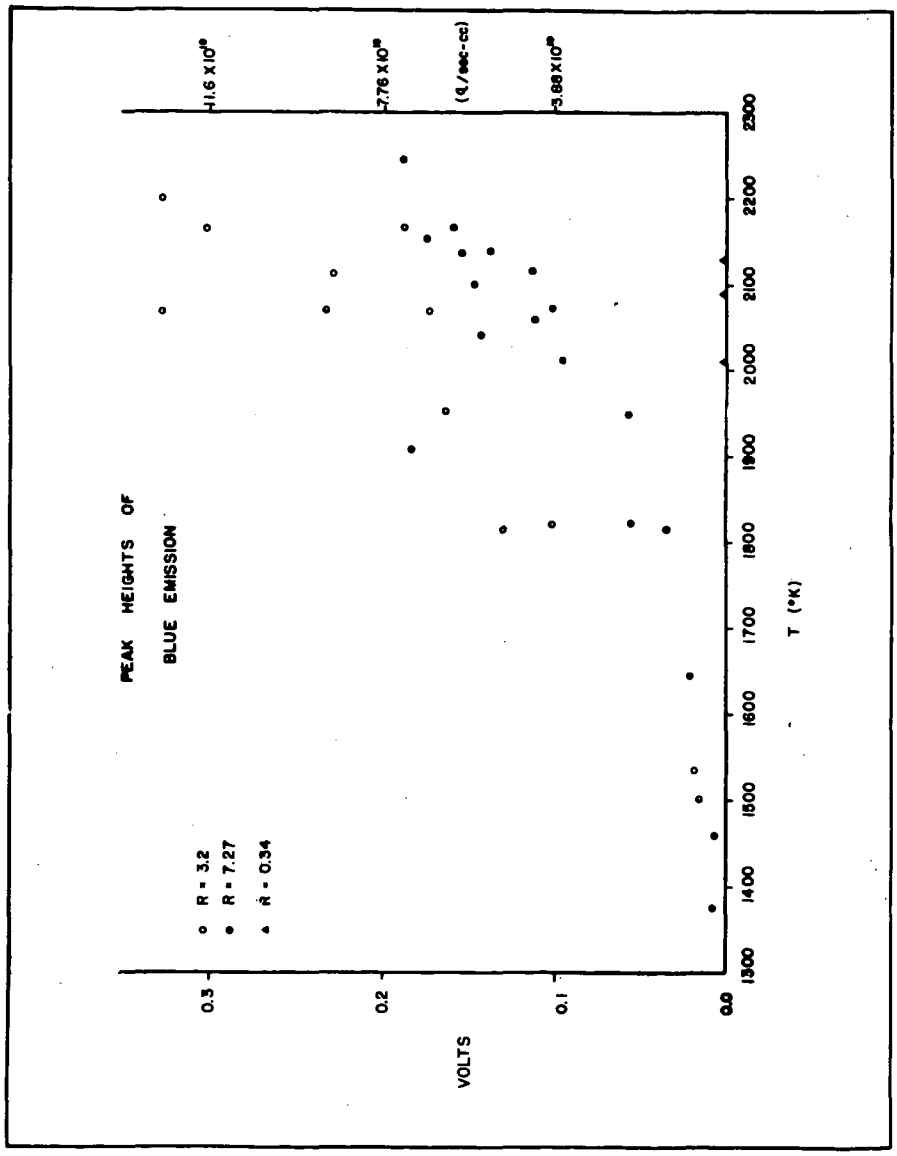

Fig. 3. Peak Intensity of Continuum Emission.

Chemi-ionization Reactions in High Temperature Hydrocarbon Oxidation

Joe V. Michael and Graham P. Glass

Chemistry Department, Harvard University, Cambridge, Mass.

Introduction

The mechanism of chemi-ionization in hydrocarbon oxidation reactions has attracted much interest in recent years. Ionization in hydrocarbon flames has been studied by means of Langmuir probes,[1,2] mass spectrometric sampling,[2,3] and microwave attenuation measurements.[4,5] By using these techniques the concentration of ions in the flames of lower hydrocarbons has been measured and has been shown to be too great to be accounted for by thermal excitation. Most investigators agree that the ions are formed by chemical reactions but the nature of these reactions as yet is not absolutely clear. The high heats of formation of most organic ions places severe energetic restrictions on the reaction which produces ions, and much effort has been spent considering reactions exothermic enough to do this. The reaction, $CH + O = CHO^+ + e^-$, has been suggested as a probable ion forming reaction, but no conclusive evidence for it has been found. To be sure CHO^+ (mass 29) has been observed by many investigators in flames, but it has always appeared in concentrations much below that of the more abundant ions (e. g. H_3O^+). Calcote[6] has pointed out that CHO^+ would be expected to undergo rapid proton transfer reactions with water, a product of these oxidations, thus explaining its presence in such low concentrations.

Calcote[2] has detected the $C_3H_3^+$ ion in a mass spectrometric investigation of low pressure acetylene-oxygen flames. This ion was observed in the flame profile ahead of H_3O^+ in quite large concentrations and its abundance was independent of the stoichiometry of the flame. It is diffucult to account for these observations on the basis of charge transfer reactions from CHO^+.

The work described in this paper was performed using shock tubes, and the reactions which occur during the oxidations of both methane and acetylene were studied by means of a Langmuir probe and also by means of a time-of-flight mass spectrometer which was adapted to detect the chemi-ions formed during the reactions.

Experimental

The apparatus in which the Langmuir probe measurements were made was substantially the same as that described by Hand and Kistiakowsky[7]. Shock waves were generated in a three inch I. D. steel tube and shock wave velocities were measured by gold film resistance gauges the outputs of which were displayed on a raster sweep oscilloscope. Radiation from the heated gas behind the shock wave passed through a lithium fluoride window and was detected by means of an RCA 1P28 photomultiplier. An interference filter was used to isolate the $A^2\Delta \rightarrow X^2\pi$ system of CH. The probe consisted of a 12 mil diameter tungsten wire placed in the shock tube in a plane defined by the optical slits. All but the last one-quarter inch of the wire was insulated with Armstrong A2 cement, the tip of the probe being near the shock tube axis. The major modification to the apparatus was the introduction of a removable piston which could be placed seven millimeters behind the cross sectional plane which contained the probe. This allowed the reactions in the stationary gas behind the reflected shock to be studied, thus removing the complicating effect of the aerodynamic interaction of the moving gas with the probe[7].

The second technique combines a shock tube and a Bendix time-of-flight mass spectometer in a redesigned apparatus which is a significant improvement over the one described by Bradley and Kistiakowsky[8]. Complete mass spectra of the reacting gases can be obtained every 20 or 50 μsec. Data is recorded by means of Polaroid 10000 ASA speed film. Normally a total of twenty-one spectra are displayed on three Tektronix 531-A oscilloscopes so that the amount of observable reaction time is a little over a millisecond with 20 KC operation. The mass range can be adjusted at will before the start of an experiment.

Sampling is through a small pinhole (.004 in. diameter) in the tip of a small conical nozzle (1 mm. by 1 mm. pointed away from the mass spectrometer) at the end of the shock tube. It is felt that this small nozzle reduces problems caused by boundary layer build up on the reflection plate onto which the nozzle is mounted.

The shock tube is one inch in diameter and 2.75 meters long. Shock velocities are measured with four thin film resistance gauges (either Pt or Au) spaced ten centimeters apart. The signals from these gauges are displayed on a raster oscilloscope. Shock temperatures are calculated using ideal shock relations in both incident and reflected shocks.

All experiments with the time-of-flight mass spectrometer reported here were carried out with five percent reactants in ninety-five percent krypton. The experiments with the Langmuir probe apparatus were carried out with one percent reactants in ninety-nine percent argon.

Results

Ions and stable products were observed using the time-of-flight mass spectrometer in the oxidations of both acetylene and methane. Both types of species arose concurrently after an induction period characteristic of a branching chain reaction. In both systems the total ionization was observed using the Langmuir probe technique. The ionization rises exponentially with time and the measured time constants provide a convenient method for determining the rates of the branching chain reactions. Ionization is not, however, a major part of the reaction since, for example, in the oxidation of acetylene, the maximum concentration which the ions achieved was about 10^{8} ions/cc. This was 10^{-6} of the initial acetylene concentration.

The individual ions produced were indentified with the time-of-flight mass spectrometer. The largest mass peaks in the acetylene-oxygen system were 39 and 19. 39, 31, 19, and 37 were observed in the methane-oxygen system. By using deuterated acetylene and methane the following assignments were made for the different species:

$$39\text{-}C_3H_3^+ \ ; \ 31\text{-}CH_3O^+; \ 37\text{-}H_3O\cdot H_2O^+; \ 19\text{-}H_3O^+.$$

Figure 1 shows the time history of the ionization in two typical experiments with acetylene-oxygen. It is seen that $C_3H_3^+$ is the first ion observed followed later by H_3O^+. In these experiments the reactant mixtures were: (A) 3 O_2 + 2 C_2H_2 + 95 Kr, and (B) 3.75 O_2 + 1.25 C_2H_2 + 95 Kr. Ionization was not observed in mixtures where acetylene was in excess over oxygen.

$C_3H_3^+$ was also the first ion observed in the oxidation of methane. CH_3O^+ arose at nearly the same time as did $C_3H_3^+$ but its concentration was much lower. H_3O^+ and $H_3O\cdot H_2O^+$ arose concurrently at still later times.

In the acetylene-oxygen system the time constant measured for the growth of ionization, using the Langmuir probe technique, was found to be identical to that measured for the simultaneous growth of chemi-luminescent radiation from the CH ($A^2\Delta \longrightarrow X^2\pi$) system.

In earlier experiments with the time-of-flight mass spectrometer, the stable products observed in the oxidation of acetylene were CO, H_2O, CO_2, and C_4H_2.[8,9] These results were confirmed in the present study. CO, CO_2, H_2O, and C_2H_2 were observed as stable products in the methane-oxygen system. CO_2 was a major product in 3 O_2 + 2 CH_4 + 95 Kr, and it was absent in 1.4 O_2 + 3.6 CH_4 +95 Kr. C_2H_2 was found to be a major product in the latter mixture but was formed in quite small quantities in the former.

Discussion

$C_3H_3^+$ has been observed by several investigators in hydrocarbon

oxidation systems. As has been stated previously, Calcote[2] detected this ion ahead of H_3O^+ in a dilute low pressure flame of acetylene and oxygen. Green and Sugden[3] have also observed this ion in flames at somewhat higher pressures. The following reaction schemes have been suggested by these workers for the formation of $C_3H_3^+$.

Calcote:

(1) $CH + O = CHO^+ + e^-$
(2) $CHO^+ + H_2O = H_3O^+ + CO$
(3) $H_3O^+ + C_3H_2 = C_3H_3^+ + H_2O$

Green and Sugden:

(1) $CH + O = CHO^+ + e^-$
(2) $CHO^+ + H_2O = H_3O^+ + CO$
(4) $H_3O^+ + CH_2O = CH_3O^+ + H_2O$
(5) $CH_3O^+ + C_2H_2 = C_3H_3^+ + H_2O$

In both of these mechanisms, $C_3H_3^+$ is formed by charge transfer reactions from CHO^+. However, the time history in the stationary gas behind a reflected shock wave is much better defined than in a flame where diffusion and cold boundary layer effects could invalidate measurements, and it is felt that $C_3H_3^+$, and CHO^+, is the first ion formed since it is the first ion observed in these experiments.

Two structures appear to be feasible for the $C_3H_3^+$ ion:

(A) $HC\equiv C-CH_2^+$ and (B) 

The cyclopropenyl ion (B) is believed to be the more probable structure, since it has great stability due to delocalization of its π electron system. Tri-substituted aliphatic and aromatic analogs of the cyclopropenyl ion have been synthesized[10] and halogen salts are completely dissociated in polar solvents. Furthermore, a plausible mechanism for it can be suggested which is energetically possible, whereas such a mechanism for the formation of (A) is difficult to justify on an energetic basis.

If (B) is the correct species it should be extremely stable and should undergo little or no charge transfer. The ion probably is removed from the system by chemical reaction, perhaps with oxygen resulting in the production of other ions. Indeed in experiments where oxygen is in excess the rate of fall off for $C_3H_3^+$ is faster and the total yield of H_3O^+ is greater that in experiments where oxygen is present in stoichiometric quantities (see Figure 1).

The following mechanism is proposed for the formation of $C_3H_3^+$:

$$(6)\quad CH + C_2H_2 = HC{=}\overset{\diagup\,\diagdown}{\underset{CH}{\diagup\,\diagdown}}CH^+ + e^-$$

The heat of formation has been determined by Wiberg et al[11] for $C_3H_3^+$ to be 271 kcal/mole. This value is higher than that estimated by a simple molecular orbital calculation coupled with thermodynamic considerations, and the value measured by Wiberg et al may refer to structure (A). However if the Wiberg value does apply to (B) then reaction (6) is nearly thermoneutral if the CH radical is in its $A^2\Delta$ or $B^2\Sigma^-$ state. If the calculated value is correct then the CH radical could even be in its ground state and reaction (6) would be close to thermoneutrality. Both CH ($A^2\Delta$) and CH ground state are known to be present in the oxidation of acetylene.[12,13] Since there is some evidence for the existence of acetylene in the oxidation of methane, reaction (6) could also explain the observation of $C_3H_3^+$ in this system.

The above mechanism has recieved some support from the observation of chemi-ionization in the reaction of iodoform and acetylene. The chemi-ionization had an "activation energy of formation" much below that usually found (55 kcal/mole), and the ionization was believed to be produced from the reaction of acetylene with the breakdown products of iodoform (CH and CHI).

This mechanism is also consistent with the observation that the time constants for the rise of ion concentration and CH($A^2\Delta \rightarrow X^2\pi$) radiation were identical in the early stages of the acetylene-oxygen reaction. However the mechanism, CH ($A^2\Delta$) + O = CHO^+ + e^-, which has previously been proposed[7] for the formation of ions in these systems is not consistent with this observation. Both CH ($A^2\Delta$) and O would be expected to be intermediates in the branching chain reaction, and therefore the concentrations of both would be expected to rise exponentially in the early stages of reaction. Thus the inverse time constant for the growth of ionization would be equal to the sum of the inverse time constants for the rise of CH and O concentrations.

The authors wish to thank Professor G. B. Kistiakowsky for his many helpful suggestions. We also wish to thank Dr. Hiromi Niki and Dr. J. L. Michael for help in the experiments with the time-of-flight mass spectrometer. The work with the Langmuir probe technique was supported by the Office of Naval Research and that with the time-of-flight mass spectrometer by the National Science Foundation.

Bibliography

1. Van Tiggelen, A.; Experimental Investigation of Ionization Processes in Flames, University of Louvain ARL Report 68, May, 1961.
2. Calcote, H. F.; Ninth Symposium (International) on Combustion, p. 622, Academic Press (1963).
3. Green, J. A. and Sugden, T. M.; Ninth Symposium (International) on Combustion, p. 602, Academic Press (1963).
4. Sugden, T. M.; Fifth Symposium (International) on Combustion, p. 406, Reinhold (1955).
5. Schneider, J. and Hoffman, F. W.; Phys. Rev. 116, 244 (1959).
6. Calcote, H. F.; Eighth Symposium (International) on Combustion, p. 184, Williams and Wilkins Co. (1962).
7. Hand, C. W. and Kistiakowsky, G. B.; J. Chem. Phys. 37, 1239 (1962).
8. Bradley, J. N. and Kistiakowsky, G. B.; J. Chem. Phys. 35, 256 (1961).
9. Dove, J. E. and Moulton, D. M.; To be published.
10. Breslow, R., Höver, H., and Hai Won Chang; J. Am. Chem. Soc. 84, 3168 (1962).
11. Wiberg, K. B., Bartley, W. J., and Lossing, F. P.; J. Am. Chem. Soc. 84, 3980 (1962).
12. Gaydon, A. G.; The Spectroscopy of Flames, p. 113, Chapman Hall, Ltd., (1957).
13. Gaydon, A. G., Spokes, G. N., and Van Suchtelen,J.; Proc. Roy. Soc. A256, 323 (1960).

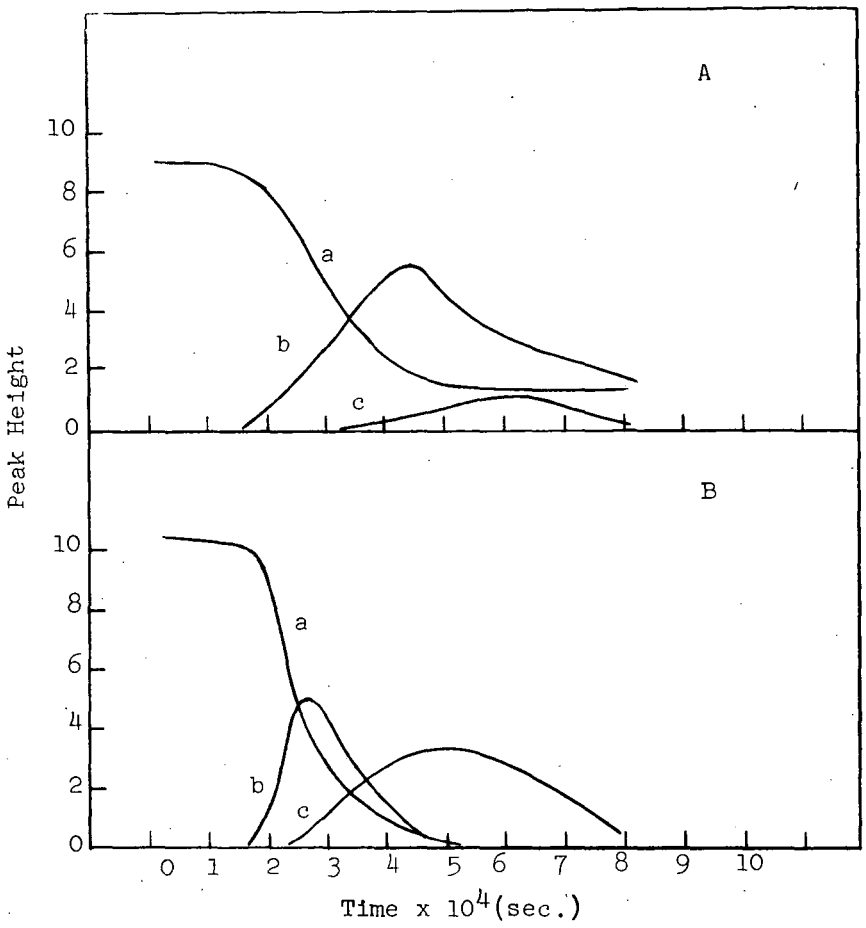

Figure 1. Height of ion peaks versus time in two experiments.

Experiment A:

2 C_2H_2 + 3O_2 + Kr at 1600°K;
curve a is acetylene, b is m = 39 ($C_3H_3^+$), c is m = 19 (H_3O^+).

Experiment B:

1.25 C_2H_2 + 3.75 O_2 + 95 Kr at 1700°K;
a, b, and c refer to the same species as in A.

SHOCK TUBE EVALUATION OF HYDRAULIC FLUIDS

Gordon B. Skinner

Monsanto Research Corporation, Dayton 7, Ohio

INTRODUCTION

While the shock tube has been used extensively in the study of gas-phase reactions, relatively few studies have been made of gas-liquid reactions. The main reason for this has been the difficulty in interpreting the data obtained when two phases are initially present, because the additional steps of drop break-up, evaporation and mixing need to be considered, as well as chemical kinetics.

A study of the combustion process when n-hexadecane is injected as a fine spray into shock-heated air was made by Mullaney (Ref. 1). By high-speed photography he was able to observe injection of the spray, evaporation of the droplets, and spontaneous ignition. In most of his experiments combustion started before evaporation was complete. Shock tubes have also been used by Morrell and co-workers (Ref. 2,3) and by Hanson, Domich and Adams (Ref. 4) to study the break-up of liquid jets by rapidly moving gas streams. These investigators used inert liquids to study atomization of the liquids without the complications introduced by combustion, and were able to obtain equations relating atomization time to physical properties of the liquid and gas.

The original intent of this work was to develop a method of rating the ignition characteristics of fire-resistant hydraulic fluids that could be related to the single-cylinder engine test (Ref. 5) currently used, yet require much less fluid for an evaluation. The results shed some light on the parameters governing liquid-gas reactions.

EXPERIMENTAL

The shock tube used for these experiments has been described in detail elsewhere (Ref. 6). Briefly, it is 3 inches in diameter, with 12-foot low-pressure and 20-foot high-pressure sections. Shock speeds are measured by timing the passage of a shock wave between stations 55 and 7 inches from the closed end of the low-pressure section. Gas temperatures and flow velocities are calculated from the shock speeds. A piezoelectric pressure transducer is mounted in the top of the tube, 3 inches from the closed end, while a fused quartz window (covered except for a 2 mm vertical slit) is in the side of the tube, also 3 inches from the end. Light emitted by combustion in the tube is detected by a photo-multiplier tube 8 inches away from the tube, which also was covered except for a 2-mm vertical slit. Because of the slits, light emitted only from gas 3 inches from the end of the tube was detected.

A 0.01 ml drop of the liquid to be tested was placed on an 18 gauge copper wire placed crosswise in the tube just below the quartz window. Since the wire curved downward slightly in the middle, the liquid remained together as a hanging drop, only a small fraction being in close contact with the wire. In all cases, the driver gas was helium at 85 psia, while the initial air pressure in the low-pressure section was variable.

RESULTS

The ignition time of a fluid sample is taken as that between the passage of the reflected shock past the pressure transducer and the moment when the light intensity reaches 10% of its maximum value. These ignition times have been plotted against the calculated temperature of the air behind the reflected shock wave. While the incident shock wave is important in causing break-up of the fluid droplet, the fluid droplets remain in the incident shock region for only about 0.3 millisecond compared to total ignition times of 1 to 5 milliseconds. Therefore the temperature behind the reflected shock wave seemed to be the most meaningful single number by which to characterize the experimental conditions.

Figure 1 shows the ignition delays found for xylene and three hydraulic fluids. MS-2110-H is essentially a light hydrocarbon lubricating oil, while MIL-H-19457 is a phosphate ester, one of the most fire-resistant fluids available of which the general formula is

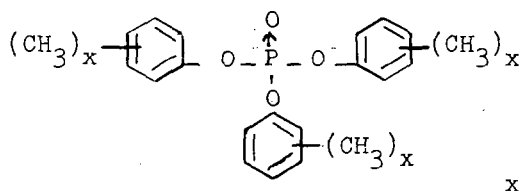

x = 0, 1 or 2

Since, in the engine test of Reference 5, the actual measured quantity is the compression ratio required to cause ignition of a spray of hydraulic fluid in 2 milliseconds time as the piston is approaching the top of its stroke, it is appropriate to compare the engine compression ignition rating (expressed as a compression ratio) to the reflected shock temperature required to give ignition of the fluid in 2 milliseconds. Engine compression ignition ratings of the above four fluids have been measured (Ref. 5), and have been plotted against the 2-millisecond shock temperatures in Figure 2. The correlation between the two tests is good, but the linear relationship found over the range covered experimentally cannot be expected to hold for higher or lower ratings.

Of a number of exploratory hydraulic fluids tested one, of formula

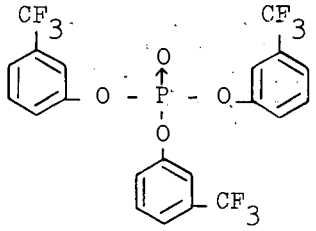

had the high ignition temperature of 1365°K., which from the extrapolation of Figure 2 would indicate an engine test rating of about 80.

DISCUSSION

There is, and probably will be for some time, a question as to the relative importance in the ignition process of the physical factors of drop break-up, evaporation, convective and diffusive mixing on the one hand, and chemical reactivity on the other.

Morrell and Povinelli (Ref. 3) have developed an equation for the time for break-up of liquid cylinders by shock waves, which should also apply approximately to drops. The break-up times of the 0.01 ml drops of "standard" liquids used in the above experiments have been calculated, as follows:

Liquid	Calculated Break-up Time, milliseconds
MS-2110-H	0.24
Fluid AV	0.31
Xylene	0.81
MIL-H-19457	0.25

These drop break-up times do not correlate with the ignition data, since the break-up times of the most and least flammable liquids are the same, while the calculated break-up times for Fluid AV and xylene, which have similar ignition temperatures, are different. Moreover, the boiling points of these latter two compounds differ considerably, being 325° and 140°C, respectively. It seems, therefore, that under these conditions the physical properties of the fluids are less important than chemical reactivity in controlling the ignition delays.

The author wishes to acknowledge the suggestion, made by Gordon H. Ringrose, that the shock tube could be used to test the reactivity of hydraulic fluids; and the assistance of Edward S. Blake and Ralph E. DeBrunner who furnished the experimental hydraulic fluids.

REFERENCES

1. G. J. Mullaney, Ind. Eng. Chem. 50, 53 (1963).

2. G. Morrell, Eighth Symposium (International) on Combustion, Williams and Wilkins Co., Baltimore, Md., 1963, p. 1059.

3. G. Morrell and F. P. Povinelli, NASA Lewis TP 3-63, Paper presented at Fifth Liquid Propulsion Symposium of the Chemical Propulsion Information Agency, Tampa, Florida, Nov. 12-14, 1963.

4. A. R. Hanson, E. G. Domich and H. S. Adams, Phys. Fluids 6, 1070 (1963).

5. C. L. Brown, NAVENGRXSTA Report 95 648 C, Fluid Structural Factors Versus Fire Resistance, November 1962.

6. G. B. Skinner and R. A. Ruehrwein, J. Phys. Chem 63, 1736 (1959).

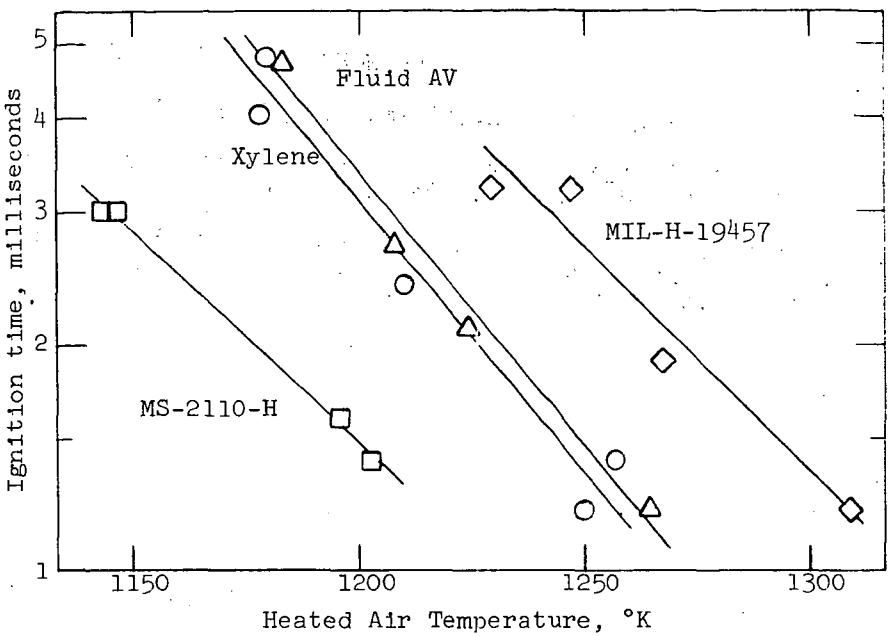

Figure 1. Shock tube ignition of hydraulic fluids

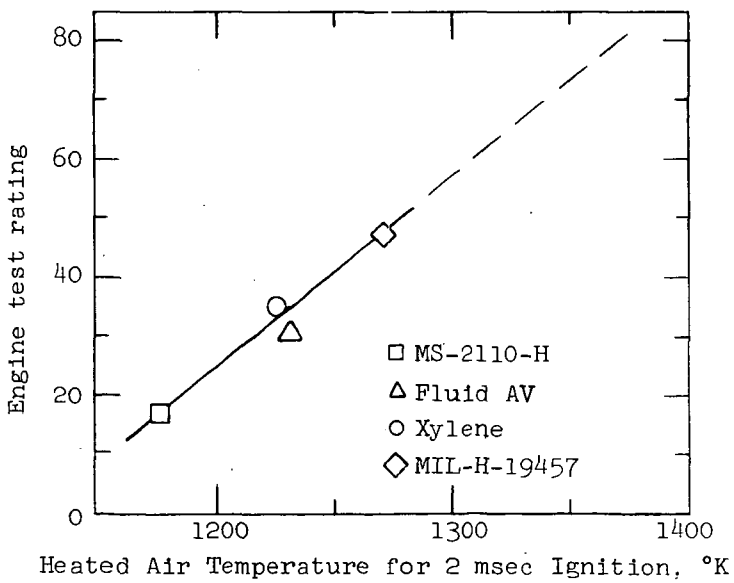

Figure 2. Calibration curve - shock tube versus engine test rating

On the Stability and Combustion Intensity of Pulverized Anthracite Flames

J. M. Beer

Pennsylvania State University
Department of Fuel Technology
College of Mineral Industries
University Park, Pennsylvania

ABSTRACT

Recent experiments on pulverized anthracite flames carried out by the International Flame Research Foundation at IJmuider (Holland) are discussed. It is shown that ignition is considerably aided by the entrainment of hot combustion products into the fuel rich primary jet. This indicates that it is advantageous if the mixing between the primary jet and the rest of the combustion air is preceded by the mixing of the primary jet with the hot combustion products. Experimental evidence to prove this point is presented. Flame stability improves also with finer grinding. Flame speeds in this case increase partly due to the increased radiation from the flame front owing to the burning of the fine particles and also due to the higher absorption of such a dust cloud. It is shown from the comparison of the values of "mixedness" and "reactedness" along the flames that the combustion of the solid residue follows mixing more closely in flames with finer ground pulverized anthracite. The rates of combustion of the anthracite calculated from measurements on jet flames are of the same order of magnitude as those determined in a laboratory "plug-flow" type flame.

Reaction Rates of Single Coal Particles: Influence of Swelling, Shape, and Other Factors

By Robert H. Essenhigh
Department of Fuel Technology, College of Mineral Industries
The Pennsylvania State University, University Park, Pa.

and G. C. Yorke
Department of Fuel Technology and Chemical Engineering
University of Sheffield, England

1. INTRODUCTION

Coal particles burning in oxygen-vitiated and enriched atmospheres, at about 1000°C, have been shown by Previous work (1,2,3) to burn in the expected two-stage process of: volatiles combustion; followed by burn-out of the solid carbon residue remaining. The same work also showed that the solid residues burned according to the Nusselt-predicted (4) "square-law", by which the burn-out time (t_b) was directly proportional to the square of the initial particle diameter (d_o). However, although the agreement between prediction of the residue behavior and experiment was generally found to be adequate to good (1,2) there were several questionable points in the theoretical assumptions made in the modified (5,6) Nusselt theory used. These assumptions centered principally on the suggested behavior of the particles on swelling, and the ultimate effect this could have on the combustion behavior, particularly if the particles formed hollow cenospheres (7,8). Several questions were set up by this, as follows: (1) How much did the particles swell? (2) Was this swelling reasonably isotropic? (3) How did swelling change with coal rank? (4) Did the particles form cenospheres? (5) Did cenosphere formation, if any, affect the mechanism of burn-out, and if so how would this affect the theoretical analysis? (6) What influence did particles shape have on the final shape after swelling, and therefore on the combustion behavior?

To answer these questions as far as possible, a number of particles from each of the 10 coals used in the previous investigations (1,2,3) were photographed during combustion, and it was found that reasonably satisfactory answers to all six questions were obtained with, in addition, further information on swelling properties of coal particles.

The purpose of this paper is now to describe the photographic experiments carried out, the results obtained, and the answers that were provided, by these, to the questions given above.

2. EXPERIMENTAL

Whilst the coal particles were burning, in the combustion unit described in the previous papers (1,2,6), they were photographed using a continuously running camera adapted to take intermittent exposures.

2.1 Combustion Unit - The method of burning the particles was exactly the same as that described in the first two publications of this work (1,2). The particles, in the size range 0.5 to 2 m.m., were cemented to fine silica

threads with a high temperature cement and then suspended, cantilever fashion, between two heating coils made of electrical resistance wire wound in flat spirals. These coils were about 1.5 m.m. across, and mounted with their planes horizontal about 1.5 m.m. apart. The coils were heated electrically, to about $1000^{o}C$.

2.2 Pyrolysis Unit - For a few experiments, carried out on one coal alone, the combustion unit described above was enclosed in a brass box, with observation windows, that could be flushed out with CO_2. This made it possible to observe the behavior, and measure the swelling of particles just pyrolysing without burning..

2.3 Optical Unit - To illuminate the particles, a 36-watt car headlamp bulb was placed at the focal point of a 10-cm. f.l. lens to produce a parallel beam of light. The particle combustion, or pyrolysis,unit, was placed in this parallel beam, about 20-cm. from the first lens, and about the same distance from a similar lens which then created a real image of the burning particle at about a one-to-one magnification. This image, therefore, could exist also as a real object, well clear of any heat source, that could be magnified to any required degree by a suitable short-focus objective close to this real object. The second image from this could then be projected onto a screen, or into a suitable camera.

2.4 Camera - The one used was a Cossor 35 m.m. Oscilloscope camera, with an adaptation to provide intermittent exposures on continuously moving film. A glass screen was lightly ground with abrasive and placed at the end of the camera tube, in the same relative position as that normally occupied by the Oscilloscope screen. The particle image provided by the optical unit was projected onto this screen, at a net magnification of about 5, and this image was then photographed (from the reverse side) by the Oscilloscope camera. This final stage diminished the image, but the overall magnification was still about 2. By trial and error it was found that the glass screen could not be too lightly, or too heavily ground: in the first instance the contrast between image and surroundings was too faint; and in the second, too little light was reaching the film.

2.5 Exposure Unit - Since the 35 m.m. recording strip was moving continuously, it would have blurred any time exposure that was of adequate duration to affect the emulsion used, even at the low speed of traverse involved. (The emulsion was on opaque recording paper, not on transparent film strip.) A rotating glass plate was therefore placed in the paralled light beam, between the particle and the second lens. As the plate rotated, it moved the image formed at the camera and, by adjusting the rate of rotation, the speed of motion of the image and recording paper could be matched (on the same principle as that used by the Fastax camera). This produced a clear image and, by incorporating a simple shutter, a series of single exposures could be taken. Finally, the rotation was synchronized with the camera by using gears and spindles of Meccano (a type of Errector set) to take a drive off the camera motor. Timing of the frames was then obtained by timing a given number of revolutions of the rotating plate.

2.6 Coal Preparation and Data - Information on grinding and sieving the coals is given in detail in the previous papers (1,2,6). They were crushed and ground by hand in a pestle and mortar, and then sieved mechanically using the complete sequence of British Standard sieves from 3/16" to 52 mesh (4760 to 295 microns). In these photographic studies, the particle sizes mostly used were about 2 m.m.

Table 1
Coal Analyses and Data

(1A) Ultimate Analysis (d.m.f.)

Coal	C	H	O	N	S	V	C_f	C_v	(C_v/C_f)
(1) Stanllyd (Blaunhirwaun)	93.00	3.35	1.59	1.33	0.73	9.9	90.1	2.9	0.03
(2) Five ft. (Deep Duffryn)	91.80	4.08	2.32	1.42	0.38	14.9	85.1	6.7	0.08
(3) Two ft. Nine -unknown-	91.20	4.35	2.54	1.65	0.26	28.8	71.2	20.0	0.28
(4) Red Vein (Cilely)	89.70	4.66	3.55	1.67	0.42	23.3	76.7	13.0	0.17
(5) Garw (Cwm Tillery)	88.90	4.99	4.50	1.33	0.28	30.6	69.4	19.5	0.28
(6) Silkstone (Elsecar)	86.90	5.79	5.50	1.51	0.30	41.5	58.5	18.4	0.49
(7) Winter (Grimethrope)	84.00	5.47	8.29	1.85	0.39	39.3	60.7	23.3	0.38
(8) Cowpen (Northumberland)	82.70	5.40	9.60	1.80	0.50	40.2	59.8	22.9	0.38
(9) High Hazel (Thorne)	81.90	5.57	10.52	1.58	0.43	40.7	59.3	22.6	0.38
(10) Lorraine (Faulquemont)	79.25	5.13	14.16	0.95	0.51	40.2	59.8	19.5	0.32

(1B) Proximate Analysis and Other Data

Coal	V.M.	H_2O	Ash	CO_2	B. S. Sw. No.	g/cc.	M	m
(1) Stanllyd	7.9	1.3	2.9	~~0.7~~3	n.c.	1.38	0.871	3.06
(2) Five ft.	12.6	0.9	3.9	0.26	1	1.40	0.993	3.20
(3) Two ft. Nine	28.9	0.8	22.2	13.3	1	1.36	1.150	3.15
(4) Red Vein	20.5	1.0	1.6	0.04	6 1/2	1.34	1.794	3.01
(5) Garw	27.7	1.0	3.7	0.05	4	1.31	0.934	3.04
(6) Silkstone	39.6	1.3	1.7	0.35	4½	1.28	0.690	3.00
(7) Winter	36.0	2.6	1.7	0.77	3	1.25	0.848	3.06
(8) Cowpen	34.6	7.3	4.1	0.95	1	1.27	1.000	3.17
(9) High Hazel	36.7	5.1	1.0	0.0	1	1.27	0.941	3.04
(10) Lorraine	35.0	5.0	5.9	0.52	n.c.	1.36	0.919	3.01

The coal analyses are given in Table 1, which also gives for the full particle size range, the size coefficients (M and m) in the empirical relation between weight (w_o) and initial diameter (d_o):

$$w_o = M.d_o^m \quad (1)$$

where M and m are empirical constants determined experimentally. The method for determining M and m has already been described (2) but, briefly, required the weighing of groups of particles from a number of sieve cuts to determine w_o (the mean weight per particle) at a given mean sieve aperture as diameter, d_o. The best values of M and m were then determined by the method of least squares.

3. THEORY

The "square-law" relation referred to in the Introduction was first derived by Nusselt (4) for heat and mass transfer to and from a sphere. This theory, and necessary modifications for application to swelling coal particles, has been adequately covered in the previous papers and publications (1-3,5,6); the purpose of this section is to indicate how the theory may be modified further if needle-like coal particles are treated as cylinders instead of spheres.

For both systems the approximation of single diffusion of oxygen through stationary nitrogen is used. The Stephan flow (9) is also neglected since the previous studies (1,2) showed this to be a valid approximation for oxygen in air and vitiated air atmospheres (though not for enriched atmospheres (3)).

The starting point for both theories (sphere and cylinder) is Fick's Law for diffusion:

$$g' = -D(dN/dr) \quad (2)$$

where g' is the number of molecules diffusing across unit area in unit time; D is the diffusion coefficient; and dN/dr is the oxygen concentration gradient at any distance r from the center of the sphere.

The next step is to write the continuity equation which is slightly different for each system. For the sphere we have:

$$a^2.g'_s = r^2.g' \quad (3a)$$

whilst for the cylinder

$$a.g'_s = r.g' \quad (3b)$$

This makes the difference in the solutions for g'_s since, on substitution for g' and integrating, we have:

sphere: $$-g'_s = D(N_o - N_s) / a \quad (4a)$$

cylinder: $$-g'_s = D(N_o - N_s) / a.\ln(r_o/a) \quad (4b)$$

where the subscripts to N are for the main stream values and the solid surface values respectively; a is the particle radius; and r_o in eqn. (4b) is the distance at which the main stream value of N is reached. In eqn. (4a) this is taken as infinity, and the term in r_o vanishes. In eqn. (4b) the equation becomes meaningless, if r_o is taken as infinity. All we can do then is to consider the equation for the mass transfer coefficient k. This is:

$$g'_s = -k(N_o - N_s) \qquad (5)$$

But the mass transfer coefficient is related to the Nusselt number for mass transfer by the definitive group;

$$Nu = k(2a)/D \qquad (6)$$

For the sphere, it can be shown from eqn. (4a) that in quiescent conditions, Nu takes the value 2. Experimentally, it has also been shown by data (10) quoted by Gruber and Erk (11) that Nu also tends to a constant value, of 0.43, for the cylinder in quiescent ambient conditions. If we assume that this holds generally, we than get the alternative equation for the cylinder:

$$-g'_s = 0.215D(N_o - N_s)/a \qquad (4c)$$

which, clearly, differs from eqn. (4a) only by the factor 0.215. From either equation, we have that the specific reaction rate is inversely proportional to the radius. Integrating, as in the previous analyses for the sphere, we get for the variation of diameter with time:

$$d^2 = d_o^2 - t/K \qquad (7)$$

where K is the burning constant, given by (2,5)

<u>for the sphere</u> $K_s = \sigma/3\rho_o D_o p_o (T/T_o)^{0.75}$ (8a)

<u>and for the cylinder</u> $K_L = K_s/0.215 = 4.65K_s$ (8b)

so a cylinder of radius a should still burn according to a square law, but take up to 4 or 5 times longer to burn out than a sphere.

3. RESULTS

3.1 <u>General Behavior</u> - In these photographic studies, between 30 and 40 particles were burned (compared with over a 1000 in the previous total-burnin time studies). The particles were mostly cubic in nominal appearance, this being the same principal basis of selection as in the previous studies, but a few were needle shaped particles selected to study the influence of shape.

The burning particles all exhibited the characteristic behavior of volatiles generation and combustion, with swelling during the volatiles combus phase; this was followed by residue burn-out. Diameters were measured from the photographic records and plotting the square of the diameter against frame number (as Time), to test eqn. (7), The Figures 1 and 2 show the type of plots obtained . Figure 1 is for the Stanllyd anthracite, and Figure 2 fo the Cowpen coal. In the latter, the effect of swelling is clearly illustrate by the sudden rise and fall of the curve at the start of combustion. Swellir in air is therefore a two-stage process; first there is a large expansion, followed by a contraction. In CO_2 there was only expansion, no contraction.

the end of the contraction, the line is seen to flatten out: this is the idue combustion. The curve of Fig. 2 is typical of all the bituminous ls, whatever their swelling number.

Swelling and Swelling Factor - f - The identification of the peak in Fig. 2 h the period of volatiles generation was more or less self-evident, but ther, positive identification was provided by simultaneously recording the ht output from the particle with a photocell. This technique had been d in the previous studies (1,2) to determine the total burning time, l it had been found during those that the period of volatiles evolution l combustion correlated with a characteristic trace in the record of the tocell output. This trace was a random high frequency oscillation due to flickering flame from the volatiles combustion. Identification of this aracteristic trace, and comparison with the photographs, showed that the rticles started to swell a little in advance of the start of the volatiles ibustion; the volatiles continued to burn right through the main expansion l contraction period; and the start of the residue combustion correlated .l with the start of the final linear portion of the plot of Fig. 2.

With this positive identification, measurements were then made of some egular shaped particles to check the degree of isotropism in the swelling. e particles selected for this were quite long, rectangular or needle-shaped rticles, the selection being based on the assumption that if they broke i-isotropically, they would be the most likely to swell non-isotropically. the event, they swelled quite uniformly, all dimensions changing in approxi-tely the same proportion, as with substantially all the other particles idied.

Swelling determinations were then carried out on selected particles of l the coals to determine their average swelling factors. The swelling ctor, f, was defined as the ratio (d_s/d_o), d_o being the initial, cold ameter, and d_s being the diameter at the start of the residue combustion. e values of this ratio, f, are summarized in Table 2 for the ten coals. As n be seen, the scatter is quite wide for any given coal, but the average very close to 1.5 for all the bituminous coals used, irrespective of the S. swelling numbers. This result was quite unexpected, and it raises in estion the meaning of such quantities as B.S. swelling number. The difference tween swelling factor and number is obviously dependent on the different perimental conditions in the methods of measurement. In contrast to the elling-factor measurements on single, unconstricted particles, as described ove, Swelling Number tests are made on groups of particles under some degree constriction, and are, therefore, partly able, and partly forced to swell to each other. Initially, at low volatile content in the bituminous range, ere is little loss, and therefore little increase in porosity. However, the volatile content (and loss) increases, there is more and more space adjoining particles for others to swell into, thus producing the characteristic inverted 'U' curve of the swelling or caking index against coal rank.

3 Residue Burn-Out - Study of the residue burn-out was the most crucial int examined. The particular point of interest here was in the change of ameter as the particle burned out. Sinnatt and others (7,8) had shown ny years ago that coal particles carbonizing in neutral or reducing atmospheres ll form hollow shells, generally known as cenospheres, the optimum tempera-rn of formation being between 600 and 700°C. If such a change occurred to e single particles before the residue combustion, then the theory of the sselt analysis, or any other similar analysis, would be quite inapplicalbe

since these depend on the assumption of reaction at the exposed nominal or superficial surface, alone; also the integral of the burning rate depends on the further assumption of uniform particle density, right down to zero radius.

This was in essence the basis of Ornings criticism (12) of one of the previous papers (2). Explicitly he mentioned the need to integrate to some finite radius as the lower limit, and not to zero radius. However, the experimental results do not support the expectations based on the cenosphere formation, but they do support the results based on the original assumption of uniform density right down to zero radius. The curves of the type of Fig. 2 show quite clearly that the results obey eqn. (10). This means that the rate of burning (dm/dt) is proportional to the radius or diameter, down to quite small radii. Few particles could be followed right down to zero radius because of the difficulty of measuring less than one millimetre on the recording strips, but most could be followed to between 70 and 90% loss of mass, so the agreement found over the measured range justified extrapolation to burn-out.

The slope of the burn-out section of the curves is given by eqn. (7) as 1/K. As a check on the magnitudes to be expected, these were calculated for many of the particles, and the values found ranged from 1000 to 2000 sq.cm./sec in good general agreement with the values previously reported (2). This is further substantiation of the conclusion that the particles are of uniform density right to the center. Because of the variation in the behavior of single particles, the scatter was about the same as that found for the total burning-time measurements made previously, but because of the much smaller numb of measurements made, these additional values have less meaning and precision compared with the previously determined values.

4. DISCUSSION

4.1 General - With the data available, there is little more that can usefully be added to comments already made on the foregoing results. To our mind these establish that the particles usually swell isotropically, with a swelling factor that is remarkably constant over a wide range of coal rank (10 to 40% V This alone is thought to be a point of considerable interest and importance. There was greater scatter in the swelling factor, f, between particles of the same coal than there was between the average values for different coals. This suggests that useful attention could well be directed towards pure maceral behavior as this might conceivably be responsible for the variations found. The particles evidently do not form cenospheres under these conditions though it is always possible that the peak swelling was a condition of true cenosphere formation, with destruction of the cenospheres as the temperature rose above the optimum for their formation. In this connection, it is not always realized that true cenosphere formation does not generally take place in oxidizing atmospheres above 1000°C. This again is thought to be a point worth further investigation. The only point not yet considered is the influence of shape factor.

4.2 Determination of Shape - To discuss the influence of shape, it is first necessary to determine what shapes the particles have. With the information on mass and diameter given in Table 2, considerable information can be obtained as to the most probable shapes of the particles. The mass/diameter data is correlated by eqn. (1). If we divide through by the coal densities, (Table 1), the data are converted to a volume/diameter correla Let us now consider a number of regular shapes as follows: (1) cube of side

(2) sphere of diameter d_o; (3) cylinder of diameter d_o and length d_o^{1+y}; (4) rectangular block of length d_o^{1+x}: (i) with square cross section of side d_o: (ii) with rectangular cross section of sides d_o and d_o^{1+y}; (5) spheroids, in both forms: (i) oblate and (ii) prolate, with minor axes of length d_o and major of length d^{1+x}. These all have volumes that can be related to the dimensions with a multiplying factor, F, as in the Table following:

Table 3

Particle Shape Factor, F

3. (A) Regular Shapes

	Volume	Factor (F)
1. Cube	d^3	1
2. Sphere	$(\pi/6)\,d^3$	0.524
3. Cylinder	$(\pi/4)d^{3+x}$	0.7855
4. Rectangular block		
(i) regular	d^{3+x}	1
(ii) irregular	d^{3+x+y}	1
5. Spheroid		
(i) oblate	$(\pi/6)\,d^{3+2x}$	0.524
(ii) prolate	$(\pi/6)\,d^{3+x}$	0.524

3. (B)

	Coal Data (x + y)	F	K(calc)	K(expt)	K(calc)/K(expt)
1. Stanllyd	0.06	0.63	2680	2125	1.26
2. Five ft.	0.20	0.708	1725	1290	1.34
3. Two ft. Nine	0.15	0.845	1365	1470	0.93
4. Red Vein	0.01	0.592	1500	1475	1.02
5. Garw	0.04	0.713	1335	1610	0.95
6. Silkstone	0.00	0.54	1080	1110	0.97
7. Winter	0.06	0.674	1095	1125	0.97
8. Cowpen	0.17	0.787	1055	1060	1.00
9. High Hazel	0.04	0.735	1075	1450	0.74
10. Lorraine	0.01	0.675	1165	992	1.07

From this it can be seen that the cube and rectangular blocks have F factors of unity; the sphere and spheroids, values of 0.524; and the cylinder is intermediate, at 0.7855. For the data quoted, the particles chosen were those that, by eye, looked closest to cubes, so we expected to find F factors close to unity. In fact, as Table 3 shows, the values indicated that the shapes approximated more closely to something between the spheroid and the cylinder than to a cube or rectangular block. Table 3 also gives the experimental and calculated values of K obtained previously (2); there seems to be no correlation between the (x+y) exponent difference, or the F factors. We therefore conclude that treating the particles as spheres was an adequate approximation to reality, the more so as the particles definitely derived a more rounded shape as they swelled, in spite of the general retention of their original shape. The final difference between the calculated and experimental values of K is most probably due to random scatter. Any closer practical identification with shape will require more precise experiments than those reported here.

4.3 Influence of Shape - Although determination of shape did not provide any further practical interpretation of the available data, the factor of shape can, nevertheless, be usefully considered and discussed in general. Shape may be partly a function of the inherent physical properties of a given coal that control the shape on breakage, but Perry (13) has shown that it is also dependent on the type of grinder used. Perry reported that a disc mill produced lamellar shapes whilst those from a hammer mill were polyhedral, tending to cubical. With decreasing particle size, the lamellar shapes tended to vanish, and even the disc mill produced substantially polyhedral shapes at very small sizes. In our experiments, the particles were crushed by hand, in a pestle and mortar and, as described above, their shapes seemed to approximate most closely to spheroids and cylinders.

In influencing combustion behavior, we might expect that, broadly speaking, the smaller the radius of curvature of any part of the particle surface, the faster that area would be likely to react, since the boundary layer above that part should be a little thinner. It is difficult to say for certain, however, from a study of the photographs, that this does or does not occur; irregularities in the shapes of the particles are maintained for quite an appreciable length of time - as long as 10 or 20 seconds - but most of the particles appeared to have been reduced to good approximations to spheres by the time they were half burned. The photographs in some instances were misleading as the ash would occasionally remain as a fairly coherent, though fragile, tracery, in the center of which the glowing, shrinking sphere could be clearly seen by eye, though the photographs showed only the barely changing outline of the ash. This was generally the case with the high-ash Two Ft. Nine coal, but occasionally happened with the others.

What we would suggest, from both the visual and photographic studies of the particles, is that reaction is in fact fastest at exposed projections, and sharply curving surfaces. This means that shapes like cubes, prolate spheroids, and polyhedral shapes in general will be reduced approximately to spheres by the time they are half burned. Short cylinders and short rectangular blocks of near uniform cross-section would therefore burn down first to something approaching prolate spheroids, and thence again would reduce to spheres. This means that excess material might burn off fairly rapidly, and the overall behavior would then approximate to spheres of diamet equal to the cube side, the shorter side of the rectangular block, or the minor diameter of the prolate spheroids. Since these are the dimensions most likely to determine whether or not a given particle would remain on, or pass through, a given sieve mesh, it may well substantiate and justify the successful use of the sieve mesh dimension in specifying the particle diamete to be used in the combustion calculations.

Other shapes such as needles, long cylinders, long regular blocks, or prolate spheroids with a big ratio of major to minor axis would be expected to burn at rates rather closer to those expected of regular cylinders. The square law relation of eqn. (7) should still obtain, but the burning rates and overall burning times should be rather longer. This expectation was neve tested quantitatively but it could quite possibly account for some of the scatter in burning times found at any particular given diameter.

Finally, there are shapes like oblate spheroids, flat rectangular plate: and lamellae. The behavior of these has yet to be investigated either theoretically or experimentally, but our expectation is that they would very likely burn in from the edges rather fast, giving burning times many times i excess of expectation on the basis of either the total mass involved, or on

sieve diameter. It is also likely to be sharply dependent on the orientation of the plane or flatter surface to the horizontal or vertical as this could strongly influence the natural convection currents and therefore the boundary layer thickness. This, however, is an area of investigation still open to study.

5. CONCLUSIONS

The conclusions that may be drawn from this study are in answer to the questions set out in the Introduction.

(1) Particles swell or not according to coal rank. Particles from anthracites (under 5% V.M.) swell negligibly or not at all. Particles from bituminous coals, on the other hand, (greater than 10% V.M.) swell in air by a net factor of about 1.5, this factor being substantially independent of coal rank.

(2) The swelling process is in two stages: first an expansion to 2 or 3 times the original diameter, followed by a contraction down to the final diameter of 1.5 times the original diameter. In CO_2, the swelling finishes at the end of the first stage; there is no contraction which presumably, therefore, is conditioned by the presence of oxygen.

(3) In swelling, the process was reasonably isotropic, and apparently uniform throughout, with no cenosphere formation.

(4) In burn-out, the particles evidently burned uniformly at the exposed surface only. There was no evidence of internal burning (as is only to be expected with boundary-layer diffusion control of the reaction). The diameters therefore dimished with time quite regularly according to the equation:

$$d^2 = d_o^2 - t/K$$

with values of the burning constant K in agreement with those obtained previously from studies of the "integrated" or total burning times.

(5) Finally, shape appeared to have no detectable effect on the burning rates, other than maybe to increase the scatter in the burning times. Detection of any such effect will almost certainly require more accurate studies, using more precisely specified materials, both with regard to composition as well as shape.

6. REFERENCES

1. Essenhigh, R.H. and Thring, M.W. Conference on "Science in the Use of Coal" (Sheffield, 1958) Paper 29 p. D21 Institute of Fuel (Lord) 1958
2. Essenhigh, R.H. J. Engrg. for Power 85 (1963) 183
3. Beeston, G. and Essenhigh, R.H. J. Phys. Chem. 67 (1963) 1349
4. Nusselt, W. V.D.I. 68 (1924) 124
5. Essenhigh, R.H. J. Inst. Fuel 34 (1961) 239
6. Essenhigh, R.H. Ph.D. Thesis (University of Sheffield: U.K.) 1959
7. Sinatt, F.S. and Slater, L. Fuel 1 (1922) 2
8. Newall, H.E. and Sinatt, F.S. Fuel 3 (1924) 424
9. Stephan, A. Ann. der Physik 17 (1882) 550; 41 (1890) 725
10. Eckert, E.R.G. and Soehngen, E. Trans. A.S.M.E. 74 (1952) 343
11. Grober, H. and Erk, S. "Fundamentals of Heat Transfer" (3rd Ed.) (Trans.) McGraw Hill, 1961
12. Orning, A.A. J. Engrg. for Power 85 (1963) 189
13. Perry, M.G. Univ. Sheffield Fuel Soc. J. 8 (1957) 28

7. ACKNOWLEDGMENT

The work described in this paper completes publication of research on single coal particles carried out as part of a general program of research on Pulverized Coal Combustion sponsored by the Electricity Supply Research Council of Great Britain. The work was carried out in the Department of Fuel Technology and Chemical Engineering, University of Sheffield, England, during the tenure by one author (R.H.E.) of the Research Fellowship granted under the terms of the sponsorship. The authors are indebted to the ESRC both for the financial support of the research appointment, and for permission to publish this paper.

Table 2

Values of Swelling Factor, f (d_s/d_o)

		c%	V.M. %	Values of f	Mean (f)
1.	Stanllyd	93.0	9.9	1,1,1	1
2.	Five ft.	91.8	14.9	1.5, 1.25, 1.9	1.55
3.	Two ft. Nine	91.2	28.8	1.1, 1.25, 2.2	1.48
4.	Red Vein	89.7	23.3	1.75, 1.6, 1.7 1.7, 1.9, 1.7	1.72
5.	Garw	88.9	30.6	1.8, 1.6, 1.4 1.9, 1.5	1.64
6.	Silkstone	86.9	41.5	1.8, 1.4	1.6
7.	Winter	84.0	39.3	1.3, 1.1, 1.6 1.9, 2.0	1.58
8.	Cowpen	82.7	40.2	1.6, 1.5, 1.9	1.67
9.	High Hazel	81.9	40.7	1.4, 1.5, 1.4 1.8, 1.6, 1.7	1.56
10.	Lorraine	79.3	40.2	1.3, 1.5, 1.5 1.8, 1.6	1.54

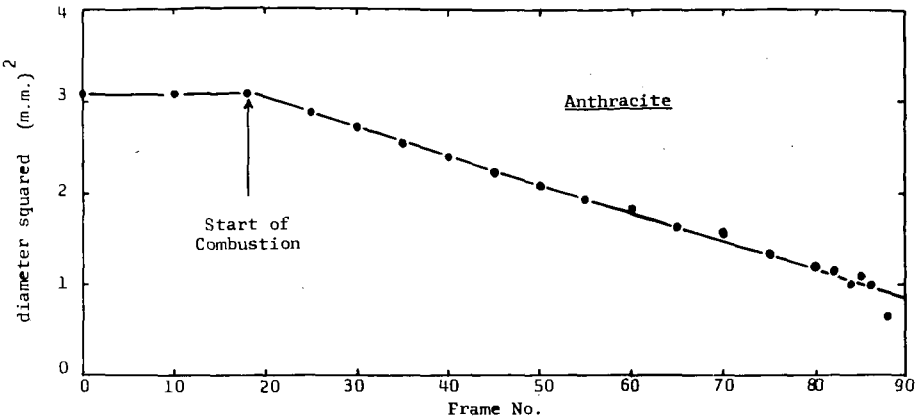

Figure 1 - Variation of diameter squared with time of burning anthracite particle (Stanllyd)

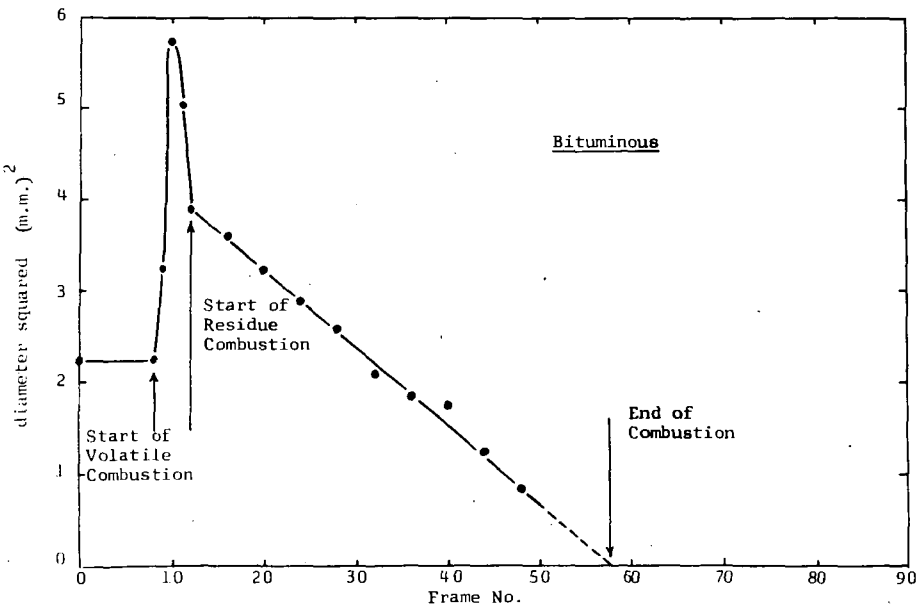

Figure 2 - Variation of diameter-squared with time of burning bituminous coal particle (Cowpen)

Predicted Burning Rates of Single Carbon Particles

Robert H. Essenhigh, Robert Froberg
and Jack B. Howard

Department of Fuel Technology
The Pennsylvania State University
University Park, Pennsylvania

1. INTRODUCTION

In spite of the immense amount of research on combustion of carbon in the last 30 years, the classic experiments of Tu, Davis, and Hottel (1) on 1" spheres are still of the best, and perhaps still the most widely quoted, of all experimental work on the subject, carried out at atmospheric pressure, and in this range of particle size and temperatures. The theory, of course, has advanced in several particulars since then (see Reviews (2-5)) and it has long been known that the original Tu et al. theoretical analysis was inadequate. In the original analysis, only desorption and boundary layer diffusion were considered as possible rate-controlling steps in the reaction: chemisorption and internal reaction were neglected. This neglect was simply that, at that time of writing, these two latter concepts had not been formulated, or not generally accepted; also, as a bias against considering adsorption, this was always assumed to be so fast as to be effectively instantaneous. According to Brunauer (6), the concept of activated adsorption was first formulated in the early 1930's - about the time of writing of the Tu et al. paper, or soon after - but, even a decade later, it still had not been generally accepted, with the consequence that many true chemisorption processes even then were being incorrectly interpreted in terms of solution, diffusion, migration (mobile adsorption), or reaction at the solid surface itself (6). Analysis of the internal reaction processes came even later, and has only been developed in the last decade or so.

Thirty years of research, therefore, has largely inverted the relation between theoretical to experimental work: that is to say, theory now leads experiment in consolidated development. Even so, the theoretical position is still confused: confidence in many of the theoretical concepts is still low as there are now almost too many theoretical possibilities available to explain any given set of new experimental data. Further definitive experiments are required to clarify quite a number of theoretical ambiguities, inconsistencies, and contradictions. One particular such point of major fundamental and practical concern at the present moment is the relative importance of the three principal "resistances" (1,7) in the carbon oxidation reaction. The three resistances are those of: boundary layer diffusion (S_0); adsorption (S_1); and desorption (S_2). For many years, only diffusion was ever considered as the rate control at temperatures in excess of 1000°K. Hottel and Stewart (8) had in fact shown conclusively, 25 years ago, that this was definitely not the case for small particles of pulverised-coal size, in flames, but little or no notice seems to have been taken of this paper till recently. Latest work, (9,10) however, has now confirmed the essential correctness of Hottel and Stewart's conclusion, but this now brings in question the basis of the previous belief, and also over what range of particle sizes and temperatures the new conclusion is valid.

In support of the original contention of diffusional control at high temperatures, the paper most frequently quoted would seem to have been that of Tu et al. Since, however, the original analysis was incomplete or inadequate, for the reasons given above, our thought was that the Tu et al. data might not be inconsistent with the new concepts, but simply had never been tested against them. It is true that their data apparently gave full support to the concept of diffusion control, but it has been shown elsewhere (2) (following Brunauer's (6) suggestion), that many combustion data can reasonably be reinterpreted in terms of an activated adsorption control, instead of the generally assumed diffusion control - if it can be accepted that the activation energy, though low, is finite, in the region of 2000 to 4000 cal., and therefore able to generate a small, but not negligible, resistance. Given this assumption, the Tu et al. data can then, apparently, be shown to give equally full support to the alternative hypothesis of adsorption control. This evident contradiction (i.e., equal support to both hypotheses(, means of course, that the intrepretation of the data, as analysed to date, is ambiguous; but it seemed to us, nevertheless, that the ambiguity was in the analysis, not in the data. Therefore, if the data were of the high quality that is generally claimed for them, it might be possible to remove the ambiguities by using the data to test the full equations now available in the literature (3-5), instead of the partial equations used hitherto (1) (see also (11,12)) which were generally based on unverified assumptions of very rapid, and therefore neglectable, adsorption.

The purpose of this paper, therefore, is to present this re-analysis It shows that the data are indeed of excellent quality (thus eliminating the need for repeat of the experiments). It also shows that adsorption presents a small, but significant resistance, which increases in importance as the particle size drops, becoming dominant at something under 100 microns. There are, therefore, no essential inconsistencies with other and more recent data, so the tested equations can be used to some extent to predict combustion behaviour of very small particles.

2. THEORY

The literature and general theory of carbon combustion has been reviewed so often, and so extensively (2-5), in the last few years, that we do not intend, in this section, to do more than set out the essential equations in the best form for our immediate purpose of testing them by re-analysis of the Tu et al. (1) experimental data. The most exhaustive of the reviews is that by Walker et al. (4) who paid particular attention to mechanism details, internal reaction, CO_2 and other reactions, and influence of radiation. For our purposes here, however, the nomenclature of the other reviews is more convenient, and has therefore been followed.

2.1 General Model - The classic picture of heterogeneous reaction between a flowing fluid and the solid it surrounds (e.g., (13,14)) is that of a three stage process. (1) The reacting fluid diffuses through a boundary layer against the counter diffusion of inerts and/or reaction products - e.g., N_2, CO_2, CO. (2) At the solid surface the reacting fluid is chemisorbed, requiring activation energy of adsorption, E_1. (3) After a finite residence time, which can be microseconds, the final reaction step is completed with the desorption of the adsorbed material which carries with it the underlying atom of the solid, so forming the reaction products: this requires activation energy, E_2. The total process is then completed with counter-diffusional escape of these products into the main fluid stream. This general process can then be treated mathematically by setting up the simultaneous equations both for boundary layer and pore diffusion and for the appropriate adsorption isotherms. These are the subjects of the next two section.

2.2 Diffusion - Potentially, this can operate in two ways: by boundary layer (external) diffusion; and by pore (internal) diffusion.

(i) Boundary layer diffusion: The existence of this process is well established, and the process well understood; and, as a result of excellent agreement between prediction and experiment (15-17), confidence in the absolute accuracy of the diffusion calculations for combustion rates is now high.

To treat diffusion mathematically, we define a velocity constant for mass transfer (transfer coefficient), k_o, by the equation:

$$R_s = k_o(p_o - p_s) \qquad (1)$$

where p is the oxygen partial pressure, with subscripts o and s for values, respectively: in the main stream, and adjacent to, the solid surface. The velocity constant, k_o, is a function of particle size and general ambient conditions, including temperature and velocity in particular. Standard analysis of this system, following Nusselt (14), leads to an equation for k_o that may be written as the temperature function:

$$k_o = A_o(T/T_o)^{n-1} \qquad (2)$$

where A_o is a velocity dependent coefficient, given below; and n is an index generally lying between 1.5 and 2, depending on the nature of the diffusing gases involved. For oxygen in nitrogen, which is the dominant system in air-combustion, experiment gives the best value for n as 1.75 (18,19). The coefficient A_o is given by:

$$A_o = (\rho_o M_c/M_o)\ (D_o/d)Nu = K.Nu \qquad (3)$$

where ρ_o is the s.t.p. density of oxygen; M_c and M_o are the molecular weights of carbon and oxygen respectively; D_o is the s.t.p. diffusion coefficient of oxygen through nitrogen; d is the particle diameter; and Nu is the Nusselt number for mass transfer. In general, Nu is a function of the Reynolds and Prandtl numbers that can be written

$$Nu = 2 + c.Re^m.Pr^n \qquad (4a)$$

where c is a numerical constant, ranging in value (according to both the heat and the mass transfer literature (20,21)) from 0.18 to 0.7, obtained by correlation of data. Grober and Erk (20), in their review of the mass transfer data, give only the one value of 0.6 (22). This is close to Khitrin's value of 0.7 (23), quoted by Golovina and Khaustovich (24). The Pr index, n, is given by nearly all as 1/3, but in any case the Prandtl number in this instance is so close to unity that its cube root can be taken as 1 with less than 1% error. The Re index, m, is also given a range of values, from 0.5 to 0.8 (see (20,21)) in the heat transfer literature, but again, the purely mass transfer literature seems to agree on 1/2. This is given by Ranz and Marshall (22) and by Khitrin, (23) and it is also the value used to correlate combustion data by Graham et al. (25) and by Day (26). Walker et al. (4) do quote lower coefficients than this for various combustion systems, but the systems are not isolated spheres. Taking the value of 0.6 for c, 1/2 for m, unity for Pr, and expanding the Reynolds number into a coefficient and a velocity, we can rewrite eqn (4a) as:

$$Nu = 2 + c'.v_o^{1/2} \qquad (4b)$$

where c' takes the value: 2.64 (at c = 0.6).

(ii) Pore diffusion: This potentially can play a part only in the event of pore or internal reaction. If it does so, however, it has been shown

elsewhere (27,5) that its effect is to generate modified velocity constants for the adsorption and desorption processes. This means that the equations to be developed in the next section (2.3) are potentially capable of accounting for pore reaction as they stand, with the sole modification of using apparent velocity constants in place of the true ones, with auxiliary equations to relate the true and effective constants. These modified and auxiliary equations are given in the literature (4,5,27), but we are not giving them here since, to anticipate our conclusion, we found no apparent or detectable influence of pore diffusion. This was not entirely unexpected since the burn-off on the whole was fairly low, and little development of internal surface would have had time to take place. An indicator to this result was also provided by the original conclusion of Tu et al. (1) that the low temperature reaction was zero order, with respect to the oxygen partial pressure, whereas this would have been a half order reaction had internal diffusion played a part.

We therefore saw no point in quoting the pore diffusion equations. We mention it here only to show that the point was considered and capable of being incorporated.

2.3 Adsorption Isotherm - (i) Basis of choice: To set up the equation for the reaction process itself requires first the selection of an appropriate isotherm. Our choice here has been made partly on the basis of the behaviour of the most likely isotherms and manipulation of the resulting equations, and partly on the basis of Occams Razor (the Principle of Minimum Hypotheses).

The two isotherms considered were the Langmuir and the Temkin isotherms. Ideally, selection of an isotherm should be carried out by experiments to test and determine the most probable one, but this has not yet been done for this system. In general, however, the literature shows that most experimental data have been correlated on the basis of a Langmuir isotherm (28,29,30).

Information based on the variation of activation energies is also inconclusive. If a Temkin isotherm is involved, these energies must change with percentage coverage of the solid surface by the adsorbed layer. Data on these energies, however, are only plentiful for the desorption process; for the adsorption process they are very scarce. For desorption, the literature (3,4,21,30) gives values ranging from 20,000 to 80,000 cal.; but these seem principally to vary with the experimental system, and with the type of carbon used: the changes are never explicitly attributed to change of percentage coverage. For adsorption, it has already been mentioned in the Introduction that the value is expected to be low. This is the summary conclusion by Trapnell (31) in view of the speed and ease of chemisorption at normal and low ($-70^{\circ}C$) temperatures. Trapnell also quotes values from Barrer (32) which start at 4000 cal. at low coverage, in agreement with Blyholder and Eyring's figure (30), and also in agreement with the re-estimates (2) of data in the literature. Barrer also shows that the value rises with coverage, the highest figure he found being 23,000 cal. At this degree of coverage, however, the activation energies are approaching those of desorption, and it will be shown below (Analysis sec. 3.3) that the effects of rising E_1 and falling E_2 with increasing coverage do in fact offset each other: the actual degree to which this occurs can only be determined by experiment, and this has never been done. This occurs in the middle range of the isotherm. At the extreme limits, at high and at low coverage, the two isotherms in any event tend toward each other, so the offsetting effect of changing E_1 and E_2 in the middle region of coverage will tend to restore a Temkin isotherm at least to a pseudo-Langmuir isotherm. Since the use of a Temkin isotherm renders the equations somewhat intractable, and in any event has never been conclusively established, we therefore decided to use the Langmuir isotherm (on the basis of Occams Razor) since this involved fewer and simpler assumptions, though this use was still with the reservation that, if such an isotherm could be used successfully, it might still be only a pseudo-isotherm.

(ii) Langmuir isotherm: This isotherm depends on only two velocity constants: one for the adsorption process, k_1; and one for the desorption process, k_2. Both are assumed to be invariant with respect both to oxygen concentration, and to percentage coverage of the solid surface by the adsorbed film. If the specific reaction rate is R_s (gm of carbon/sq. cm. sec.), the Langmuir isotherm then gives us (5)

$$1/R_s = (1/k_1 p_s) + (1/k_2) \tag{5}$$

where p_s is the oxygen concentration adjacent to the solid carbon surface. The velocity constants can be written in general as

$$k_1 = A_1 . \exp(-E_1/RT) \tag{6a}$$

$$k_2 = A_2 . \exp(-E_2/RT) \tag{6b}$$

where the E's are the activation energies as already defined; and A and A are the pre-exponential constants or frequency factors. Like E_1 and E_2, A_2 can only be determined experimentally for the particular system under consideration; but A_1 can, in principle, be calculated from Kinetic Theory, which gives

$$A_1 = B_1 \sqrt{T/T_o} \tag{7a}$$

and

$$B_1 = M_c P \eta / \sqrt{2\pi MRT_o} \tag{7b}$$

where: P is the absolute total pressure (dynes/sq.cm.); M is the mean molecular weight of the ambient gas; R is the gas constant; and η is a steric, orientation, or entropy factor for the oxygen as it is adsorbed on the solid surface.

For reasons to be explained below (Analysis, sec. 3), it is convenient to incorporate the root-temperature term in an apparent or effective activation energy E_1', whence we may write

$$k_1 = B_1 . \exp(-E_1/RT) \sqrt{T/T_o} \tag{8a}$$

$$= B_1' . \exp(-E_1'/RT) \tag{8b}$$

The objective of this is to reduce the temperature-dependent factor A_1 to a temperature-independent factor B_1, and hence to B_1', ($=B_1/b$, where $b = 3.9$), where the factors B are also independent of velocity.

2.4 Combined Kinetics - To take all the possible factors into account simultaneously, it is clear that we must set up the equation for the combined kinetics by elimination of the unknown partial pressure p_s by solving for this between eqns (1) and (5) and equating. This gives the quadratic:

$$R_s^2 - (k_o p_o + k_2 + k_o k_2/k_1) R_s + (k_o p_o) k_2 = 0 \tag{9}$$

This is already cumbersome: it is clear that if the expressions for the velocity constants (k) are also inserted, the equation becomes totally unweildly. There are then so many coefficients that the expression could be fitted to anything at all, relevant or not. For this reason, we have tried, in our Analysis (sec. 3, below) to consider special cases that can be legitimately extracted, and to test the expression, unit by unit. For this reason we derive two of the special cases of importance, in this section, for use in the analysis below.

(i) k_2 large: For this special case, we divide the equation through by k_2 and, find that, when k_2 is large, the two terms (R^2/k_2) and $(k_o p_o/k_2)$ both become vanishingly small.[2] This leaves only the familiar "resistance" equation:

$$1/R_2 = (1/k_o p_o) + (1/k_1 p_o) \quad (10a)$$

$$= S_o + S_1 \quad (10b)$$

where 'S' is the appropriate resistance.

The significant point of this equation is that the reaction rate is first order (proportional to p_o) whatever the relative values of k_o and k_1. This is important as this resistance equation applies only when k_2 is large, i.e., at high temperatures. This was the central error of the original Tu et al. (1) analysis since the authors started by assuming that the reaction was first order, over the whole temperature range; they then showed experimentally that the first order reaction was true only above 1100 or 1200°K, with a zero order reaction below this temperature (as later confirmed by others (33,34)); but yet they continued to analyse the full data in terms of their only-partially applicable equations. For these reasons, the activation energy was mis-identified, and the part played by adsorption in the high temperature region was not appreciated.

(ii) k_1 large: The original Tu et al. analysis therefore was based on the concept of full chemical control at low temperatures, and full diffusional control at high temperatures. This only follows if adsorption is so fast that k_1 is very large, and we than have another special case of great interest. For k_1 large, the term $(k_o k_2/k_1)$ in eqn. (9) vanishes, and the resulting expression then factorises:

$$(R_s - k_2)\ (R_s - k_o p_o) = 0 \quad (11)$$

What this implies is that: k_2 is controlling at low temperatures; $k_o p_o$ is controlling at high temperatures; but, between the two, there is no transition region. Change from one region to the other is quite discontinuous. There is, of course, continuity in the reaction rate values; but there is complete discontinuity in the slopes of the two curves at the junction of the two regions. Experimentally, this has been shown explicitly for the carbon-hydrogen reaction (35), and implicitly for the carbon-oxygen reaction under such conditions that the reaction is possibly that by CO_2, with the carbon, in a double film at the onset of diffusion (24).

(iii) k_o large: For this condition, inserted for completeness, eqn. (9) reduces to the Langmuir isotherm of eqn. (5), though with p_o substituted for p_s. We can then write in the resistance notation:

$$1/R_s = S_1 + S_2 \quad (5a)$$

3. ANALYSIS

In this analysis, now to be developed below, our essential objective was to extract experimental values, from the experimental data, in such a form that it would then be possible to check one dependent variable against one independent one, according to the developed equations, all other variables remaining constant in the particular process being checked. This seemed to us to be the only valid way of testing such involved and elaborate equations as those given above, though it is conceded that the methods of extracting the operating values may perhaps be regarded as somewhat questionable in one or two particulars. However, it is difficult to see what other approach could have been adopted.

The analysis starts with a re-presentation of the data.

3.1 Data Plot - Fig. 1 shows the plot of the original Tu, Davis, and Hottel data (1), but as an Arrhenius plot instead of the double-log plot that they used; also using carbon surface temperatures as being more relevant then furnace temperature.

On this plot, the almost-vertical dotted line on the right is the k_2 term, fitted to the data, with an activation energy (E_2) taken as 40,000 cal. This value was selected as it gave a better fit to the data than the 35,000 cal. quoted by the original authors; it was also closer to other values found for electrode carbon (see (3,4,21)).

The heavy lines are "back-plots" calculated according to eqn. (9) using values of the constant coefficients as determined by this analysis.

3.2 Empirical Correlation - If the calculated back-plots of Fig. 1 are carefully compared with the original curves drawn in the original Tu et al. paper, which latter were drawn empirically, the two sets will be seen to follow each other very closely. This agreement was quite fortuitous, but it so happened that the original curves were of considerable assistance in providing us with a starting point in the analysis. In the first place, the marked curvature of the lines in the original plot showed that the limiting approximation of eqn. (11) clearly did not apply. Therefore, if any approximation applied, it would be closer to a Langmuir isotherm; moreover, this expectation was strongly supported by the shape of the curves. These all have a common starting point at low temperatures, with "fine-structure" splitting at high temperatures due to both oxygen concentration, and velocity. What, therefore, we had to investigate was the possibility that the curves were modified Langmuir isotherms, obeying a two-term equation of the form:

$$1/R_s = 1/k_2' + 1/k_2 \qquad (12)$$

where k_2 is identified from the start with the same k_2 desorption step as in the previous equations; but k_2' is inserted empirically. This is initially defined, also empirically, by:

$$k_2' = A_2' . \exp(-E_1'/RT) \qquad (13)$$

where E_1' is an effective activation energy that is identified below as the E_1' of eqn. (8b), and so is written as such here; and A_2' is an empirical velocity and concentration-dependent coefficient or frequency factor.

Our procedure now is: first, to show that this formulation has empirical value in correlating the data, to reduce these to specifications in terms of empirical equations, incorporating empirical definitive, coefficients; and secondly, to show that the empirical definitive coefficients also have fundamental justification and meaning.

3.3 Data Fit - To correlate the data by means of eqn. (12), the method used is illustrated in Fig. 2. This illustrates the method for just three of the data sets: namely, for the three oxygen concentrations, 21.0%, 9.69%, and 2.98%, at the single approach velocity of 3.51 cm./sec. All the other data were treated similarly (plots not reproduced). On these data plots, two "fitting" lines were drawn, one equivalent to a slope of 2,000 cal., for E_1', and the other equivalent to a slope of 40,000 cal., for E_2. Parallel to these two lines, further lines were drawn which were expected to be the limiting assymototes of the "Langmuir" curves when these were calculated and drawn in on top of the data. For the data of Fig. 2, this gave us, as can be seen, four such fitted lines, three for the slopes of E_1', and one for the slope of E_2.

As mentioned above, the k_2 line was retained as common to all the data (common A_2 and E_2), for all velocities and oxygen concentrations, but there were nine different values obtained of the empirical frequency factor A_2', though at the common value of 2,000 cal. for E_1. This splits the data into temperature-dependent, and temperature-independent groups or coefficients (i.e., exp(-E/RT) and A).

Once the k_2 and k_2' lines had been drawn in, the "Langmuir" curves were easily calculated and drawn in, as shown in Fig. 2. Because this was an empirical procedure, several tries were required for some of the lines to get a placing of the k_2' line that would give the best looking fit (by eye) of the Langmuir curves to the experimental data. In this fitting process, a value of 4,000 cal. was also tried for E_1', but the fit given was very poor in comparison to the finally-adopted value of 2000 cal. Two other values for E_2 were likewise tried: 35,000 cal. as proposed by Tu et al., and 58,000 cal. as proposed by Wicke (36). It was found by this that, within the limits of the experimental scatter, the fitted curves were somewhat insensitive to increase of E_2 above 40,000 cal. (the value finally selected), but the finally selected value seemed to be the best compromise between the slightly conflicting demands of all the data sets. It can also be seen, however, on both Fig. 1 and 2, that the final Langmuir curve has a long traverse at the lower temperatures, particularly for the 50.0 cm./sec. line at 21% oxygen, that has very little curvature and, within little error, a straight line could be drawn in, as an approximation, that would have an effective slope of close to 35,000 cal. This would appear to be the origin of Tu et al's figure of 35,000, and therfore substantiated our conclusion that our value should exceed theirs.

One final point can also be illustrated on Fig. 2. If we accept that the value of E_1 will rise, and E_2 will drop, with increasing surface coverage, (i.e., decreasing temperature), the effect is shown in Fig. 2 by the dotted curved lines. It is quite clear from this that, in plotting out the composite Langmuir curve, the two tendencies could very well offset each other, as described above, thus restoring what might be a Temkin isotherm to a pseudo-Langmuir isotherm. This helps to justify our procedure, at least from the empirical point of view.

3.4 Identification - The procedure outlined above demonstrates that the data can be described, to some degree of accuracy, by eqn. (12), with the k_2 and k_2' components described by eqns. (6b) and (13). Now, if the experiments had all been carried out at temperatures in excess of about 1100°K, and had been continued to higher temperatures still, the k_2 term would have been relatively unimportant, and the data could have been described empirically by the k_2' term alone. If, therefore, we now concentrate solely upon the k_2' term, what our fitting procedure has done is to correct the data for the k_2 component, and it now allows us to treat the data as if the k_2 term were very large - i.e., the low temperature resistance, S_2, is very small. But, under these circumstances, the original eqn. (9) reduces to the familiar resistance approximation of eqn. (10), which can be written in the alternative form:

$$R_s = k_1 p_i / (1 + k_1/k_o) \quad \text{(for } k_2 \text{ large)} \qquad (14)$$

and this can now be compared with the empirically derived equation:

$$R_s = k_2' = A_2' . \exp(-E_1'/RT) \qquad (15)$$

this being the contraction of eqn. (12) when k_2 is very large. The A_2' coefficients are temperature independent, but still concentration and velocity dependent. If, therefore, the empirical coefficients A_2' have any fundamental justification, we must be able to set up an identity between eqns. (14) and (15). Testing this presumed identity is the subject of the rest of this section (3).

3.5. Concentration Properties of Empirical Coefficient A_2' - The identity between eqns. (14) and (15) may be simplified by writing:

$$A_2' = A_1' . p_o \qquad (16a)$$

and so

$$R_s = k_1' . p_o \qquad (16b)$$

whence, if the identity holds, the new empirical coefficient A_1' should now be independent of temperature and oxygen concentration, and dependent only upon velocity. This can be substantiated, in the first instance, by testing the relation of eqn. (16) against the experimental data. This can only be done for the two lower velocities, at 3.51 and 7.52 cm./sec., but the results, shown in Fig. 3 support the identity. For completeness, eqn. (16) has been assumed to hold for the other three velocities, even though measurements were made only at one oxygen concentration, and straight lines for these three velocities have also been included. The slopes of these lines give the empirical coefficients A_1', which should now be functions of velocity alone, with the temperature and concentration dependence eliminated.

3.5 Values and Properties of Empirical Coefficient A_1' - The variation of A_1' with velocity is shown graphically in Fig. 4; also shown, for reasons that will be developed, is its variation with $v_o^{1/2}$. This variation with the square root of the velocity follows from the identity between A_1' and k_1, which now reduces to

$$R_s = A_1' . p_o . exp(-E_1'/RT) = B_1' . p_o . exp(-E_1'/RT) \; / \; (1 + k_1/k_o) \qquad (17a)$$

or

$$A_1' = B_1' \; / \; (1 + k_1/k_o) \qquad (17b)$$

This formally incorporates the identification of E_1' in eqns. (8b) and (13) as being the same in both cases. It will be seen immediately from this that, if the adsorption rate is indeed very fast compared with the transport rate, k_o, then the ratio k_1/k_o would be large compared with unity, so we would get A_1' proportional to k_o: hence - from eqns. (2), (3), and (4) - to $v_o^{1/2}$. The significant curvature on the square-root plot of Fig. 4, substantiated by later plots, shows that k_1 is not very large compared with k_o. However, before these additional plots can be examined, one further point concerning the temperature dependence of the identity must be investigated.

3.6 Temperature Dependence of Empirical Coefficient A_1' - By the method of derivation, the coefficients A_2' and A_1' are necessarily defined as being temperature independent. It is apparent, however, from the proposed identity of eqn. (17b) that the right hand side of the identity still contains temperature-dependent terms. The coefficient B_1' is defined as being temperature independent; the dependency is incorporated solely in the two velocity constants, k_o and k_1. Since the two constnats appear in their ratio, k_1/k_o, what we must establish, for the identity not to fail, is that this ratio has negligible temperature dependence. From eqns. (2) and (8b) we can write:

$$k_o/k_1 = (A_o/B_1') . f \qquad (18a)$$

where

$$f = (T/T_o)^{0.75}/exp.(-E_1'/RT) \qquad (18b)$$

the quantity, f, being the temperature function ratio. Taking E_1' as 2,000 cal. this temperature function ratio has been calculated out for the temperature range 900 to 1700°K, and the result of the calculation is shown graphically in Fig. 5. It is clear from this that the ratio is very constant indeed. For the range from 1000°K, the value of the ratio can be taken as 7.1 ± 0.1. This represents less than 1.5% variation which, compared with the scatter of the original experimental points, is quite acceptable. This confirms that the coefficient A_1' has now been reduced to a function of velocity alone.

3.7 Velocity Dependence of Empirical Coefficient A_1' - By using the temperature function ratio, f, of eqn. (18b), we may now re-write eqn. (17b) in the form:

$$1/A_1' = (1/B_1') + (1/fA_o) \qquad (19a)$$

or

$$= (1/B_1') + 1/f.K(2 + c'\sqrt{v_o}) \qquad (19b)$$

The only variable terms now left in this are: the independent variable of velocity, v_o; and the dependent variable, A_1', obtained by reduction from the experimental data. Eqn. (19) is not a function that can be tested directly as it stands but, as a first approximation, we may assume that 2 is small compared with $c'\sqrt{v_o}$. The appropriate plot to test this is given in Fig. 6, which like the square-root plot of Fig. 4, also shows detectable curvature. In point of fact, apparently good-fit straight lines could have been run through both plots but, when this was tried, there was then an inconsistency amounting to an order of magnitude in the values of the ordinate intercepts of the two plots. By successive approximation between the two plots to remove the inconsistency, an ordinate intercept in Fig. 6 of value 100 was finally adopted for the quantity $1/B_1'$. This value was then used to test the following final arrangement of eqn. (19b):

$$1/\left[(1/A_1') - (1/B_1')\right] = 2fK + (fKc')\sqrt{v_o} \qquad (19c)$$

This final equation was tested by the plot of Fig. 7. This shows that the function is satisfactorily obeyed with an intercept of value 0.6×10^{-3}, this being the value of the quantity (2fK).

This functional agreement thus substantiated the identity of the empirical coefficient A_1' with the theoretical quantity $B_1'/(1 + k_1/k_o)$, as in eqn. (17b).

3.8 Coefficient Values - What we have now established is that the proposed equations have the correct functional form, which therefore provides qualtative substantiation of the picture developed. However, the graphical plots do more than this: they also provide experimental values, by way of slopes and intercepts, of the various coefficients involved, and these experimental values can now be compared with the values predicted from theory. In general, these will be seen to show agreement between prediction and experiment that varies from adequate to excellent.

3.8.1 Diffusion and Velocity Coefficients - (i) Zero velocity: At zero velocity, we get the limiting value of 2 for the Nusselt number. Physically, this represents the situation where the particle is surrounded by a totally quiescent diffusion film exerting its maximum influence. To compare theory and experiment, the experimental coefficient relating to zero velocity is the ordinate intercept on Fig. 7. From this plot, this intercept has the value: 0.6×10^{-3}. By eqn. (19c), this value is predicted by the quantity (2fK); i.e., $2f(\rho_o M_c/M_o)(D_o/d)$. Taking the following values for these quantities: ρ_o as $1.43^o \times 10^{-3}$ g/c.c.; M_c and M_o as 12 and 32 respectively; D_o as 0.181 sq. cm./sec.; and d as 2.54^c cm.; we have $K = 3.83 \times 10^{-5}$. Since ^of, from Fig. 5, has the value 7.1, we also have

predicted value: $2fK = 14.2 \times 3.83 \times 10^{-5}$

$= \underline{0.545 \times 10^{-3}}$ compared with

experimental value: $= \underline{0.60 \times 10^{-3}}$

This agreement is clearly acceptable. It is, however, no more than we now expect from diffusion calculations in view of the excellent agreement already obtained elsewhere (15-17) using such calculations. Confidence in the accuracy of diffusion calculations is now very high.

(ii) Finite velocity: In the following system, the agreement on coefficients is as good, though the order of agreement depends on whose equation is chosen from the literature for comparison of the coefficients; there are also two points that can be queried about the method of the theoretical calculation. To compare theory and experiment, we have in this instance the comparison of the values for the slope of Fig. 7. The experimental value, from the plot, is 0.725×10^{-3}. The predicted value is given, again from eqn. (19c), by its second term, as: fKc'. The value of fK is given above as 0.2125×10^{-3}; and for c' is given (from Ranz and Marshall's data (22)) under eqn. (4b) as 2.64. Hence we have:

predicted value: $fKc' = 0.2125 \times 10^{-3} \times 2.64$

$= \underline{0.7175 \times 10^{-3}}$ compared with

experimental value: $= \underline{0.725 \times 10^{-3}}$

This agreement is also excellent. The only reservations on the predicted value are concerned with: the use of the s.t.p. gas viscosity in evaluation of the c' coefficient (in eqn. 4b). Since the gas viscosity increases roughly in proportion to the square root of the temperature then, taking a mean temperature of 1500°K, the correction factor to be applied is division by the fourth root of 1500/273. This gives us about 1.5. However, we should also correct for the increased velocity past the sphere at its perpendicular diameter to the gas flow due to the constriction of the tube. This gives us a multiplying correction factor, for both corrections combined, of about 0.75. If, however, we then use Khitrins coefficient of 0.7 (23), instead of Ranz and Marshall's of 0.6 (22), the correction factor is about 0.9. This would still put the agreement between the predicted and experimental values within an acceptable 10%, but quite clearly, the possibilities of selecting values that will fit becomes so wide that better agreement finally becomes meaningless.

3.8.2 High Temperature Rate Coefficients - (i) Energy of Activation, E_1: The choice of apparent energy of activation, E_1, has been fully discussed above. This is not a quantity that can easily be predicted from first principles. A few have been (e.g.: adsorption of H_2 on carbon (37)), but no simple general method yet exists.

The apparent value is related to the true value by eqn. (8). The effect of dividing the Arrhenius exponential by $\sqrt{T/T_o}$ is to reduce the true value by about 1400 cal. By calculating the quantity $\exp(-E_1'/RT) \times \sqrt{T/T_o}$, and making an Arrhenius plot, a value of 3,400 cal. was obtained for the true activation energy E_1. This is clearly in line with the values given by Blyholder and Eyring (30), and by Barrer (32) for low area of coverage; it is also in line with the estimates made elsewhere (2). Another interesting figure can be extracted from the low temperature and pressure studies of Laine, Vastola, and Walker (38). They quote activation energies of 44,000 cal. for carbon gasification with oxygen, and 36,000 cal. for the simultaneous oxygen depletion. As with Gulbransen and Andrew (39) (whose respectove figures were: 40,000 and 35,000 cal.), these represent respectively the values for the desorption process alone, and for the total reaction. If the latter figure is the value of $(E_2 - E_1)$, then we have a subtraction, values for E_1 of 8,000 and 5,000 cal.

from Laine et al. and Gulbransen and Andrew respectively. Both figures are in line with Barrer's values (32) at low to medium coverage, and the higher is close to Bannerjee and Sarjants value (40) of 8,300 cal.

(ii) Frequency factor: This is the quantity A_1, or B_1 as the temperature-independent form of the coefficient, given theoretically by eqn. (7). It is related to the experimental quantity, B_1', through eqns. (7) and (8). The experimental value of B_1' is 0.01, obtained as described in sec. 3.7 by successive approximation. By eqn. (8) we get, for B_1, a value of 0.039. This, however, is substantially lower than the predicted value of B_1 when the orientation coefficient is unity. Taking P as 1.013×10^6 dynes/sq. cm.; M as 30; and R as 8.37 ergs/degree mole; we get a calculated value of 5.89 for B_1. Since this is substantially above the experimental value of B_1, we may reasonably infer, following Laine et al. (38), that the difference is due to the orientation or steric factor, η. This can be calculated from the identity:

$$\eta = B_1(\text{exptl.})/B_1 \text{ (predtd.)}$$

$$= 0.039/5.88$$

$$= 1/150$$

This is within a factor of 2 or 3 of the values for η given by Laine et al. (38), which ranged from 1/56 to 1/83. If the adduced explanation for the discrepancy between the two B_1 values is correct, the values of η are at least in order of magnitude agreement.

3.8.3 Low Temperature Rate Coefficients - Little need be said about the low temperature coefficients. The identification and interpretation of these has never been in dispute. The values of A_2 and E_2 adopted, as described above, of respectively: 1.05×10^4 g/sq.cm.sec., and 40,000 cal., are in line with other values given in original papers and reviews, to which reference may be made for comparison.

4. DISCUSSION

4.1 General - What these results clearly establish, to our mind, are: first, the general validity of the approach; second, substantiation of the high reliance that may be placed on the diffusion calculations; and, third, the degree of confidence to which the quoted equations may be used for calculating mass transfer in a flowing system. Given these, the most important final conclusion that may be drawn is the relative importance of the high-temperature resistance, S_1, in comparison with the diffusional resistance, S_o. This final point is now amplified in the sections following.

4.2 Resistance Ratios - (i) S_1/S_o : To show the relative importance of S_1 to S_o, which former has hiterto been generally neglected as too small, Fig. 8 shows a plot of their ratio as a function of velocity. The single line given is valid over the temperature range 1100 to 1700°K, to within about 1%; it is also independent of oxygen concentration. This shows that, over the velocity range of the experiments, the resistance ratio rises from 0.18 to 0.57. As percentages of the total reaction resistance, these figures show that S_1 rises from 15% to 36%, which clearly is not negligible. This confirms the conclusion drawn from eqn. (11) that continuity in the slopes of the curves can only mean that S_1 is significant.

At zero velocity, the ratio does become very small, dropping to about 20:1. This however, is true only for these very large spheres. Since S_o is proportional to the sphere diameter, d, by eqns. (10), (2), and (3), we then have that the resistance ratio is inversely proportional to the diameter, d. Thus,

even in a quiescent system, reduction of d from one inch to 2.5 mm would raise the resistance ratio up to 2 to 1: i.e., the two would be comparable in value. At 250 microns, the ratio goes to 20 to 1 in favour of the chemical resistance; and at 25 microns, or pulverised coal particle size, the diffusional resistance, S_o, becomes totally unimportant, in agreement with previous predictions and calculations (41,42) (also see below).

If, on the other hand, the high temperature frequency factor, A_1 ever attained its full theoretical value, the S_1 resistance would not become important till the particle size dropped below 100 microns. Above this, it would not matter. This may well have been the case for the carbons formed in situ from burning coal particles since no evidence of a chemical resistance was ever found (15-17) for particles ranging in size as low as 300 microns. This suggests that A_1 may depend as much on the inherent reactivity of the material as it does on any accomodation or orientation factor.

(ii) S_1/S_2: This alternative plot is shown in Fig. 9. In this instance the two resistances are independent of velocity, but are very strongly influenced by temperature and oxygen concentration. Even so, the two resistances are equal, over the range 5 to 21% oxygen, at a temperature of around 1200 ± 100°K; and there is substantially change from S_2 control to S_1 control (if S_o is absent) in the temperature range 1200°K ± 200°. For the 1" spheres, inspection of Fig. 2 indicates a transition temperature of about 1000°K ± 200° (cf. data in Review (3)), thus implying a surface oxygen concentration (p_s) of 1% or less. Since the oxygen concentrations can be read as surface values (i.e., of p_s), rather than main stream values, the progressive reduction of the diffusion layer, due to a rising velocity, or falling particle size, is seen to increase the surface oxygen concentration, and to raise the transition temperature.

4.3 Small Particle Behavior and Other Data - As mentioned above, the diffusion resistance, S_o, becomes neglible as the particle size drops below 100 microns. Small particle behavior, as in pulverised coal flames (9), or soot particles in cracked hydrocarbon flames (10), can therefore be evaluated from eqn. (10) and Fig. 9. According to these, we should find that, even in the most favorable conditions for the resistance S_2, the S_1 resistance should predominate above 1400°K. Data (9,10), however, show that high activation energies, of about 40,000 cal., can be adduced over the range 1300 to 1700°K. This, of course, is quite feasible if the S_1 value for particles formed from coal in situ can indeed drop by a factor of 10^2, as discussed above. At 5% oxygen concentration, the S_2 resistance would not drop below 10% of the total resistance till the temperature exceeded 1900°K.

Such behavior would satisfactorily account for the results obtained, except that both reactions are claimed to be first order. A possible reason for this further discrepancy may be that there is even a fourth resistance or mechanism coming into play at the higher temperatures. Smith and Gudmundsen (43) measured burning rates of small spheres, 2 or 3 mm in diameter, at temperatures ranging from 1450 to 1750°K. At the lower temperatures in this range, the reaction rates obtained substantially agree with prediction from the equations developed in this paper, using the same experimental coefficients. The initial slopes of the curves with respect to temperature are also similar; but above 1650°K, where Tu et al. had very few data, the slopes of the Smith and Gudmundsen curves increase very rapidly indeed, with the activation energy evidently high. Golovina and Khaustovich (24) have shown the same effect, also using spheres of very similar diameter to those used by Tu (of 1.5 cm.) and in a 60 cm./sec. air flow. In agreement with Tu, the reaction rates rose fast up to 1000 or 1100°K, then levelling off at about 30 x 10^{-5} g./sq.cm.sec.

(cf. Fig. 3). Then, in agreement with Smith and Gudmundsen, they rose fast again over the temperature range 1400 to 1750°K, rising to about 70×10^{-5} g./sq.cm.sec.; but then they levelled off again, with calculated rates in agreement with a double film diffusion system, this being maintained up to the experimentalltemperature limit of 3000°K.

This phenomenon shown by Smith and Gudmundsen (43) and by Golovina and Khaustovich (24) in the temperature range 1500 to 1700°K may, therefore account for the Lee et al. (10) anomalies, but clearly this is a region now requiring examination, both theoretically and experimentally in much greater detail.

5. CONCLUSIONS

From this analysis, of the Tu, Davis, and Hottel data (1), on the burning rates of 1" carbon spheres, presented in this paper, we conclude that:

1. The three-resistance concept of: boundary-layer diffusion (S_o), activated adsorption (S_1), and desorption (S_2), which are deemed to take place physically in series, is essentially correct.

2. At low temperatures (below 1000°K) the desorption resistance (S_2) predominates, and the reaction order is zero. At high temperatures, (above 1000°K), the diffusion and adsorption resistances (S_o and S_1) are both, simultaneously important, and the reaction is first order. For the 1" sphere at low velocities, S_1 is the lower of the two resistances, being 1/6 of S_o at 3.5 cm./sec. gas velocity; but rising to 1/2 of S_o at 50 cm./sec.

3. At higher velocities, or smaller particle sizes, the diffusion resistance, S_o, becomes progressively less important. In general, it should be possible to neglect it with little error, at particle sizes less than 100 microns (pulverised coal size), even in quiescent ambient gas conditions.

4. The reciprocal of the three resistances are related to the velocity constants of the three processes, given generally by:

$$1/S_o = k_o p_o = A_o . p_o . (T/T_o)^{0.75}$$

$$1/S_1 = k_1 p_o = A_1 . p_o . \exp(-E_1/RT) = B_1' . p_o . \exp(-E_1'/RT)$$

$$1/S_2 = k_2 = A_2 . \exp(-E_2/RT)$$

the coefficients A_o, A_1, And B_1' being given by eqns. (3) and (7). A_o is velocity dependent, and temperature independent; A_1 is temperature dependent, and velocity independent; and B_1' and A_2 are both temperature and velocity independent.

5. The relation between specific reaction rate (R_s) and the velocity constants is given by the quadratic of eqn. (9) However, the data may be approximated by the modified Langmuir isotherm.

$$1/R_s = (1/k_1' . p_o) + (1/k_2)$$

where $$k_1' = A_1' . \exp(E_1'/RT)$$

A_1' and E_1' are empirical quantities determined by experiment. A_1', by definition, is independent of both temperature and oxygen concentration, but is velocity dependent.

6. The empirical activation energy, E_1', is identified with the effective activation energy, obtained from first principles, after combining the $T^{1/2}$ term of A_1 with the E_1 term in S_1 (E_1 being the true activation energy). The value of the effective energy, E_1', is found by best fit to experiment to have a value of 2000 cal./mole. By calculation from this, the true value, E_1, is 3400 cal./mole, in adequate agreement with other values for this quantity in the literature.

7. The empirical frequency factor, A_1', is identified with the theoretical group obtained from first principles:

$$A_1' = B_1' / (1 + k_1/k_o) \qquad (17b)$$

From this, the following relation with velocity is obtained:

$$1/[(1/A_1') - (1/B_1')] = 2fK + fKc'\sqrt{v_o} \qquad (19c)$$

Comparison with experiment confirmed the functional form of this equation; and excellent agreement was found between the predicted and experimental coefficients involved in the diffusion and velocity components of the calculation.

8. Agreement between the predicted and experimental values of the A_1 and B_1 frequency factors are in error by a factor of 150. This is attributed to an orientation or steric factor, $\mathcal{P}$, for which other values in the literature are in the range of 50 to 80. For this identification, agreement is therefore adequate.

9. A final point developing from this analysis is an ambiguity or inconsistency in higher temperature data, obtained by others, that just overlap in their bottom ranges with the top temperature range of those obtained by Tu et al. In the overlap, the data agree; but at higher temperatures, beyond the overlap, the data show a much more rapid rise in reaction rate than the equations and mechanism should permit. This phenomenon requires further study.

6. LIST OF SYMBOLS

A - frequency factor
A_o - " " for diffusion = $K.Nu$
A_1 - " " for adsorption = $M_c P \eta / \sqrt{2\pi MRT}$
A_2 - " " for desorption
A_1' - first empirical factor = $B_1' / (1 + k_1/k_o)$
A_2 - second empirical factor = $A_1' p_o$
b - conversion factor (numerical) in $B_1 = b.B_1'$: value 3.9
B_1 - adsorption frequency factor (temp. indep.) = $A_1 . \sqrt{T/T_o}$
B_1' - effective adsorption frequency factor = B_1/b
c - numerical constant in Nusselt/Reynolds No. equation
c' - revised value of c for velocity equation = $c\sqrt{\rho_o d/\mu}$
d - particle diameter (this paper = 2.5 cm.)
D_o - diffusion coefficient at s.t.p. (for O_2 in N_2 = 0.181)
E_1 - adsorption activation energy (true) = 3400 cal/mole
E_1' - empirical and effective adsorption activation energies = 2000 cal./mole
E_2 - desorption activation energy (true) = 40,000 cal./mole
f - temperature function ratio: $(T/T_o)^{0.75}/\exp(-E_1'/RT)$: value = 7.1
k - velocity constant
k_o - velocity constant for diffusion = $A_o(T/T_o)^{0.75}$

k_1 - velocity constant for adsorption = $A_1.\exp(-E_1/RT)$
k_2 - " " for desorption = $A_2.\exp(-E_2/RT)$
k_1' - first empirical velocity constant
k_2' - second empirical velocity constant = $k_1' p_o$
K - diffusional constant group = $(\rho_c M_c/M_o)\ (D_o/d)$
m) - general indices, for Re and Pr numbers
n)
M_c - molecular weight of carbon
M_o - molecular weight of oxygen
Nu - Nusselt number for mass transfer
p_o - oxygen partial pressure, main stream value
p_s - oxygen partial pressure, solid surface value
P - total pressure (1 atmos.)
Pr - Prandtl number
Re - Reynolds number
R_s - specific reaction rate - g/sq.cm.sec.
S_o - diffusional resistance = $1/k_o p_c$
S_1 - adsorption resistance = $1/k_1 p_o$
S_2 - desorption resistance = $1/k_2$
T - temperature (absolute)
T_o - s.t.
V_o - s.t.p. gas velocity
ρ_o - s.t.p. density
η - orientation or steric factor in adsorption
μ - gas viscosity

7. REFERENCES

1. Tu, C.M.; Davis, H.; and Hottel, H.C. Ind. Eng. Chem. 26, (1934) 749.
2. Essenhigh, R.H. Sheffield Univ. Fuel Soc. J. 6 (1955) 15.
3. Essenhigh, R.H. and Perry, M.G. Introductory Survey "Combustion and Gasification", Proc. Conf. "Science in the Use of Coal", Sheffield, 1958, p. D1: Institute of Fuel, London, 1958.
4. Walker, P.L., Rusinko, F. and Austin, L.G. Advances in Catalysis, Vol. II, pp. 134-221, Academic Press Inc., New York 1959.
5. Thring, M.W. and Essenhigh, R.H. "Chemistry of Coal Utilization": Supplementary Volume ch. 17, pp. 754-772, Wiley; New York, 1963.
6. Brunauer, S. "Adsorption of Gases and Vapors, p. 10, Oxford University Press, 1945.
7. Fischbeck, K.Z. Electrochem 39 (1933) 316; 40 (1934) 517.
8. Hottel, H.C. and Stewart, I.M. Ind. Eng. Chem. 32 (1940) 719.
9. Beer, J.M. and Thring, M.W. 1960 Anthracite Conference Proceedings: M. I. Experiment Station Bulletion No. 75 (Sept. 1961) p. 25 Pennsylvania State University.
10. Lee, K.B., Thring, M.W. and Beer, J.M. Combustion and Flame 6, (1962) 137.
11. Godsave, G.A.E. Nat. Gas Turbine Estab. Report No. R.126 (1952).
12. Spalding, D.B. Proc. Inst. Mech. Engrs. (Lond) 168 (1954) 545.
13. Noyes, A. and Whitney, K. Z. phys. Chem. 23 (1897) 689.
14. Nusselt, W. V.D.I. 68 (1924) 124.
15. Essenhigh, R.H. and Thring, M.W. Inst. Fuel Conference "Science in the Use of Coal", Sheffield, April 1958, Paper 28, p. D21. Inst. Fuel (London) 1958.
16. Essenhigh, R.H. J. Engrg. for Power, 85 (1963) 183.
17. Beeston, G. and Essenhigh, R.H. J. Phys. Chem. 67 (1963) 1349.

18. Sherwood, T.K. and Pigford, R.L. "Adsorption and Extraction", p.2, New York 1952.
19. International Critical Tables 5 (1929) 62.
20. Grober, H. and Erk, S. "Fundamentals of Heat Transfer", pp. 282, 283, 4.2, 3rd ed. (trans.) McGraw Hill 1961.
21. Frank-Kamenetskii, D.A. "Diffusion and Heat Exchange in Chemical Kinetics" Ch I and II: Princeton Univ. Press (Trans.) 1955
22. Ranz, W.E. and Marshall, W.R. Chem. Eng. Prog. 48 (1952) 403.
23. Predvoditelev, A.S., Khitrin, L.N., Tsukhanova, D.A., Colodtsev, H.L. and Grodzovski, M.K. Gorenic Ugleroda (1949), Izdatelstvo AN SSSR.
24. Golovina, E.S. and Khanstovich, G.P. 8th International Combustion Symposium (1960) Paper 84, p. 784, Williams and Wilkins Co., Baltimore 1962.
25. Graham, J.A., Brown, A.R.G., Hall, A.R. and Watt, W. Conf. on Ind. Carbon and Graphite, Soc. Chem. Ind. (Sept.) 1957.
26. Day, R.J. Ph.D. Thesis, The Pennsylvania State University, 1949.
27. Essenhigh, R.H. and Fells, I. Faraday Soc. Discussions "The Physical Chemistry of Arosols" (Bristol 1960), p. 208, Faraday Soc. 1961.
28. Gadsby, J., Long, F.J., Sleightholm, P. and Sykes, K.W. Proc. Roy. Soc. A193 (1948) 357.
29. Gadsby, J., Hin shelwood, C.N. and Sykes, K.W. Proc. Roy. Soc. A187 (1946) 129.
30. Blyholder, G.D. and Eyring, H. U.S. Air Force: Office of Scientific Research Report (Technical Note) O.A. NoXX August 1956.
31. Trapnell, B.M.W. "Chemisorption", pp. 70,71, Butterworths Scientific Publications (London) 1955.
32. Barrer, R.M. J. Chem. Soc. (1936) 1261.
33. Parker, A.S. and Hottel, H.C. Ind. Eng. Chem. 28 (1936) 1334 - Analysis by D.A. Frank-Kamenetskii, (ref. 62 to 64.
34. Arthur, J.R. and Bleach, J.A. Ind. Eng. Chem. 44 (1952) 1028.
35. Barrer, R.M. and Rideal, E.K. Proc. Roy Soc. A149 (1935) 231, 253.
36. Wicke, E. 5th Internation Sumposium on Combustion 1955, paper 17, p. 245 (Reinhold Pub. Corp. 1956).
37. Sherman, A. and Eying, H. J. Am. Chem. Soc. 54 (1932) 2661.
38. Laine, N.R., Vastola, F.J. and Walker, P.L. J. Phys. Chem. 67 (1963) 2030.
39. Gulbransen, E.A. and Andrew, K.F. Ind. Eng. Chem. 44 (1952) 1034, 1039, 1048.
40. Bannerjee, S. and Sarjant, R.J. Fuel 30 (1951) 130.
41. Beer, J. M. and Essenhigh, R.H. Nature (London) 187 (1960) 1106.
42. Essenhigh, R.H. J. Inst. Fuel, 34 (1961) 239.
43. Smith, D.F. and Gudmundsen, A. Ind. Eng. Chem. 23 (1931) 277.

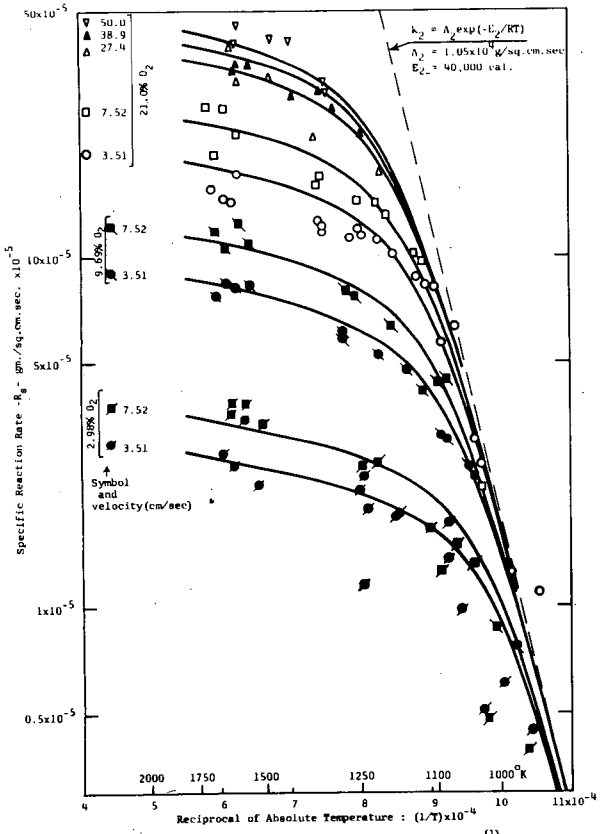

Figure 1 - Data Plot - Original data from Tu, Davis, and Hottel[1] Arrhenius plot, showing agreement with calculated curves (full lines) according to equation (9) (see text) of: Specific reaction rate (R_g) against reciprocal of temperature (1/T).

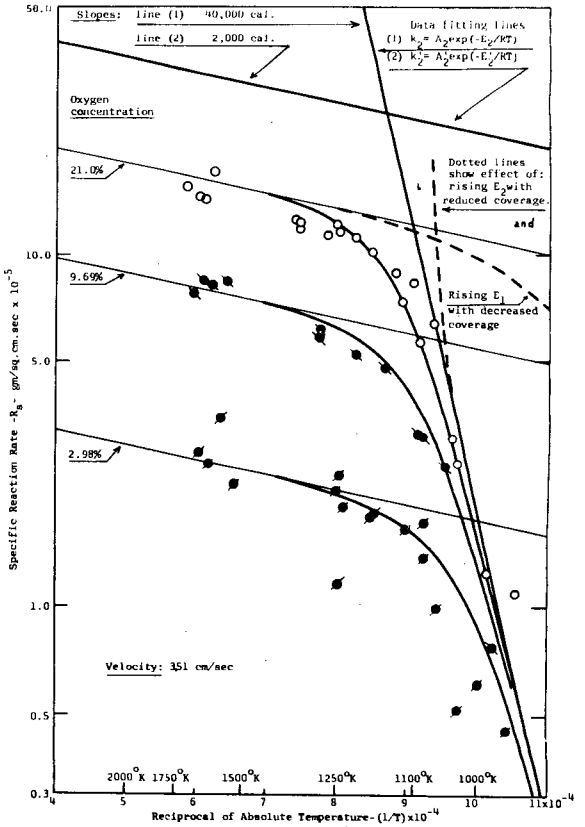

Figure 2 - Fitting Plot. Curves drawn according to equation: $1/R_g = (1/k_2') + (1/k_2)$. Data from Tu, Davis, and Hottel[1]

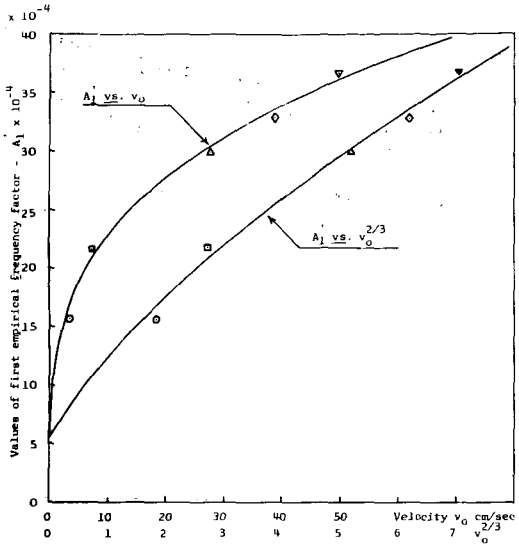

Figure 4 - Plot of first empirical frequency factor (A_1') against: (1) Velocity (v_o); (2) Square-root velocity ($v_o^{2/3}$)
Data: Derived from Tu, Davis, and Hottel[1]

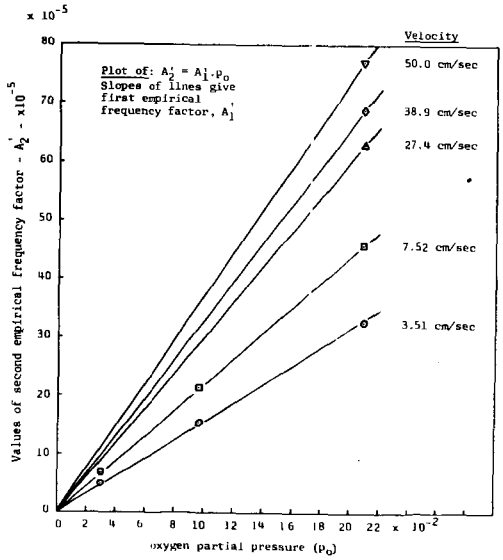

Figure 3 - Plot of second empirical frequency factor (A_2') against oxygen partial pressure (p_o), to show linear relationship - for two lower velocities. Three higher velocities (27.4, 38.9, and 50.0) added for comparison.
Data: Derived from Tu, Davis, and Hottel[1]

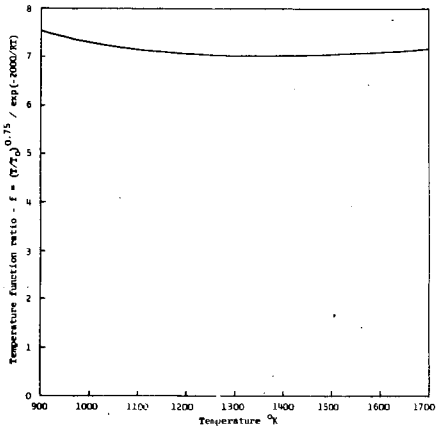

Figure 5 - Plot of temperature function ratio (f) against temperature (T) to show the constancy of 'f' with 'T'.

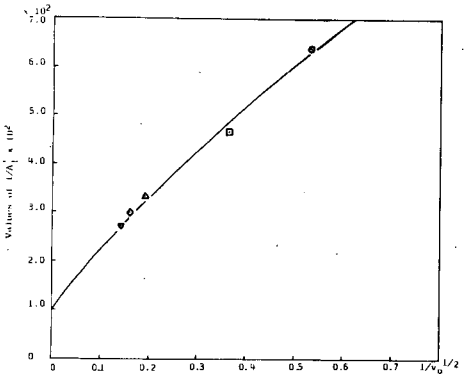

Figure 6 - Plot of reciprocal of first empirical frequency factor ($1/A_1'$) against reciprocal of square-root of velocity ($1/v_o^{1/2}$)
Data: Derived from Tu, Davis, and Hottel[1]

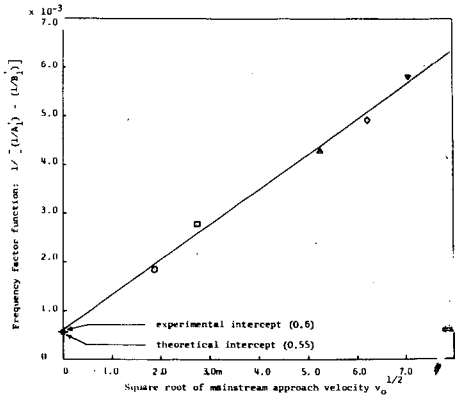

Fig. 7 - Test of eqn. (19c). Plot of frequency factor function against square root of velocity ($v_o^{1/2}$)
Data: Derived from Tu, Davis, and Hottel

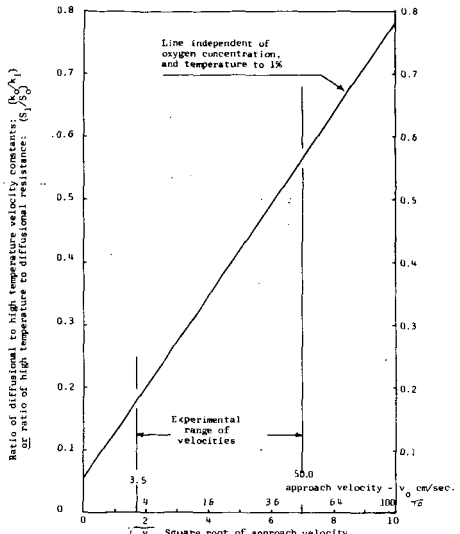

Fig. 8 - Plot of calculated ratio of high temperature to diffusional resistance (S_1/S_o) against velocity (v_o and v_{o_2})

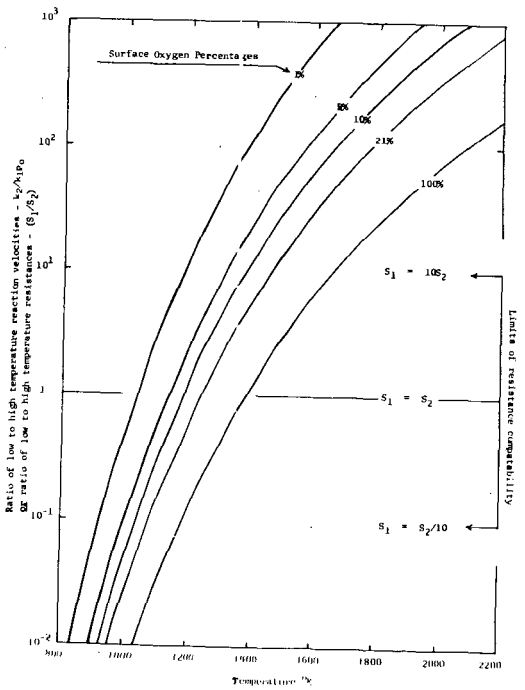

Figure 9 - Plot of calculated ratio of high to low temperature resistances (S_1/S_2), as a function of temperature, for 5 levels of oxygen concentration.

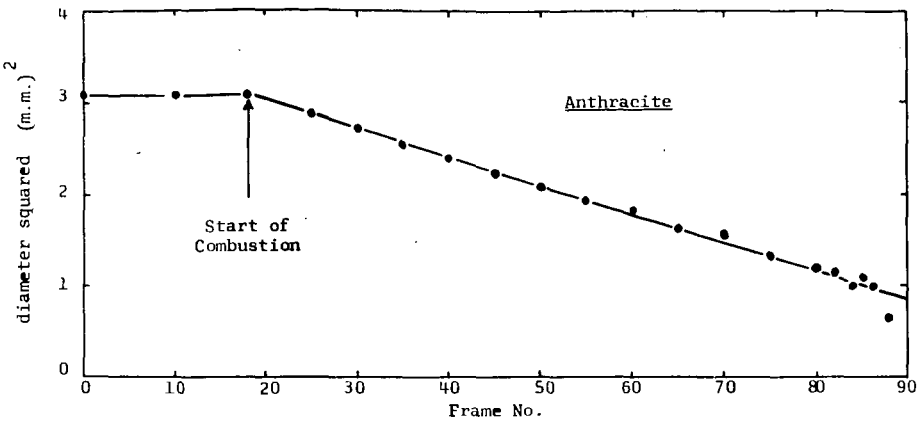

Figure 1 - Variation of diameter squared with time of burning anthracite particle (Stanllyd)

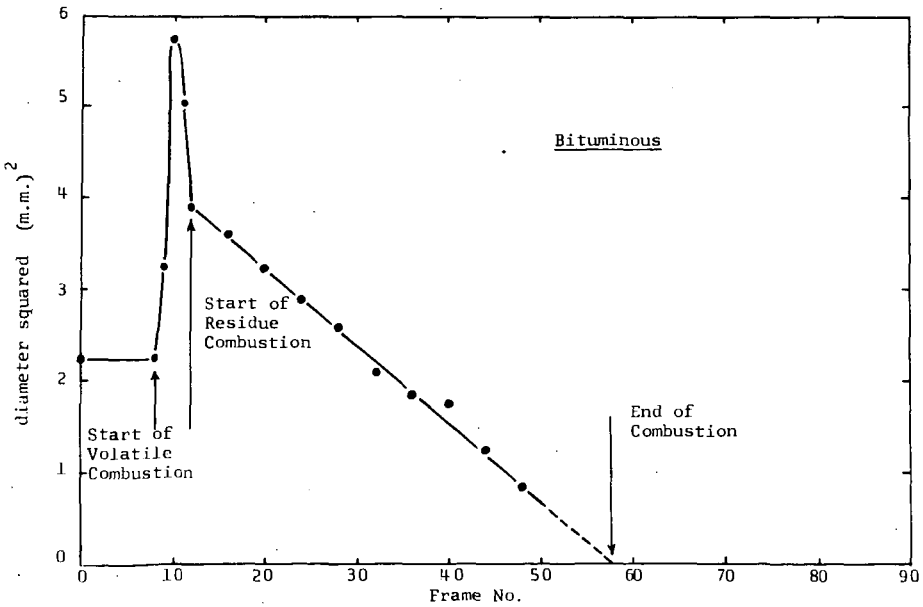

Figure 2 - Variation of diameter-squared with time of burning bituminous coal particle (Cowpen)